AIR TECHNICAL INTELLIGENCE
TRANSLATION

STAT

TITLE (UNCLASSIFIED)

PROCESSES OF FRICTION IN THE BRAKES OF AIRCRAFT WHEELS SELEC-
TION OF FRICTIONAL PAIRS

(PROTSESSY TRENIYA V TORMOZAKH AVIAKOIES. PODBOR FRIKTSIONNYKH
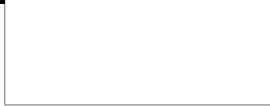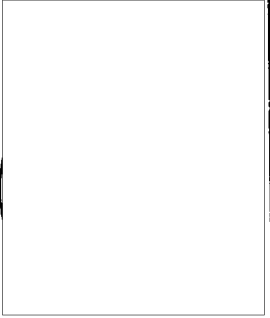PAR)

BY

I. V. KRAGEL'SKIY, G. YE. CHUPILKO, A. V. CHICHINADZE

SOURCE: ACADEMY OF SCIENCES USSR, MOSCOW

1955

190 pp.

STAT

STAT

STAT

BOOK

(UNCL) PROCESSES OF FRICTION IN THE BRAKES OF AIRCRAFT WHEELS

SELECTION OF FRICTIONAL PAIRS

(PROTSESSY TRENIYA V TORMOZAKH AVIAKOLES.

PODBOR FRIKTSIONNYKH PAR)

AUTHOR: I.V.KRAGEL'SKIY, G.Ye.CHUPILKO, A.V.CHICHINADZE

SOURCE: ACADEMY OF SCIENCES USSR, MOSCOW

1955

190 pp.

STAT

ACADEMY OF SCIENCES USSR

INSTITUTE OF MACHINE STUDIES

I. V. Kragel'skiy, G. Ye. Chupilko,

A. V. Chichinadze

PROCESSES OF FRICTION IN THE BRAKES OF AIRCRAFT WHEELS

SELECTION OF FRICTIONAL PAIRS

BASIC SYMBOLS

A_s – Kinetic energy of an aircraft at the instant of ground contact

A_T – Kinetic energy transmitted to the brakes

$A_{..}$ – Kinetic energy of the body.

a_{sbl} – Magnitude of reciprocal surface penetration

a_{kr} – Depth of deformation, leading to the given kind of destruction

a – Temperature conductivity

C_{sam} – Coefficient, considering the aerodynamic characteristics of an aircraft, and the resistance to rolling

c – Heat capacity

E – Elasticity modulus

F_{st} – Static friction force

F_k – Rolling friction force

f – Coefficient of friction

$\psi_{k\ max}$ – Maximum coefficient of tire friction against ground

G_{pos} – Aircraft weight on landing

H_B – Brinell hardness

J_{ch} – Numerical intensity of wear

J_v – Weight intensity of wear

J_l – Linear intensity of wear

K_{sam} – Coefficient considering the aerodynamic qualities of an aircraft, on landing

K_{per} – Coefficient of resistance to nose-over

i

STAT

K_{zh} – Coefficient of rigidity

μ – Poisson's ratio

M_T – Brake moment of wheel

$M_{T\,max}$ – Maximum brake moment of wheel

$M_{T\,mean}$ – Mean brake moment

N_{max} – Maximum brake power

N_T – Power absorbed by brake

$N_{T\,ud}$ – Brake horsepower

P_{st} – Radial stationary load   on wheel

P_k – Radial ground reaction, acting on the wheel

P – Load

p_T – Pressure in brake system

$P_{f\,sr}$ – Mean actual specific pressure upon contact

P_{ud} – Specific pressure

p_o – Tire inflation pressure

S_f – Actual area of contact

S_p – Calculated area of contact

S_H – Nominal area of contact

S_K – Contour area of contact

S_T – Friction area

τ – Specific force of friction

t – Time

V – Volume

v_{sk}^{∂} – Sliding speed of disk

v_{sk}^{k} – Sliding speed of drum, relative to brake shoe

v_{pos} – Landing speed

v_{okr} – Peripheral speed of wheel

L – Length

ii

STAT

n_{ok} - Number of contact points per unit contour area

n_o - Number of contact points per unit nominal area

n - Number of brakes in wheel

α, β - Coefficient in the elementary law of friction

α_{st} - Stability of friction coefficient

α_{tp} - Coefficient of distribution of thermal flow

β_{eff} - Coefficient of efficiency

Δ - Linear wear, in mm

Δh - Height

Δ_{gm} - Loss of weight of material during friction

γ - Specific weight

η_{ud} - Coefficient of fatigue in friction

δ_{gl} - Magnitude of tearing in depth

δ_{st} - Stationary contraction of a tire

θ_S - Mean temperature of friction surface

θ_V - Temperature at various points within the volume of the material

λ - Heat conductivity

q_{tp} - Specific thermal flow

σ - Coefficient of heat transfer

σ' - Coefficient of external heat transfer

φ_{kol} - Total angle of wheel revolution during braking, or brake path of the wheel

r_T - Mean friction radius

g - Acceleration of gravity

γ_{gl} - Tangent of smoothness

STAT

ERRATA

EDITOR'S NOTE - "Brake Chamber", or "Brake Chambers" (passim) should read

"Expander-Tube Brake or "e.t."bs respectively.

"Chamber" (passim) should read "Expander Tube", or

"Expander Tubes" respectively.

STAT

DESIGN AND OPERATION OF WHEEL BRAKES

IN JET-AIRCRAFT LANDING GEARS

The development of aviation is accompanied by increased landing speeds and aircraft weights. In connection with this, the kinetic energy of the aircraft at the time of landing and the length of the ground run have greatly increased. According to information in the foreign press (Bibl.1), some jet aircraft already have landing speeds of 250-300 km/hr and it is quite probable that aircraft will have landing speeds of 320-350 km/hr in the very near future.

Aerodynamic resistance during the landing run of modern jet aircraft is considerably less than that of piston-engine aircraft. The force of resistance to the rolling of wheels, equipped with roller bearings and high-pressure tires, along the hard airfield surface is also very small. Therefore jet aircraft have a high kinetic energy on landing and, with special braking, require a landing run of 3500 m or more. Operating such aircraft without braking devices would require airfields of very large dimensions. The use of wheel brakes makes it possible to shorten the landing run of the aircraft 3-4 times, i.e., to reduce it to 800-1000 m, thereby greatly reducing the size of airfields.

Braking a modern jet aircraft at the time of landing, at a landing speed of 300-350 km/hr, presents a very difficult technical problem.

During the 15-25 sec of a landing run it is necessary, by means of the aid of wheel brakes, to convert a tremendous amount of kinetic energy into heat and then dissipate this heat. The most difficult problem of the wheel-brake designer is to

1

STAT

place, in the rather limited area of the wheel, brakes with sufficient power to work dependably under the difficult conditions of rolling, and at the same time provide good ventilation of the brake junction and wheel to dissipate the heat. To provide brakes with good performance and the required life, it is necessary to select materials for brake pairs which will retain their mechanical and frictional properties at temperatures and specific pressures which, in the braking process, reach considerable magnitudes.

The aircraft wheel brakes (Bibl. 2, 3, 37) now in use may be subdivided into three types: brake shoe, brake chamber, and disk types. Brake shoes are rarely used on high-speed aircraft since they are highly sensitive to any change in the friction coefficient and to deformation of the brake drum, caused by heavy thermal loading of the frictional pair. Moreover, any faulty installation of wheel and brake on the axle of the landing gear, no matter how minor, impairs the working of the brake shoes and power brake. However it is interesting to note that despite their shortcomings, brake shoes were widely used by the Germans on almost all their military aircraft during World War II.

Expander-Tube Brakes

Expander-tube brakes are less subject to thermal deformation of the brake drum and changes in friction coefficient in the brake lining. Beginning in 1936-1937, this type of brake (Fig. 1) was being developed along with brake shoes in our aviation, however, when high-speed jet aircraft appeared and the need for serious attention to brake temperature conditions arose, expander-tube brakes superseded brake shoes since they were less subject to temperature changes.

For the last 17 years, expander-tube brakes have undergone practically no changes in structural design. Improvements have been made only in the types of material used (protected expander-tubes, electronic casting of the brake body, friction plastic, laminated return springs).

The development of expander-tube brake is closely connected with the development of

STAT

brake drums: Improvement in brakes has been accompanied by improvement in brake drum design. The first changes in the brake drum were concerned with preventing drum deformation caused by thermal loadings, and with providing energy dissipation at increased operating temperatures but without any particular increase in structural weight.
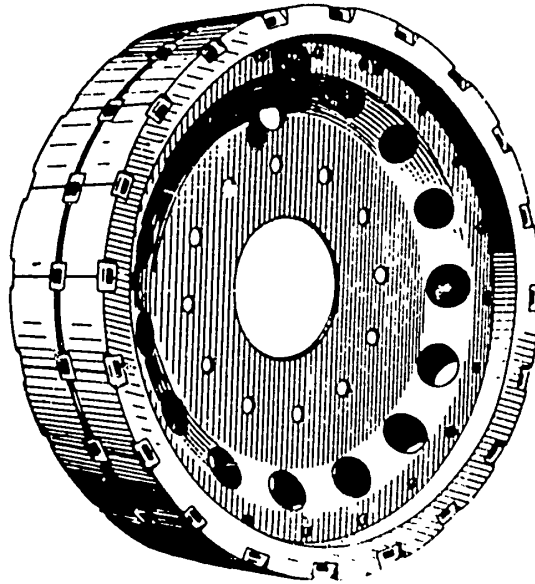

Fig.1 - Exterior View of Brake Chamber

The main improvements in the brake drum were its insulation from the rim of the wheel to avoid overheating and failure of pneumatic tires, the introduction of a finned radiation surface, and the use of bimetal drums in the form of a steel shell, reinforcing the inner cast iron layer. The friction surface of these drums is made of alloyed cast iron which makes it more durable when operating at high temperatures, and their outer surface radiates heat (Bibl.4).

At present the brake drum is made smaller along its diameter (Fig.2) than the rim of the wheel, providing an insulating air layer between the radiating surface of the drum and the rim, to which the tire with its inner tube adheres.

The shortcoming of such a construction principle is that all braking energy must be mainly absorbed and dissipated by the brake   drum, while the mass of

STAT

3

the wheel and tire barely participate. Therefore, a heavy drum must be used, calculated to absorb all the kinetic energy of the aircraft, transmitted to the brakes on landing. In earlier designs of small aircraft wheels, the brake drum was pressed into the body of the wheel (Fig.3).
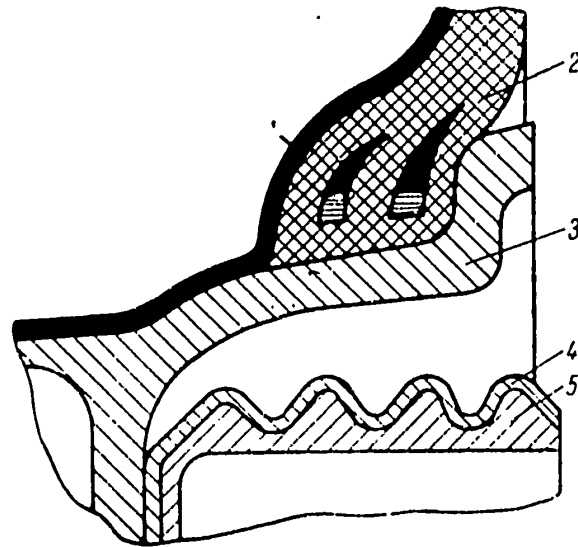

Fig.2 - Modern Design of an Aircraft Wheel with an Insulating Air Layer between the Radiating Surface of the Bimetal Drum and Rim

1 - Inner tube; 2 - Tire; 3 - Rim of wheel; 4 - Steel shell;

5 - Alloyed cast iron

The solution to the problem of increasing the resistance to wear and the constancy of the friction coefficient of the frictional brake pair is found not only through research on new and more durable materials but through improvement in conditions for the elements of the pair, i.e., through lowering the temperature of the brake pair working surface and thus eliminating increased wear of the brake shoe and lowering of brake efficiency.

Lately, bimetal drums of a different design have been used as an experiment:

STAT

the friction surface of these drums is made of a thin layer of cast iron or steel,
and remainder of the drum, which accumulates and radiates heat, of a thin aluminum
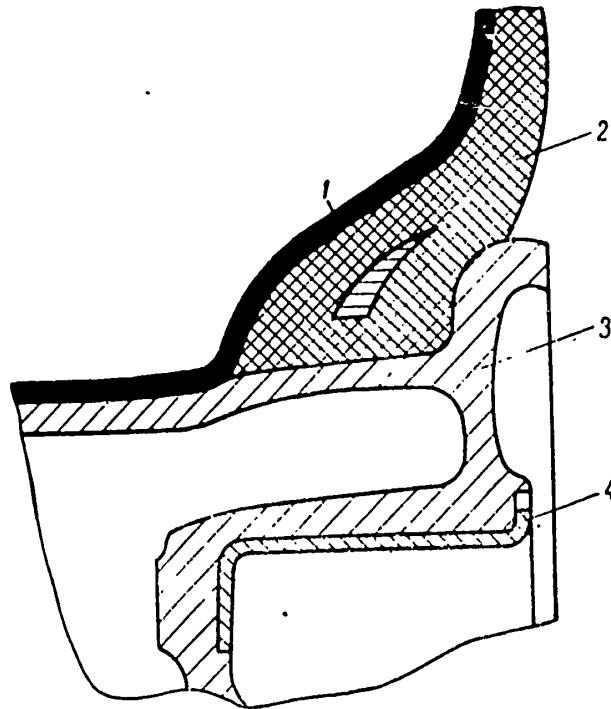alloy which has good heat conductivity and heat capacity (Bibl.5). The aluminum

Fig.3 — Early Design of an Aircraft Wheel for a Medium-size
Aircraft, with the Brake Drum Pressed into the Wheel Body

1 — Inner tube; 2 — Tire; 3 — Wheel body; h — Thin-walled
steel brake drum

alloy of the basic body of the drum and the cast iron or steel film forming the
friction surface of the drum are alloyed in a special way, so as to provide full
contact; this allows full heat transfer from the friction surface into the main
body of the drum. The cooling properties of such a drum are quite high, according
to our experimenters. Therefore, maximum temperatures on the friction surface are of
shorter duration. This improvement of the drum makes it possible not only to de-

STAT

crease the structural weight but also to improve the brake heat conditions and to provide easier working conditions for the brake linings and the friction surface of the brake drum.
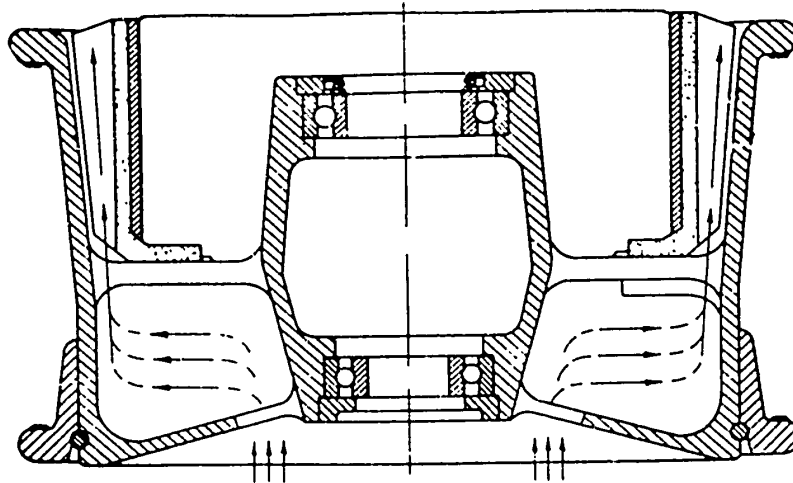
Fig.4 - Design Aircraft Wheel with Self-Ventilated Wheel Body and Exterior Radiating Surface of Brake Drum

Forced cooling of the drum after braking is used to improve the temperature conditions in the work of the lining and the friction surface. The exterior radiating surface of the brake drum is finned. Hollow brake drums with a cooling fluid or cooled with salts have been tried. Ventilation of the wheel body has also been tested (Fig.4). In this system, the exterior radiating surface of the brake drum and the wheel body are cooled by the flow of air.

In practice, however, many of these measures have proved ineffective or have not at all justified themselves. Lately, brake designs have been worked out in which the exterior radiating surface of the brake drum is ventilated and thereby cooled, also cooling the friction surface of the brake pair. Such ventilation noticeably improves the thermal conditions of the frictional brake pair. Further details on these designs are given below.

6

STAT

Disk Brakes

In modern aircraft, the need for wheels of minimum over-all dimensions to facilitate maintenance has led to the use of high-pressure tires with narrow profiles barely covering the widths of the sides of the rims. The body of such a wheel has considerably less width, which makes it difficult to place a brake drum of the necessary width in such a wheel. There is need for designing a highly efficient brake with minimum over-all dimensions. Disk brakes meet these requirements.

Disk brakes (Fig.5) are superior to brake chambers. This type of brake does not require a brake drum and therefore does not have the disadvantage of being subject to thermal radial contraction, expansion, warping, or displacement of the brake drum friction surface which would disrupt operation of the brake (Bibl.6).

Brake disks have two-sided heating, which makes them more effective and more rugged than a brake drum. At the time of braking, the disk generates heat on both of its friction surfaces, heats more uniformly and faster, and cools faster. This decreases the danger of warping.

Cooling of the friction surfaces of disk brakes is accomplished more easily than in brakes having a brake drum (Bibl.7).

Brake disks are connected to the body of the wheel by means of grooves, providing minimum contact. Therefore, contact heat transfer from the disks to the wheel body is considerably lower than from a brake drum.

Better insulation of brake disks from the wheel body is one of the most important features of a disk brake; also important is the absence of dangerous thermal deformations. The possibility of damaging the inner tube of a tire at high temperatures, while brakes are heated, is decreased.

Disk brakes usually have one (Fig.5a) or several disks (Figs.5, 6).

Unidisk brakes differ in that a large part of their friction surface is exposed, so that when they become red-hot from friction and are then cooled by an airflow they give off heat quickly to the immediate surroundings.
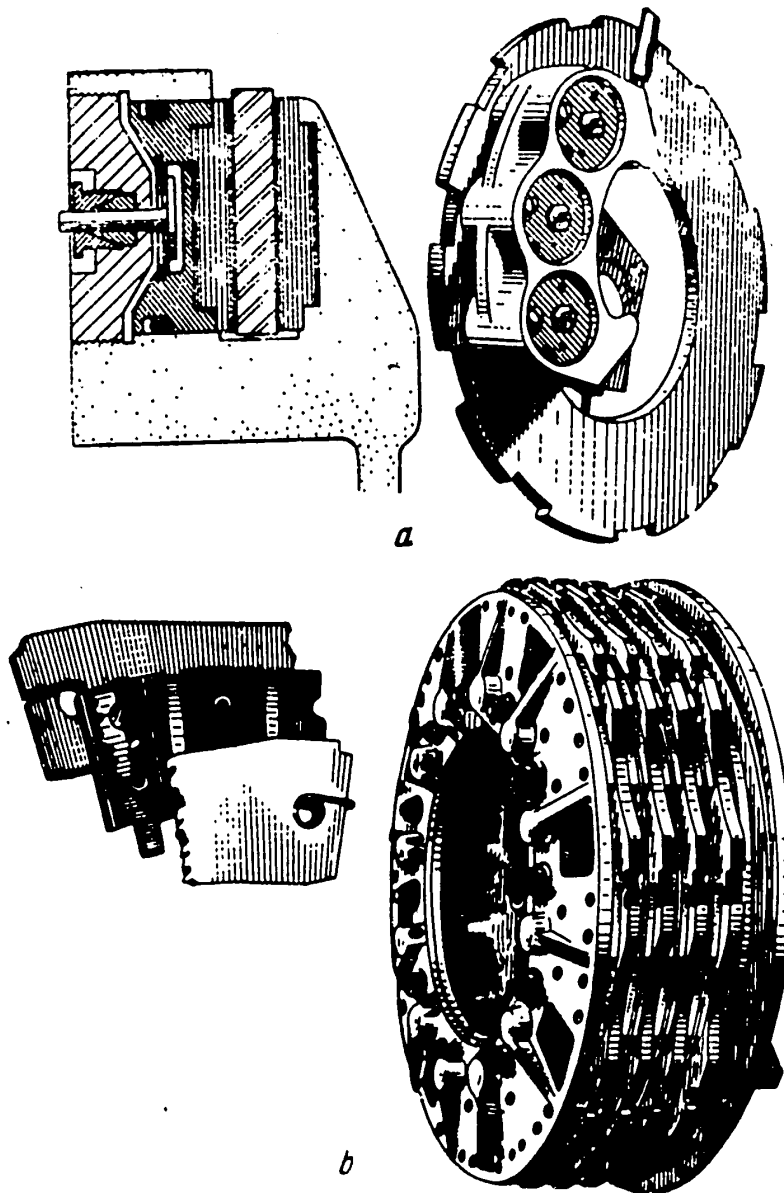
7

STAT

Fig.5 — Disk Brakes

a — Outside view and design of a unidisk brake

b — Outside view and design of a multidisk brake

STAT

Unidisk brakes with open friction surfaces are of great interest. However, unidisk brakes also have the following disadvantages:

1) Not being protected in any way, the disk may be subject to the harmful effect of sand, which contributes to the rapid wearing out of brake linings; also, in brakes with open disks the use of projecting tough (therefore heavy) brackets is necessary.

2) Despite the fact that the use of smaller friction surfaces at high specific temperatures allows maximum exposure of the disk friction surface for cooling, which is quite advantageous, the considerable increase in specific pressure on the friction lining may cause it to work unsteadily: the inconstancy of the friction coefficient, the appearance of tears etc., all in turn, will help speed deterioration.

3) The larger the mass of the disk, the greater will be the quantity of heat it accumulates; however, the thicker the disk, the higher will be the temperature gradient. The allowable average temperature of about 500°C will correspond at the time of braking, to a temperature of the disk surfaces of 1000°C or higher. Besides, impairing the frictional qualities of the pairs, this will cause oxidation of the friction surface (Bibl.8). It would be possible to chromium-plate the disks to increase their resistance to oxidation and wear, but high surface temperatures may cause formation of an oxide film on the chromium, whose mechanical strength is poor; this will cause the chromium layer to be torn off when the brake is in operation.

Multidisk brakes, in which the mass of a single disk can be reduced to an acceptable size, provide considerable absorption of kinetic energy.

Multidisk brakes consist of a number of fixed disks, joined to the body of the brake, and of revolving disks joined to the body of the wheel.

At the time of braking, the block of movable and stationary disks is compressed by a piston ring, ring-shaped piston actuated by the hydraulic system. The development of multidisk brakes has been in the direction of using thick ventilated disks.
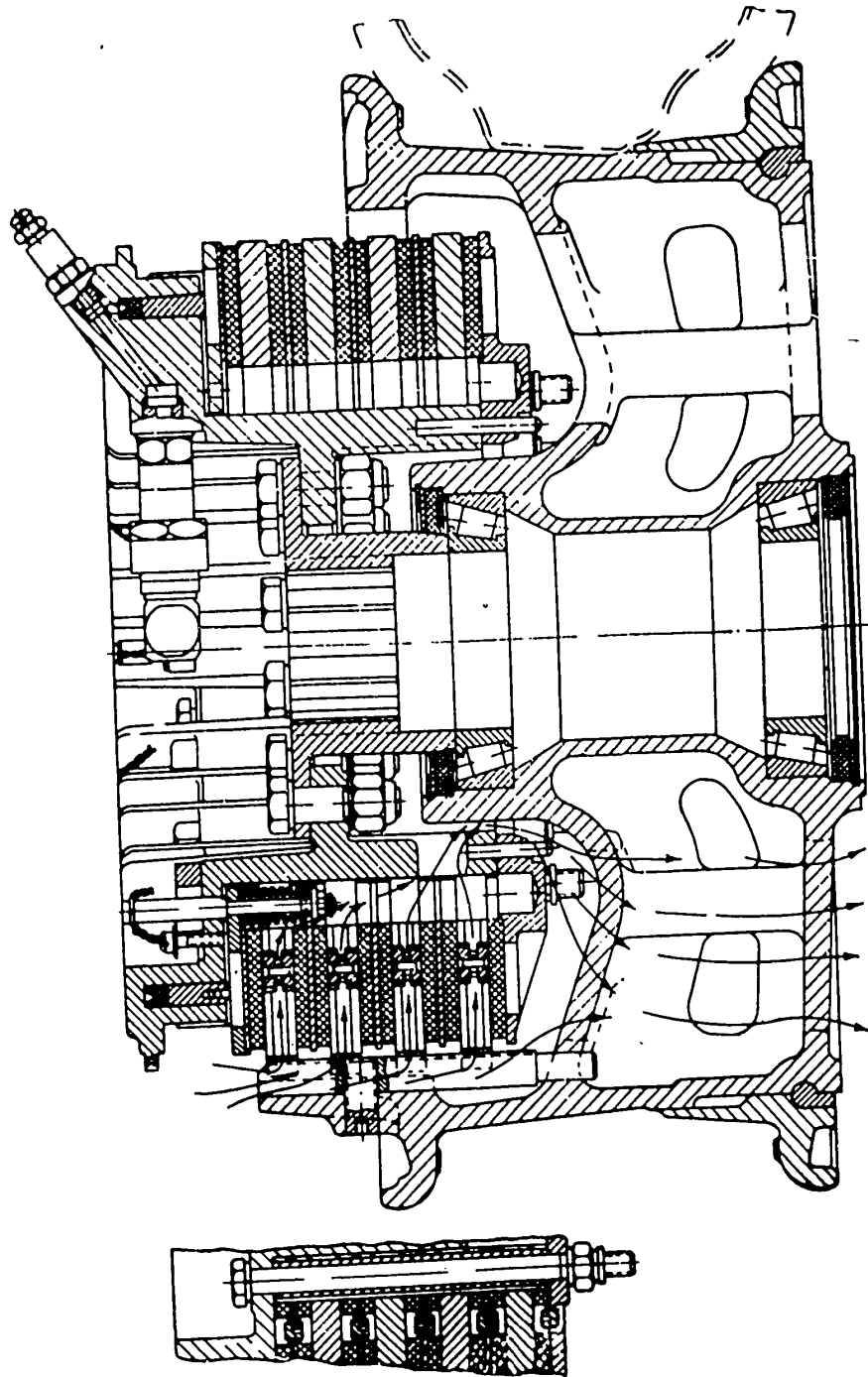
9

STAT

Fig.6 — Design of a Wheel with Multidisk Brakes

Having Thick Ventilated Disks

STAT

(Figs.5b and 6) and cooling the friction surface of the brakes by air.

Together with cermet coatings of the stationary disks, plastic frictional materials are now being used. Movable metal polished disks are plated with chromium to increase the resistance to wear and oxidation.

A multidisk brake with thick ventilated disks differs greatly from earlier multidisk brakes, both in design and operation of its parts. Revolving metal brake disks are thick solid plates, capable of accumulating a considerable amount of heat. Each revolving disk in' such a brake consists of separate segments, hinge-joined with special links (Fig.5a). Therefore, such disks do not warp or crack from heat-expansion even at quite high temperatures, while the reverse is true of solid unsegmented disks. A brake with segmented disks automatically provides complete adherence of the segments to the brake lining at the time of braking.

Segmented disks are fastened to the wheel with splines along the outer perimeter, so that they revolve with the wheel and have the axial motion required when applying and releasing the brake. These segmented disks are pressed against thin revolving disks covered with friction linings. The stationary disks are attached to the body of the brake by splines. Like the revolving disks, they have limited movement along the axle of the wheel.

The friction lining of the stationary disks consists of separate segments, forming ventilation channels in their interspaces through which air circulates (Fig.6) and cools the disks. An important result of this internal ventilation is that the efficiency of the brake is retained during prolonged braking. Moreover, dust from wear of the linings is entrained through the ventilation duct, providing better contact between disk surfaces and decreasing the amount of pressure necessary to achieve the required braking moment. The body of the brake is solidly fastened to the landing-gear support. The annular chamber contains a pressure piston which, under the action of hydraulic pressure, compresses the disk block and actuates the brake.

STAT

An advantage of multidisk brakes is that they are easily adapted to the special features of a given wheel, by changing the diameter or number of disks. Moreover, by decreasing or increasing the number of disks, the energy capacity of the existing brake can be changed within wide limits.

The power, service, and reliability of modern brakes depends to a great extent on the quality of friction linings.

The basic problem in improving the quality of brake linings lies in increasing their wear and friction stability factor in the braking process. At present the resistance of the lining to wear is a more important requirement than the stability of its friction coefficient (Bibl.2, 7, 9).

The problem of making friction materials more wear-resistant can be more easily solved only when the problem of improving temperature conditions in the operation of the brake pair is solved. Brake shoes require friction materials that are highly heat-resistant, and the selection of satisfactorily performing linings for disk brakes is complicated by the fact that the sliding speed of linings is not uniform at various distances from the revolving axle.

Effectiveness of braking relates to the length of the aircraft landing run and depends not only on the quality of the brakes but on the braking ability of the pilot. Best results are obtained if the brakes are so applied that the braking moment is close to maximum during the entire landing run. In other words, if the braking power of the wheel is coordinated with the ground traction of the wheel during the entire run, the wheel will roll without jamming.

It is difficult for a pilot to achieve such braking conditions since, at the time of landing, his attention is centered on other, more important, matters. To provide the most effective maximum braking, an automatic device is used which maintains the most advantageous braking conditions during landing. Use of this automatic device cuts the length of the run by 20-25% without risk of jamming which involves extensive tire damage and uncontrollable swaying.

STAT

Prospects for further increases in aircraft landing speeds create the problem of changing the principles of braking during landing. This requires the use of compound braking systems, i.e., auxiliary systems which supplement the existing brakes on landing. These auxiliaries are reverse-thrust, parachute, or rocket devices which absorb and dissipate a portion of the kinetic energy of the aircraft. Another possibility not to be overlooked is the use of braking cables on airfields. These would be set up on concrete landing strips, similar to those on the decks of aircraft carriers.

Operation of Frictional Brake Pairs

Absorption of kinetic energy by brake wheels can be subdivided into two phases: 1) generation of heat on friction surfaces by frictional pairs; 2) removal of heat from generating surfaces.

To achieve these phases in modern aircraft wheel brakes, which differ in their highly compressed over-all dimensions, requires the solution of several difficult engineering problems. Especially difficult is the removal of heat from the generating sliding surface of frictional brake pairs and the distribution of the corresponding heat flow along the elements of the wheel and brake structure.

The difficulty in dissipating heat from the friction surface of an aircraft frictional brake is that, in a very short interval of time (15-25 sec), it is necessary to divert a considerable amount of heat into the depth of the brake drum wall or brake disk (where it accumulates before dispersing) and into the depth of the brake linings. In the process of braking an aircraft during the landing run, such a tremendous amount of heat is passed to the generating brake surface that a heat flux forms, which is directed toward the depth of the brake drum and the brake shoes. Therefore, special measures are needed to provide prompt heat dissipation and to soften the shock . The intensity of heat flow passing from the brake shoe friction surface at the time of braking is determined by the amount of the kinetic energy of the aircraft that must be absorbed and displaced by a wheel of a given

13

STAT

size in a given interval of time.

The total kinetic energy of an aircraft at the instant it touches the ground is equal to

$$A_c = \frac{G_{pos} v_{pos}^2}{2g},$$ (1)

where G_{pos} = weight of aircraft on landing,

v_{pos} = landing speed,

g = acceleration of gravity.

Not all of the kinetic energy A_s is transmitted to the brake wheel of the air-craft. Part of the energy is expended in overcoming the aerodynamic resistance of the aircraft and the resistance of the wheels to rolling.

Part of the kinetic energy transmitted to the brakes of one wheel is determined by the formula

$$A_T = C_{sam} P_{st} v_{pos}^2,$$ (2)

where P_{st} = radial stationary stress on wheel,

C_{sam} = coefficient, considering the aerodynamic performance of the aircraft on landing, resistance of the wheels to rolling, traction of the engines during the landing run, etc.

Equation (2) indicates that the kinetic energy of the brake depends on the weight of the aircraft, landing speed, and landing performance.

The thrust of the engines, operating at minimum rpm on landing, causes a con-siderable increase in the amount of kinetic energy transferred to the wheel brake of the jet aircraft. For example, if the kinetic energy of engine thrust is disre-garded in the equation, then, in the case of a landing gear with a nose wheel, the coefficient is C_{sam} = 0.034. If the engine thrust is considered, then C_{sam} = 0.047. Therefore, the amount of kinetic energy absorbed by the wheel brake of a jet air-craft is increased 13% by the engine thrust during landing.

14

STAT

The propeller thrust during landings of aircraft with piston engines is so small that it can be neglected in calculating the kinetic energy transmitted to the brakes. Compared to piston-engine aircraft serving the same purpose, jet aircraft weigh more and have higher landing speeds. For example, fighter aircraft with piston engines, assigned to aerial combat in World War II, had a landing weight of $G_{pos} = 3500-4000$ kg and a landing speed of $V_{pos} = 150-165$ km/hr, while the newest jet fighters serving the same purpose have a landing weight of $G_{pos} = 6000$ kg and a landing speed of $V_{pos} = 250$ km/hr.

The kinetic energy transmitted to the wheel brake of a piston-engine fighter, having a landing gear with a tail wheel, equals $A_{tp} = 82,600$ kg, while the energy in the jet-fighter wheel is $A_{tp} = 550,000$ kg, or an increase of six or seven times.

The wheels of these two types of aircraft are almost the same because of considerations of compactness and minimum structural weight. The main wheels of the landing gear of the piston-engine fighter were 600×155 in size, and the wheels of the jet fighter were 660×200. Besides a slight difference in diameter and width, these wheels also differ in that the 660×200 wheel has two brakes instead of one. However, even in the 660×200 two-brake wheel of the jet fighter, the kinetic energy transferred to unit brake-friction area rose from 160 to 500 kg/cm^2. This is 3.12 times the energy passing to a single unit of brake friction surface of a 600×155 wheel of a piston-engine aircraft.

The same can be said about brake wheels for jet bombers which have tricycle landing gears with separate main wheels.

The magnitude of kinetic energy determines the size (weight) of the brake drum or brake disk. However, if the size of the brake drum is limited by its structure or over-all wheel dimensions, then the degree to which it is heated, its volumetric temperature, and brake horsepower depend on the magnitude of the kinetic energy: The given kinetic energy must be absorbed in a minimum interval of time, allowing for maximum wheel traction on the runway surface.

15

STAT

The greater the kinetic energy of a given size of brakes, the higher will be the temperature intensity of the friction couple.

At the most effective braking, which is correlated with maximum linear reduction in the landing run, the wheel brakes of the jet aircraft absorb the following horsepower

$$N_{\text{мах}} = 0{,}43 P_{\text{st}}\, \psi_{\text{к. мах}}\, \frac{\sqrt{K_{\text{заm}}}}{n_{\text{т}}}\, v_{\text{pos}}, \tag{3}$$

where K_{sam} = coefficient, considering the aerodynamic qualities of an aircraft on landing (in case of a tricycle landing gear, K_{sam} = 2.4),

$\psi_{\text{k max}}$ = maximum friction coefficient of a wheel tire against the ground (in the case of a dry concrete runway ψk max = 0.4);

n_{T} = number of brakes in the wheel,

P_{st} = radial stationary loading of the wheel,

V_{pos} = landing speed of the aircraft.

When landing an aircraft on a concrete airstrip, the required maximum brake horsepower of the brake wheel of a jet fighter equipped with bicycle landing gears and landing gear with an extra wheel, is 500-700 hp, while the brake horsepower of jet bombers is as high as 2500-3000 hp. Therefore, since the dimensions of jet aircraft wheel brakes have remained practically the same as those of piston aircraft, the increase in horsepower has resulted in a significant increase in power applied to 1 cm^2 of brake friction surface, i.e., an increase in friction horsepower.

Maximum effective braking can be achieved during the braking run if the following condition is observed, i.e., the change in the braking moment M_{T} of the wheel will follow the law of change in maximum tire traction. This condition can be expressed by the formula

$$M_{\text{т}} = \psi_{\text{к}} P_{\text{к}} r_{\text{к}}, \tag{4}$$

STAT

where M_T = wheel braking moment,

P_K = radial ground reaction, acting on the wheel,

ψ_K = friction coefficient of tire against ground.

From eq.(4) it is apparent that maximum braking of a wheel is possible on an airfield where the tire traction force ψ_K is greatest. Such airfields have concrete and metal runways.

Radial loading of the wheel at the time of the landing run correlates with the force of ground reaction P_k, which depends on the lifting force of the aircraft wing which, in turn, does not remain constant during the landing run. The force P_k and therefore r_k change their magnitude according to the aerodynamic characteristics of the wing. This force is proportional to the square of the forward speed of the aircraft. In maximum braking, there is the danger of jamming the wheel, which usually results in ruining the tire. Such jamming is caused by the fact that the magnitude of the braking moment does not correspond to the torque of the wheel.

To provide a change in the braking moment M_T during the braking process, according to the law of change of maximum tire traction $\psi_{k\ max}\ P_k$, an automatic device is installed into the brake-control system of the jet aircraft. This device maintains the magnitude of the braking moment close to the magnitude of the wheel torque during the landing brake run of the aircraft. As soon as there is danger of jamming or even partial slipping of the wheel, the automatic device immediately disengages the brake and releases the wheel. As soon as the jamming or partial slipping stops, the automatic device engages the brake again.

Such a system makes it possible not only to avoid jamming but to increase somewhat the braking efficiency of aircraft on landing, thus reducing the length of the landing run of the aircraft even more than in conventional braking. However, at automatic maximum braking, the brake wheels are subject to an additional thermal load. On maximum braking, the amount of kinetic energy transmitted to the brakes increases.

17   STAT

The thermal loading of brakes depends not only on the magnitude of the kinetic energy of the aircraft, but directly on its landing speed, since the slip speed of the brake pair depends on the landing speed and the relation to the brake friction radius r_T and the radius r_k of the rolling wheel:

$$v_{sk} = \frac{r_T}{r_k} v_{pos},\qquad (5)$$

while the temperature of the friction surface is proportional to the slip speed.

In modern brake wheels, the relation $\frac{r_T}{r_k}$ is within the limits of 0.4—0.5, while the landing speed of jet aircraft is within the limits 60–100 m/sec. Therefore, the slip speed of a modern brake pair will be within the limits of V_{sk} = 25–50 m/sec. This speed is more than twice as high as the slip speed of the brake pair of a piston aircraft.

In a modern jet fighter the thermal equivalent of kinetic energy transmitted to the brakes equals 1800 kcal. Every square centimeter of the generating surface of the brake wheel of such an aircraft gives off 350 kcal in 15–20 sec. Such a quantity of heat is enough to melt more than 1 kg of cast iron in a cupola furnace. Therefore, if the heat given off during the braking process on landing is not promptly removed from the generating surfaces of the friction pair, there is the danger of not only softening but even melting of the layers bordering the friction surfaces.

As seen in the diagram (Fig.7) in which the wear Δ of the friction material No. 22 is plotted as a function of the mean brake horsepower up to about 18 kgm/cm^2sec, the wear is almost directly proportional to the mean horsepower (Bibl.10). However, starting with a horsepower equal to 20 kgm/cm^2sec, the wear (which is already high) increases sharply. For example, the wear during one braking, at a mean horsepower of 25 kgm/cm^2sec, is six times greater than at a mean horsepower of 15 kgm/cm^2sec.

STAT

Increased wear of brake linings in brake wheels of jet aircraft also results from high temperatures forming in the friction pair. In earlier brake designs, the weight of the brake drum was so selec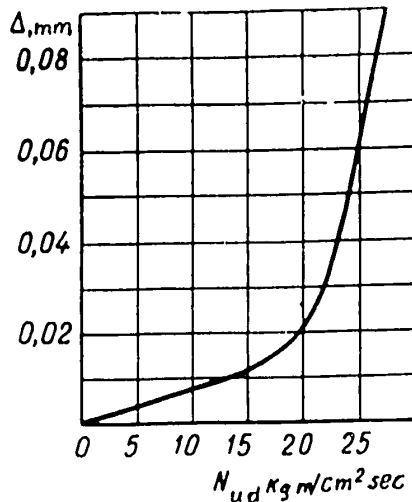ted that, in absorbing the given kinetic energy of the aircraft, its volumetric temperature would not exceed 300–350°C. Nowadays, mainly for considerations of providing minimum over-all wheel dimensions, the sizes and weights of brake drums are so selected that, in absorbing kinetic energy, the drum heats up to 400–450°C. The friction surface temperature can be two to three times more than the volumetric temperature.

Fig.7 – Linear Wear Δ of the Friction Material No. 22 as a Function of the Mean Brake Horsepower

We made laboratory tests on the heating process in an actual brake drum during braking on an inertia stand. Brakings were performed at the peripheral speed of V_{okr} = 173 km/hr at a pressure in the brake chamber of p_T = 25 kg/cm^2 and a kinetic energy of A_T = 158,000 kg.

Several brake drums were tested on a 660 × 160 wheel of the type used on fighter aircraft.

Ten thermocouples connected with an oscillograph system were placed into the wall of each drum, tested at different depths from the friction surface.

The temperature distribution along the cross sections and their change according to braking time for a steel drum C = 45, measured and recorded on the oscillograph, is shown in Fig.8. The slope of the curves for a cast iron drum was analogous.

The curves in Fig.8 show that a maximum temperature equal to 900–1000°C devel-

19

STAT

ops in the braking surface of drum-wall layers located at a depth of 0.5-1 mm from

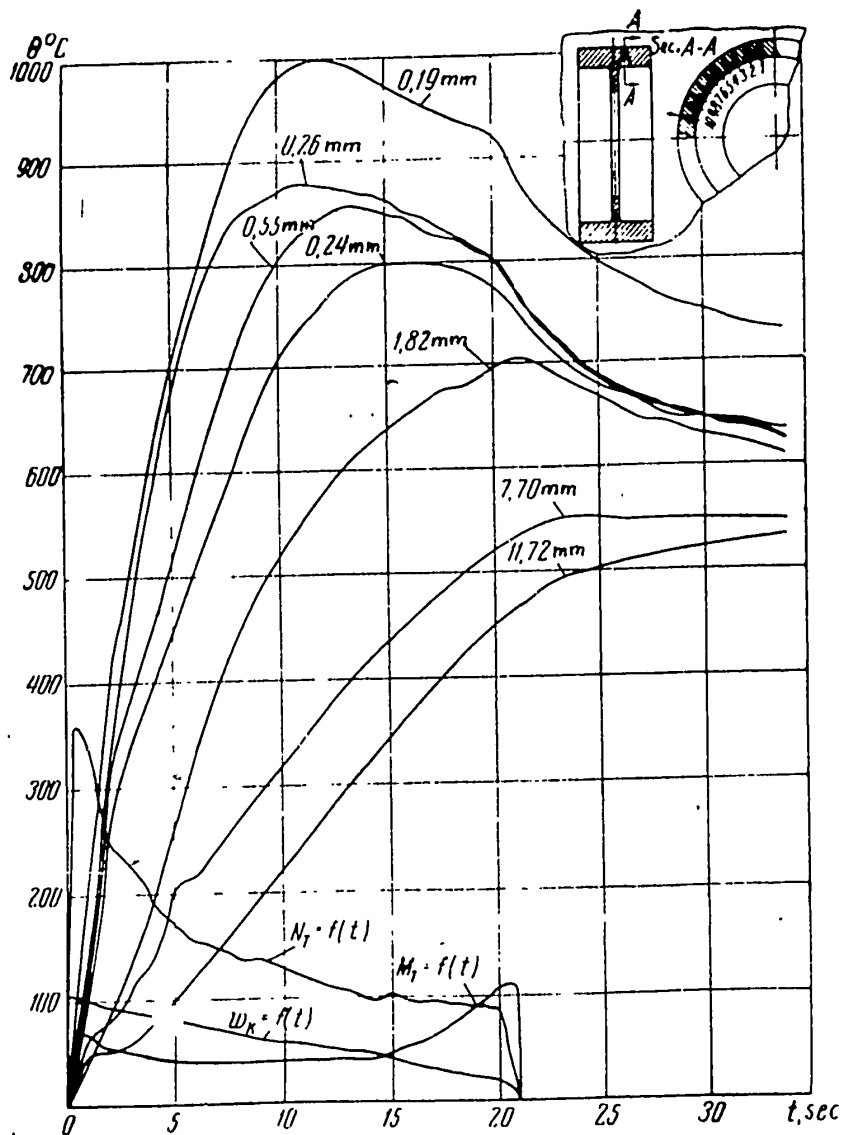the generating friction surface. This temperature prevails at about the middle of

Fig.8 – Temperature Distribution Curve for a Steel Brake Casing,
as a Function of Thickness and Braking Time t.

the braking process, and lasts 3-5 sec, and then decreases. The temperature of the

brake drum at any given moment decreases toward points more distant from the fric-

20

STAT

tion surface. The maximum temperatures along the thickness of the drum were of the following magnitudes:

Distance from friction surface, in mm	0.19	0.84	0.82	7.5
Magnitude of maximum temperature Θ, in °C	1000	800	700	550

Present requirements for brake wheels in jet aviation are such that it is advisable not to increase the over-all dimensions of the wheel and brake, or at least to leave them as they were in piston-engine aircraft. Keeping the same over-all wheel dimensions, while increasing the radial loading, specific work, and slip speed, makes the operation of frictional brake pair quite difficult under such conditions. A solution to the problem of manufacturing and selecting materials for frictional brake pairs and designing the most efficient brake is possible only on the basis of very thorough studies of the physical processes during friction and wear.

21   STAT

PROCESSES OCCURRING DURING FRICTION AND WEAR, AND THE EFFECT

ON THEM

Types of Friction

Friction is the resistance generated when two touching bodies change relative positions in their plane of contact. A resistance force directed opposite to the displacing force is called friction force.

Friction force acts in the common contact plane toward the surface of the interacting bodies and is always directed to the side opposite to the relative rate of change in positions (for each of the bodies). Like all forces it is correlated with a change in the contour of the bodies — not a macroscopic change but a microscopic one which is localized in the surface layers.

The following are differentiated by their exvent of displacement and its dependence on the applied force: a) kinetic friction; b) incomplete friction of rest; c) complete friction of rest, generally known simply as friction of rest or static friction.

Kinetic friction is correlated with very large irreversible relative displacements whose magnitudes do not depend on the applied force. The latter, in this case, is counteracted by the kinetic friction when movement is uniform.

Incomplete friction of rest is correlated with very small partially reversible displacements whose magnitudes are proportional to the applied force. The degree of displacement correlated with the incomplete friction is known as preliminary displacement. It is usually difficult to detect preliminary displacement visually,

22

STAT

since, it is measured in micromillimeters. In the case of preliminary displacement, the applied force is counterbalanced by the incomplete friction, and the body is at rest. Incomplete friction depends on the applied force and changes with increases in the latter, from zero to some maximum value, during which it becomes known as static friction. In this case, preliminary displacement develops into relative.

Friction is differentiated by kinetic characteristics: sliding, rotating, and rolling.

The first of these takes place when the same nominal contact surface of one body progressively changes its position along the surface of the other body. The second takes place when the same nominal contact surface of one body is displaced along the surface of the other body, rotating about an axis perpendicular to these surfaces. The third takes place when one body changes its position along the other under the action of the moment of force during which new elements of the nominal surface successively come into contact.

The study of friction has not yet sufficiently progressed since little is known about the surface properties of bodies.

The following types of friction are differentiated by the condition of the rubbing surfaces of a body, with respect to lubrication:

a) Pure friction, forming on rubbing surfaces when there is total absence of any contaminating substance (liquids and gases in an adsorbed state). In practice, pure friction is very difficult to achieve and can be accomplished only in vacuum.

b) Dry friction, forming when there is no lubrication or impurities between the surfaces. Often this type is called friction of unlubricated surfaces (this term is not recommended).

c) Boundary friction (boundary lubrication), in which the surfaces are separated by such a thin film of lubricant (0.1μ or less), that it has special properties which differ from the volumetric properties of lubrication but which are dependent on the nature and state of the rubbing surfaces. In this case the ordinary hy-

23

STAT

drodynamic equations for viscous fluids do not apply. The boundary layer has a flaky structure. The more active molecules are distributed closer to the metal; they attach themselves to the metal surface with their active ends and form a nap-like surface of the lubricant molecules.

d) Fluid friction (viscous lubrication) takes place when the surfaces are completely separated by a fluid film and the outside pressure, because of a specific type of clearance, is transferred to a viscous film of moving fluid.

e) Semidry friction is a combination of boundary and dry friction.

f) Semifluid friction (incomplete lubrication) is a combination of fluid and boundary lubrication or of fluid and dry friction.

The coefficient of friction of rest is the ratio of the maximum force expended to overcome the contact produced by two touching bodies being brought out of a state of rest, to the load compressing the bodies in contact.

The coefficient of sliding friction is the ratio of force expended to overcome the resistance of the relative displacement of two bodies (beyond the limits of preliminary displacement) to the load compressing the bodies in contact. The coefficient of rolling resistance is the ratio of force expended on rolling and applied to the rotating axis, to the load compressing the bodies in contact.

The coefficient of rolling friction is known as the coefficient of proportionality in Coulomb's equation:

$$F_K = k \frac{P}{r} \; .$$

(6)

It has a linear dimension since, according to modern concepts, it is characterized by a semichord of an arc of warping.

The coefficient of traction of a driving or wheel brake is the ratio of the force generated in the contact plane of the wheel with the support surface, to the force compressing the bodies in contact.

24

STAT

Surface Contacts

The contact of two hard surfaces, as a result of their roughness and waviness, is always discrete.

Microscopic protrusions and depressions on the body and the lack of parallelism of the two surfaces prevent close contact. The height of protrusions on even a highly polished optical surface is not less than 100 Å. Therefore, two superimposed surfaces come in contact only at the points of protrusion; such contact area of these protrusions comprises an insignificant part of the entire surface area and grows with an increase in pressure. These protrusions are concentrated in areas having surface waviness.

The area of each protrusion depends on the microgeometry of the surface and the dimensions of the elements (crystals) comprising the surface. It varies from one micromillimeter to $30 - 50\,\mu$ (with a height of the unevenness up to 80μ).

As the load increases, each spot grows in diameter, but any later area growth is mainly the result of an increased number of contact spots.

In this connection, the areas are differentiated as follows:

a) Nominal (geometric) area of contact, specified by the outside dimensions of the bodies in contact.

b) Contour area of contact, or the area formed by volumetric warping of the entire body on which actual areas of contact are found (the contour area S_k depends on the load).

c) The actual physical contact area S_f, or the total of all actual small areas touching the bodies.

The latter is also a function of loading and changes within wide limits - at high temperatures which form in the aircraft brake pair the ratio of actual area of contact to the nominal area of contact reaches $0.1 - 0.2$.

The dispersity of real contact is characterized by the closeness of the contact, which represents the number of contact points per unit of contour area or per unit of

25

STAT

nominal area.

The closeness of contact in the first case is proportional to the specific contour pressure.

To illustrate the point, an uneven surface with spheric waviness is represented diagramatically in Fig.9. The actual contact spots are represented by encircled points - the contour area, the product ab - nominal area.

In the most simplified concept it is assumed that the contact has a flexible na-
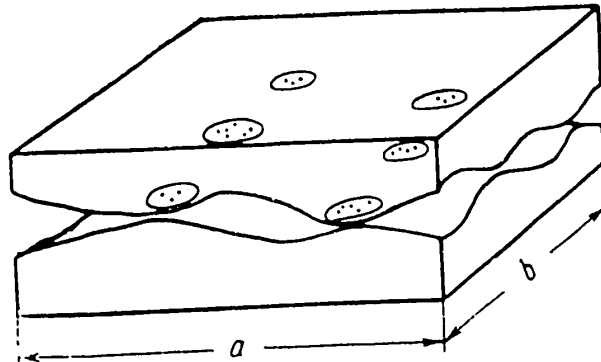
Fig.9 - Diagram Representing Uneven Surfaces with Spheric Waviness

ture, i.e., at all contact points the stress is uniformly equal to the hardness of the material. Naturally, such a concept should lead to the conclusion that the deformation in contact areas has an irreversible nature. In studying contact conditions of various materials, experiments showed that these concepts are correct only in particular cases.

It has been established that the total number of contact spots and the growth in size of each is correlated with an increase in load. However, the size of a separate spot grows only in the area of small loads, when a considerable part of the spot contacts elastically (Bibl.11).

With an increase in load, the spots are under various stresses and therefore the mean actual specific pressure grows. Only at high enough a load does the specif-

STAT

ic pressure tend toward the maximum value, whose magnitude is not determined by hardness. In some cases it constitutes half of it, in other cases two or three times the hardness. This is obvious since hardness represents the index characteristic which is connected to a great extent with the form of the penetrated indenter or penetrator and the tension of the material which it penetrates.

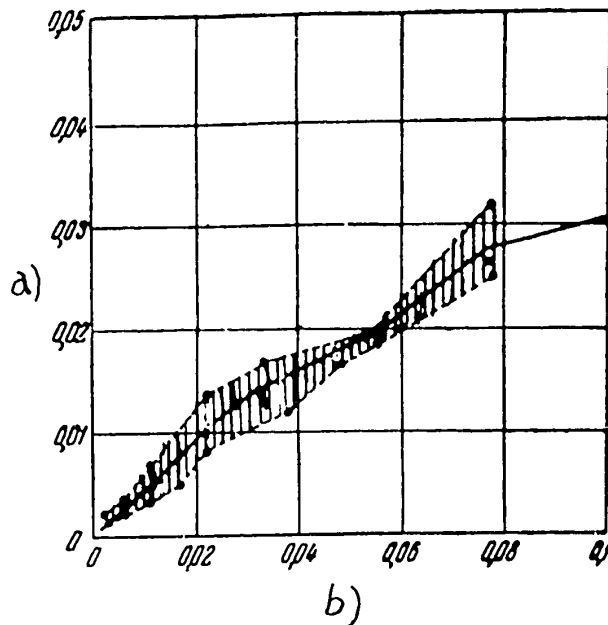The fact that contacting has a resilient, pliable nature is quite important;

Fig.10 — Actual Contact area versus Load for Silver Chloride

a) Actual area of contact in contour units; b) Specific pressure on contour area in hardness units;

i.e., in removing the load, a large share (30 to 70%) of the contact spots disappears because of the resiliency of the protrusions, the semispace, and because of the fact that the individual protrusions are loaded differently due to unevenness and waviness.

The actual area of contact of the friction material Ts-4-52 with a glass prism,

27

STAT

formed by disrupting the entire inside reflection, is shown in Fig.11.

The contact spots have an insignificant magnitude - from 5×10^{-3} to 1.5×10^{-2} cm in diameter.

Fig.11 - Actual Area of Contact (Dark Spots) of the Friction Material Ts-4-52 with the Surface of a Glass Prism: Specific Pressure P_{ud} 15 kg/cm^2; Diameter of Specimen 5 mm; Elliptic Contact Due to Distortion of Size along the

Ordinate $y = y_o \cos 45°$

All data given are for fixed contacts. In the case of sliding, the data are applicable to the speeds which result in temperatures that change the mechanical prop-

STAT .

erties of the contacts. Essentially the same phenomenon takes place, but the lowering of mechanical strength leads to an increase in the actual area of contact and thus to smaller mean actual specific pressures.

The Physical Nature of Friction

At present, friction is believed to have a dual nature. Atoms on the surface of a hard body are subject to special conditions, since their forces of interaction with atoms inside the body are considerably greater than with those of the outer medium. The interacting atoms of the two surfaces, when drawn together, exert a mutual attraction. Molecular friction forces are formed when there is tangential shifting of contiguous surfaces, due to the broken formation of the field.

B.V.Deryagin worked out the theory of this phenomenon in detail, and it was further developed by the research of V.S.Shchedrov.

Molecular interaction appears at quite small distances, comparable to the size of the atoms. In view of the fact that the roughness of the real surface exceeds by many times the roughness due to its atomic structure, molecular interaction in some points is connected with mechanical interaction and in other points is due to a reciprocal penetration of the protrusions on opposite surfaces. Reciprocal penetration takes place in separate contact points due to the heterogeneous hardness of the surface elements or due to the shape of protrusions on separate parts of the body penetrating into the counterbody. Therefore, surface roughness seems to form under loading, and sometimes, before loading, the reciprocal traction of two completely smooth surfaces may be greater than that of two uneven surfaces.

The diverse nature of reciprocal deformation in contacting members takes place during tangential displacement, which depends on the properties of the body and depth of deformation. If the deformation is not connected with destruction of the material which participates in the mechanical contacts formed, then this idealized case of interaction is actually friction in its pure state. In fact, this is the most favora-

29

STAT

ble type of interaction, in which tangential resistance forms without wear. On the other hand, if during tangential displacement complete destruction of the material participating in the contacts takes place, then this phenomenon of cutting, dispersion of material, and tangential forces contributing to the destruction of materials should actually be viewed not as friction, but forces of cutting, polishing, and others.

Generally, tangential forces are the sum of two forces - properly the friction force and the destruction force.

Our problem is to create such interaction conditions and select materials under which the ratio of these two forces would be highest, since it is constantly required to achieve conditions providing for minimum wear.

As for the friction force itself, in some cases attempts are made to increase it - friction pairs; in other cases, to decrease it - antifriction pairs.

The friction force can be determined by totaling the elementary tangential resistances which form at separate contact points, i.e.,

$$T = \sum_{1}^{n} \tau.$$ (7)

Since the number of contact points is proportional to the actual contact area, so that

$$T = \tau \cdot S_f,$$ (8)

where τ is the specific friction force.

The specific friction force, with a known approximation, may be expressed by the following binomial:

$$\tau = \alpha + \beta q,$$ (9)

where q is the actual specific pressure on contact.

30

STAT

Accordingly,

$$T = \alpha S_f + \beta N, \tag{10}$$

and the friction coefficient

$$f = \frac{\alpha S_f}{N} + \beta. \tag{11}$$

The actual area of contact in the case of a plastic contact is directly proportional to the load, i.e.,

$$S_f = K_1 P. \tag{12}$$

where $K_1 = \dfrac{1}{\sigma} = \dfrac{1}{H_B}$.

In the case of an elastic contact

$$S_f = K_2 P^x, \tag{13}$$

where the exponent of x may change within the limits of 0.5 to 1. For example, in the case of contact of a cylinder with a surface $x = \frac{1}{2}$, it follows

$$K_2 = L \cdot r^{1/2} \cdot 1{,}6 \cdot \left(\frac{1 - \mu_1^2}{E_1} + \frac{1 - \mu_2^2}{E_2} \right)^{1/2},$$

where P = load on the cylinder;

      r = radius of the cylinder;

      L = length of the cylinder.

In the case of contact of a sphere with a surface

$$S_f = K_3 P^x, \tag{14}$$

where x = 2/3.

$$K_3 = r^{1/3} \cdot 2{,}6 \left(\frac{1 - \mu_1^2}{E_1} + \frac{1 - \mu_2^2}{E_2} \right),$$

31

STAT

where r = radius of the sphere;

P = load on the sphere.

When an uneven surface touches a smooth one, we have

$$S_f = \sqrt{\frac{N\gamma_r L}{2K_{zh}}} \, . \tag{15}$$

According to this formula, the smoother the surface and the smaller the elasticity modulus of the material, the larger will be the friction coefficient.

The coefficient of rigidity is not an invariant for the given material but depends on the radius of the contact spot and, in first approximation, may be expressed by Bussine's formula, useful in a given case of surface deformation, in the load is uniformly distributed over a section of the radius r

$$K_{zh} = \frac{E}{2r\,(1 - \mu^2)} \, . \tag{16}$$

Equations (11) and (12), under conditions of plastic deformation, will yield

$$f = \frac{\alpha}{H} + \beta \, . \tag{17}$$

Because of the dual nature of friction, α and β depend on the mechanical properties of the material as well as on the molecular characteristics.

Applicable to mechanical interaction, α grows proportionally with the increased resistance of the material to shear (τ).

From the above it is clear that the material having the highest ratio $\frac{\tau}{H}$ at elevated temperatures corresponding to the friction temperatures, will have the largest friction coefficient.

Discontinuity in Friction

Sliding friction is often accompanied by skipping displacement of friction sur-

32

faces. During this, torsional vibrations, jerking, and other phenomena may appear which disrupt the normal operation of the friction unit.

Skipping during friction consists of relaxation mechanical vibrations which appear when there is considerable variable friction and a significant difference between the inertia force and the restoring force.

In the same case, when the variable friction is small and hardly disrupts the balance between inertia forces and restoring forces, vibrations appear in the system which in their nature are close to sinusoidal oscillations.

There are several theories to explain this phenomenon. According to one of the theories (Bibl.13) a decrease in friction force and an increase in speed are the conditions which cause self-oscillations in the system.

If the principal diagram of the friction system is pictured as consisting of the load A, securely fixed by the spring K and placed on the conveyor belt B moving at a speed v_0 (Fig.12), and assuming that the curve "friction force - speed" has the form represented in Fig.13, then if the speed of the belt B lies on the descending branch of this curve, i.e., if $v_0 < v_{min}$, the state of equilibrium in the system ($x = a$, $v_1 = 0$) will be unstable.

The vibrations will take place in the following manner:

As long as the belt B and the load A (Fig.12) move together, the increased elasticity of the spring K is constantly counterbalanced by the continuously growing friction force of rest F_{st}. This process is represented in Fig.13 by the straight line AB.

The moment the elastic force of the spring becomes equal to the maximum friction of rest F_{st}, a jump in speed with the value $v = 0$ to $v = v_{sk}$ will take place. This process will be expressed by the straight line BC, parallel to the abscissa.

Further, starting with the point C, the change in speed as well as in friction will take place continuously up to the minimum value of the sliding friction F_{min} and of the speed v_{min}. This period corresponds to the section CD.

STAT

At the instant the system is at the point D, there will be another jump in speed with an invariable friction force equal to F_{min} and a speed v_{min} to $v = 0$, i.e., up to the state of relative rest of the load A and the belt B, when the load will be
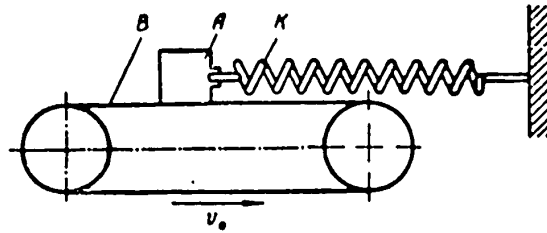

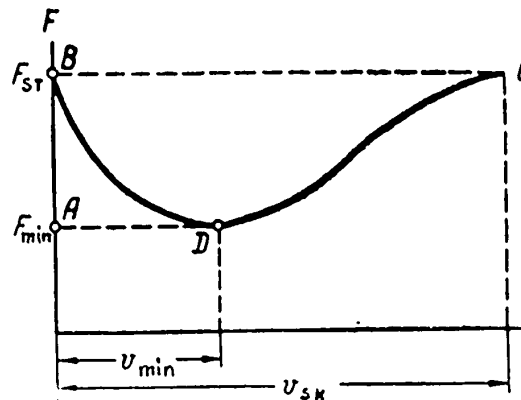Fig.12 - Mechanical Model of a Frictional Pair Having Elasticity

Fig.13 - Diagram "Friction Force F versus Speed v" (Kaydanovskiy,Khaykin)

picked up by the belt. This period is represented by the straight line DA (broken line).

Subsequently, the process will be repeated. Therefore, the skipping process is divided into four phases. In the first two phases represented by the lines AB and CD in Fig.13, the system moves continuously with a continuous change in speed and friction force. These phases are characterized by the movement of the contained system, which is determined mainly by the elastic force and friction force since the elastic forces in these phases are much greater than the inertia forces.

34

In the two other phases, which are represented by the broken lines BC and DA in Fig.13, the system moves in jumps with a sharp change in speed and a constant friction force since, for the sake of simplicity, consideration of changes in spring elasticity have been disregarded.

In these two phases inertia forces and friction forces mainly determine the movement.

However, this theory is unable to explain certain facts characterizing the skipping movement of the rubbing surfaces. For example, it is impossible to explain why the magnitude of skipping at the start of the movement is greater than the magnitudes of all the subsequent skippings, or why in zones of small speeds where there is also friction skipping, the experimental data show that the friction in these zones (at v up to 1 - 2 m/sec) in some cases does not decrease with increasing speed but actually increases.

Another theory (Bibl.12) explains the appearance of skipping during friction by the growth of the coefficient of friction of rest, which depends on the duration of the fixed contact.

As is known, the contact of two bodies does not take place along all their area, but only at individual points. As a result, the load is distributed only over the area of the contact points, which causes high specific pressures there. This, in turn, results in reciprocal surface penetration leading to plastic flow of the material (Bibl.14). The nature of the contact is viscoelastic during which time the strengthening of the contact takes place in time according to the law of damping.

If we examine the same principal diagram of a friction system studied earlier (Fig.12), then the skipping of friction forces can be explained in the following manner: While the load A and the belt B move together and the stretching of the spring increases continuously, the increase in spring elasticity will be constantly counterbalanced by the friction force of rest, whose magnitude will increase continuously because of the duration of the fixed contact.

STAT

Since the resistance of springs increases, in time, faster (Fig.14, straight line Al) than the friction increment from the duration of the contact (curve A-4-1), a disruption (Bibl.15) will take place at some period of time. At this instant, the friction drops sharply in magnitude, which is determined by the equation

$$\Delta F = F_0 \left[\left(e^{-\beta t_2} - e^{-\beta t_1} \right) \left(1 - \frac{F_\infty}{F_0} \right) \right], \qquad (18)$$

where $t_2 - t_1$ is the duration of time of the fixed contact (on the diagram, the sector 1K) and β is a constant characterizing the mechanical properties of the material.
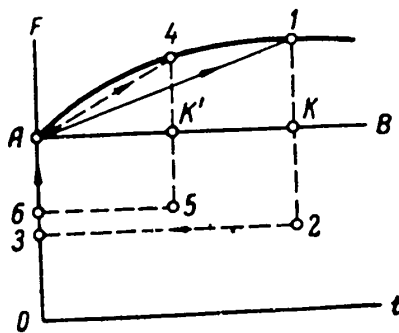
Fig.14 - Diagram "Friction F versus Time t" (Ishlinskiy, Kragel'skiy)

The load will move in the opposite direction. Under the influence of the inertia force, the load will pass through a state of equilibrium, after which the relative movement of the load and belt will stop, and the load will again be picked up by the belt B (Fig.12), and will then remain fixed for a while relative to the belt.

During this time, the friction force of rest again increases. This again causes skipping which, in magnitude, will be somewhat smaller than the first skipping if the duration of fixed contact was shorter.

It is quite clear that, at an increase in speed of motion of the belt B, the duration of the fixed contact decreases, which should lead to changes in magnitude and in the nature of the skipping. This is confirmed by experiments.

Actually, as the speed increases the magnitude of skipping decreases, the number of skippings in a unit of time increases, and finally the skippings become so small and frequent that it is impossible to measure them by instrument.

STAT

Thus, it may be stated, for all practical purposes, that skipping disappears when a certain speed is reached. The change in friction force, as a function of time, is shown in the coordinates "force – time" in Fig.14. The process of the first skipping is characterized by the following group of points A – 1 – K – 2 – 3 – A. The second skipping correspondingly is A – 4 – K' – 5 – 6 – A.

The velocity, at which the disappearance of skipping is observed, is expressed, according to the third theory, by the following equation:

$$v = \frac{2\delta \, (F_m - F_1)}{K_{zh}}, \qquad (19)$$

where K_{zh} is the rigidity of the system;

δ is a constant, depending on the surface properties.

Therefore, the zone in which the skipping of friction forces is observed will be limited by the expression

$$v_1 < v. \qquad \cdot (20)$$

Equation (19) indicates that the properties of rubbing surfaces have a considerable influence on the magnitude of relaxed vibration zones, i.e., the magnitude δ and the rigidity of the friction system K_{zh} itself. Therefore, it is obvious that it is impossible to study the formation of skipping on the rubbing pair separately from the friction system itself.

The third theory explains the appearance of skipping in friction forces by processes which take place during relative rest of the rubbing surfaces, and does not exclude the first theory, which explains the skipping in terms of kinetic characteristics of the friction force.

These two theories combined give a clearer picture of the mechanics of skipping and the causative factors.

The grapho-analytic method, using friction characteristics resulting from an ex-

STAT

periment (Bibl.16), may be applied to calculate the relaxation oscillations which develop in elastic friction systems.

Relaxation oscillations can be controlled by increasing the rigidity of the system and raising the relative sliding speeds, or by selecting frictional pairs whose friction coefficient does not decrease with increasing speed and does not significantly increase with greater duration of the fixed contact.

Dependence of the Friction Coefficient on Sliding Speed

The force necessary for destroying interpenetrated elements of two touching surfaces depends on the rate of the applied load and the sliding speed, which is the result of contact viscosity. On the other hand, viscosity causes an artificial smoothening of the roughnesses of the body surface which had been subject to impact. In connection with the above, during an elasto-plastic contact, the magnitude of the force of friction with increased sliding speed passes a maximum.

Heating the surface layers results in a change of their mechanical properties, a decrease in the coefficient of rigidity, an increase in contact area and, simultaneously, in a decrease in shear strength.

It is also necessary to consider that, as a result of the discrete nature of the interaction of two touching bodies, dissipation of energy takes place as a result of oscillations, and plastic deformation is accompanied by generation of heat which is likewise dissipated. Therefore, sliding friction is always accompanied by oscillation and heat generation.

The magnitude of the friction coefficient at increased relative sliding speed generally passes a maximum.

The dependence of the friction coefficient f on the sliding speed v is expressed by the following formula:

$$f = (a + bv)\, e^{cv} + d, \tag{21}$$

where a, b, c, d are constants, depending on the nature of the bodies and the

38

STAT

pressure.

The position of the maximum on the curve depends on the pressure of the rubbing pair and on the hardness of each of the rubbing bodies: the greater the pressure and the harder the body surface, the closer will be the maximum to the origin of the co-ordinates.

The conditions of interaction and surface destruction which cause changes in the surface and friction coefficient vary in accordance with the sliding speed.

Therefore, the friction coefficient which depends on various external conditions may change to a considerable extent.

During this, the following are generally applicable rules:

1. When the contact load and rigidity are increased, the maximum shifts to the origin of the coordinates. Therefore, in some cases there is only the descending branch of the curve.

2. The friction coefficient passes a maximum, depending on the speed.

3. In some materials, a significant change in friction surfaces takes place at high sliding speeds, due to the generation of a great quantity of heat which leads to a deviation from the indicated rule (increase in friction coefficient at high sliding speeds).

Effect of the Number of Elements of a Friction Surface on the Magnitude of the Friction Coefficients

From the generalized friction rule it follows that an increase in the actual area of contact, with the same force acting on the contact, leads to an increase in the friction coefficient. A practical means of increasing the actual area of contact is to improve the conditions of osculation of friction surfaces by improving one of the friction surfaces of the individual elements, loaded independently of the other.

In all cases, such constructions lead to an increase in the actual area of contact since, as a result of roughness and waviness, the actual area of contact, at constant load and increase in nominal surface size, increases very little. Two sur-

39

STAT

faces, each loaded with the force P, have a common contact area more than twice the size of a larger surface loaded with the force 2P. This naturally is due to the fact that the contact area, according to Hertz does not increase proportionally to the
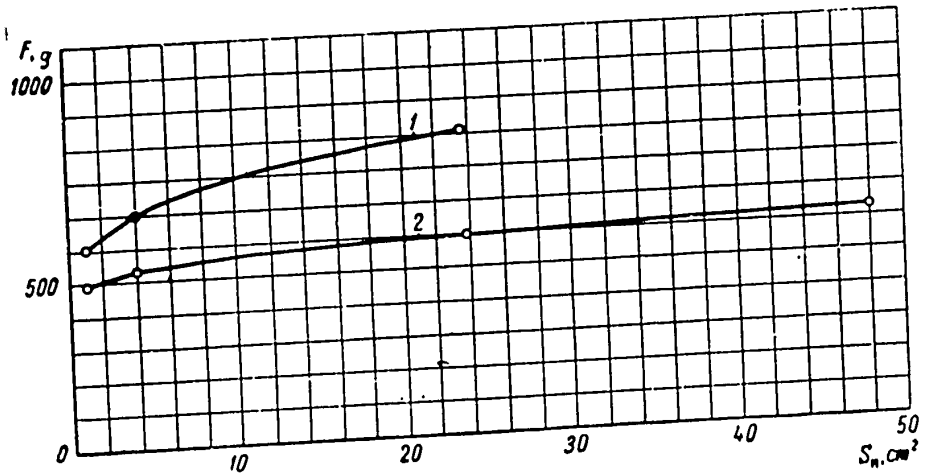

Fig.15 — Friction Force F as a Function of the Size of the Nominal

Surface S_n, with a General Load of 5 kg.

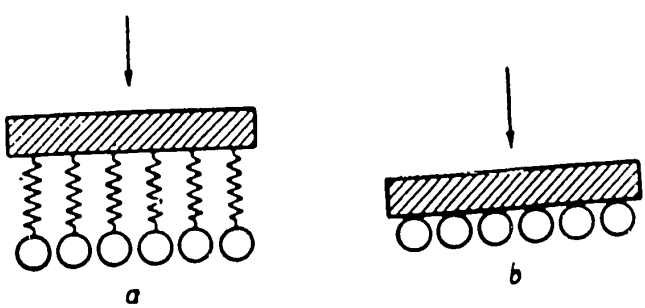1 – Leather – steel; 2 – Felt – steel

Fig.16 — Diagram of a Core Model

load but depends on a load with a ratio of 2/3 for the contact of a sphere with a plane, and on a load with a ratio of 1/2 for the contact of a cylinder with a plane. In Fig.15 experimental data are presented for characterizing the dependence of

40

STAT

the friction force on the size of the nominal surface, during friction of leather on steel and felt on steel.

We constructed a special mechanical model of the surface (Fig.16) to illustrate this case.

Value of Friction Coefficient for Various Surface Arrangements with Different Cleansing

(Materials: Balls – Steel ShKh15, Plate – Steel KhNM)

Type of Surface	Arrangement a	Arrangement b
Surface, thoroughly polished and cleaned (dry friction)	0.70	0.38
Same surface, slightly lubricated	0.24	0.20
Rough surface, cleaned (dry friction) . . .	0.25	0.21
Rough surface, slightly lubricated.	0.17	0.17

The contact surface, composed of 50 balls each of which is loaded by a separate spring (Fig.16a), results in a higher value of the friction coefficient than the same balls loaded by an ordinary plate (Fig.16b).

When neglecting the effect of the roughness of the balls, application of Gert's formula for each ball loaded by an ordinary plate will give the following for a complex of balls:

$$F = \alpha\, S_f + \beta P = C_{sp}\, n\, (v_1 + v_2)^{2/3} \sqrt[3]{\left(\frac{P}{n}\right)^2 r^2}\; \alpha + \beta P. \tag{22}$$

Here, n is the number of balls and P the general load, in kg:

$$C_{sp} = 2,6; \quad v_1 = \frac{1 - \mu^2}{E_1}; \quad v_2 = \frac{1 - \mu^2}{E_2}.$$

41

STAT

As this formula shows, with an increase in the number of balls one of the terms, expressing the friction coefficient, will increase proportionally to the cubic root of the number of balls.

These statements explain the effect of the increased rigidity of the frictional coatings and the sizes of the component elements on the magnitude of the friction.

As the Table shows, an increase in the friction coefficient takes place only on smooth surfaces without lubrication; this is natural since, in the presence of lubrication the coefficient α_{kn} is very small so that the size of the correction is also small.

By eq.(22), the friction coefficient is expressed in the following manner:

$$ f = C_{sp} n^{i/s} r^{i/s} P^{-i/s} + \beta_{kn}. \qquad (23) $$

Each surface of a real body, as a result of the presence of waviness, may be modeled as a group of balls or cylindrical segments.

Then, the nominal area is expressed as follows:

$$ S_n = (2rn)^2, \qquad (24) $$

from which the magnitude of the friction coefficient is determined:

$$ f = \frac{C_{sp} \eta^{i/s} S_n^{i/s}}{P^{i/s}} + \beta_{kn}. \qquad (25) $$

Therefore, the friction coefficient depends on the nominal surface size with a ratio of 1/6. The curves shown in Fig.15 correspond to this ratio.

The above circumstance explains the phenomenon that, at an increase in the number of independently acting elements distributed in the same nominal area, the friction force increases.

Physical Nature of the Phenomenon of Wear

Wear is the gradual undesirable change in the sizes of machine parts which takes

42

STAT

place under the action of the force of friction.

The phenomenon of wear is extremely diversified. This diversity is due to various combinations of physical-mechanical properties of rubbing bodies and exterior conditions in the friction unit, of which the most essential are the following:

Nature of loading: static or shock. Conditions: sliding speed, specific pressure, ratio of friction surface to contour area of contact part, temperature in the friction unit, surrounding medium. Type of motion: sliding or rolling, back and forth, or simply forward.

Despite the innumerable possible combinations of these factors, science now has some general laws with respect to wear which make it possible to control the processes of wear. There are at least two of these laws in existence.

The first law, applicable to mechanical interaction, is important for providing mutual penetration of contacting bodies when the surface layers maintain their contact with the main mass of material. This may be accomplished either by decreasing the magnitude of mutual penetration for quite rigid materials (principle of maximum rigidity) or by using soft materials which, despite considerable penetration, are capable of repeated deformation without losing contact with the main mass of material (principle of maximum pliability).

The second law, applicable to molecular interaction, is essential for localizing destruction contacts in the proximity zone of the place of molecular interaction.

During friction, the material is subject to the simultaneous action of compressing and displacing stresses. The material here becomes more plastic and deforms more readily. Heating of the surface layers also contributes to this: the material flows in the sliding direction, which results in an enlargement of the general contact area and a drop in the actual specific pressure. The contacting spots gradually shift, making the surface smooth; the actual specific pressure decreases still more.

The above has to do with the presence of run-in rubbing surfaces. Run-in surfaces differ from not run-in bodies in that contact in the former is made by very

STAT

small contact spots which are distributed more uniformly in the contact zones of the rubbing surfaces.

During sliding, destruction of the parts of the contacting spots inevitably takes place.

The numerical intensity of material wear is the ratio of the disintegrated spots n_p to the total number of spots n_Σ:

$$J_{ch} = \frac{n_p}{n_\Sigma} . \tag{26}$$

If we introduce the concept of compactness of a sliding contact, which represents the number of contact spots formed in a unit area (1 cm^2) during the sliding of one surface relative to the other, and if we consider that during destruction of each spot Δg_M of material is carried away, then we will obtain the following characteristic of weight intensity of wear relative to a unit path and contact area:

$$J_B = \frac{n_p \Delta g_M}{n_0 l S_n} . \tag{27}$$

The weight of the worn material is

$$g_M = n_p \Delta g_M = \gamma V,$$

where V is the volume.

For a contact area equal to unity, we have

$$g_M = \gamma \Delta h,$$

where Δh is the height of the worn layer of material.

Then,

$$J_B = \frac{\gamma \Delta h}{n_0 l} . \tag{28}$$

The ratio $\dfrac{\Delta h}{l}$ is known as the linear wear of material J_L, i.e.,

44

STAT

$$J_\perp = \frac{\Delta h}{l} .$$

(29)

This is the most important characteristic of wear since, generally, in coupling machines an increase in clearance puts the engine joints out of action.

With an increase in clearance, the uniformity of surface contiguity is disrupted, leading to overloading of separate contact spots, which contributes to an increase in the number of disintegrating spots. If the dimension of the clearance ("cylinder - piston", "shaft - bearing" and others) increases by arithmetic progression, then the intensity of wear grows by geometric progression. The maximum of wear is correlated with a rapidly growing decrease in machine production.

In other junctions of the "brake friction" type, where close reciprocal contiguity is always assured, there is no clearance: The part normally operates until it is completely worn.

From the above it follows that

$$\Delta h = \frac{n_p \Delta g_M}{\gamma} .$$

(30)

Apparently, to decrease the wear it is necessary to decrease the number of contact spots found under conditions of destruction and the size of the particles separated during destruction.

The creation of such interactions is of great significance in the destruction resulting from repeated action rather than from single action.

Let us examine how the process of destruction of surface friction takes place and in what manner it can be affected.

The interacting contact spots can be destroyed during a single interaction; during repeated interaction they may be deformed elastically without being destroyed. An analysis of the process is complicated by the fact that, during the interaction of rubbing surfaces, the deformation of contacting roughnesses cause a

45

STAT

significant change in the friction surface.

These changes are due partly to an intensive deformation of the surface layers, leading to a torsion of the crystal lattice of the material and to cold-hardening, and partly to the temperature conditions of the friction unit.

Friction and temperature essentially are two aspects of one and the same phenomenon.

Engels shows that friction and impact lead from molar motions, a subject of mechanics, to molecular motion, a subject of physics.

Heat developed in a body is produced by the motion of molecules of which it consists.
This motion forms as a result of mechanical deformation. All deformations during reciprocal sliding concentrate in a thin layer contiguous to the body surface. This deformed area is called the surface layer. It is in this layer that elevated temperatures develop whose magnitude is functionally connected with the sliding speed.

As the degree of deformation is attenuated in accordance with the depth of the deformation zone, so does the temperature decrease according to depth. The variation in temperature with depth is characterized by the temperature gradient $\frac{\partial \theta}{\partial n}$.

Temperatures on the friction surface easily reach high values (of the order of $100 - 200°C$ or higher under dry friction conditions).

The temperature gradient may reach extremely high values (up to $1000°/mm$ and more).

From the surface layer, the heat spreads into the body, is characterized by a much smaller gradient, and partially dissipates from the friction surface in the case of incomplete osculation of the rubbing parts. High temperatures and significant temperature gradients lead to chemical and structural changes of the material (D.K.Chernov, I.A.Oding, V.V.Chernyshev).

Any change in material properties affects the nature of wear, replacing one type of destruction by another, which in some cases leads to a change in the type of

STAT

interaction (Bibl.17). Therefore, the process of wear may be divided into three kinds of phenomena, which continuously exert a mutual influence interaction followed by destruction of some contacting sections and physical-chemical changes in others. For a given section of material, the physical-chemical changes which may be called friction precede destruction, and this phase is completed by the phase of wear.

Breaking up the processes of wear into separate successive phases makes it possible to perceive those factors which, under given concrete conditions, are most easily affected: in some cases changes in the conditions of interaction, in others the physical-chemical processes. The result of these changes will be a change in the type and intensity of destruction.

There are two types of interaction:

1) mechanical - penetration,

2) molecular - attraction and cohesion (Fig.17).

The second interaction accompanies the first but depends on external conditions and material properties which manifest themselves to a different degree in each case.

Several types of destruction have been noted. The following types of destruction are observed during mechanical interaction (Fig.17):

1) Gouging (breaking away of particles during abrasion);

2) Mechanical scaling, resulting from repeated interaction in the smoothing process (abrasion without formation of wear particles);

3) Chipping, resulting from the smoothing process during thermo-chemical changes in the surface layers;

4) Formation of dust (micro-gouging, microscaling, microchipping, and fusion).

Other types of destruction are probably possible.

The following types of destruction are possible during molecular interaction:

depth tearing or cohesion if the molecular interaction is great.

STAT

Two, three, or four types of destruction by mechanical interaction take place during repeated molecular interaction if it is low (attraction).

The physical-chemical changes in the surface layers may differ in many ways since they are determined by the variety of material properties used in friction
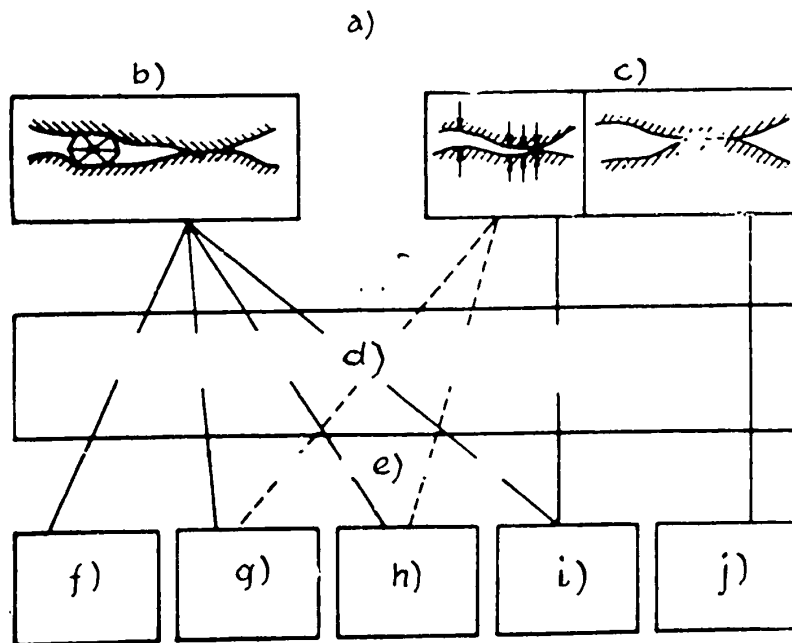

Fig.17 - Types of Interaction and Destruction

a) Types of interaction; b) Mechanical penetration; c) Molecular: Attraction, gripping; d) Types of physical-chemical changes in surface layers: mechanical, structural, chemical, and others; e) Types of destruction; f) Gouging; g) Chipping; h) Scaling; i) Microdestruction; j) Depth tearing

units (metal, wood, stone, etc.). For metals the changes are: consolidation during deformation (down to the interfaces), recrystallization, formation and dissociation of solid solutions, coagulation, diffusion, saturation of surrounding medium with elements, etc.

To control the wear of the unit, it is necessary to determine the form of interaction taking place, the type of resultant destruction, and the physical-chemical

STAT

changes taking place in the surface layers.

The products of destruction and physical-chemical changes remain on the worn surfaces of the parts. If the distinguishing characteristics, sequence, and nature of the development of the separate links in this chain of events are known, the entire process of wear may be determined from the products of disintegration.

For example, in aircraft wheel brakes the by-products of wear, depending on the temperature conditions, form a hard deposit which is a liquid or a mixed intermediate fluid, coating the friction plane between the elements of the pair in a thin layer. The disintegration products continuously change positions in the direction of movement of the movable member of the pair, until they gradually exceed the limits of the friction plane.

The intermediate layer, observed in testing of brakes, influences both the frictional qualities and the process of wear.

It has been noted that, if the friction brake surface is scavenged with a strong jet of compressed air, removing the products of wear from the friction plane, the brake moment of the brake will increase. If the products of wear are improperly removed from the friction plane the decrease in the effectiveness of the pair will be accompanied by an irregular wearing of the brake coating: the part of the coating at the leading rim of the shoe wears out more than the one at the trailing rim.

The quantitative characteristic which specifies this or any other forms of interaction, change, or destruction is the magnitude of penetration of the contacting spots. In the case of mechanical interaction, this determines the deformation zone, surface roughness during sliding friction, and nature of the destruction. The distinguishing characteristic of mechanical interaction is that the destruction zone exactly reflects the penetrated member (Fig.18a). In the case of molecular interaction, the degree of penetration does not determine the deformation zone since destruction may take place at a considerable depth (Fig.18b) or a connection may form

49

STAT
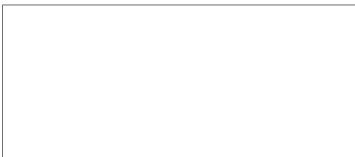
which depends on the extent of the molecular interaction and the mechanical proper-
ties resulting from the molecular connection.

Since the surface is formed of roughnesses of different heights, the penetra-
tion due to reciprocal compression varies widely and leads to different types of
surface destruction.

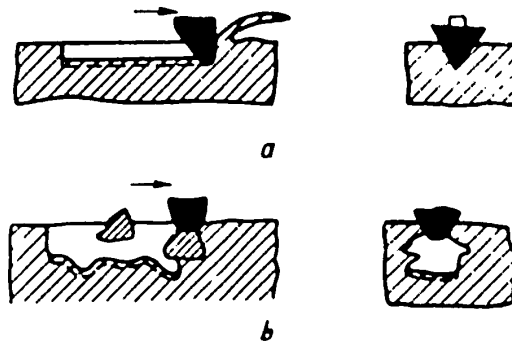Under conditions of mechanical interaction, some form of destruction takes

a

b

Fig.18 – Destruction Zone as a Function of the Penetration Depth
a)– At mechanical interaction, b – At molecular interaction

place, depending on the magnitude of penetration (Fig.19).

A geometric analysis of the contact conditions of sliding surfaces (Fig.20)
leads to the following simple formula, which determines the intensity of weight
wear (Bibl.18):

$$J_B = (a_{sbl} - a_{kr})\frac{\gamma}{\Delta L}, \qquad (31)$$

where a_{sbl} = magnitude of mutual surface meshing (embedding);

a_{kr} = depth of deformation leading to a given form of destruction;

ΔL = sliding path, equal to the base of the supporting surface curve;

γ = specific weight of the material.

Equation (31) refers to destruction due to a single action. In the case of de-

50

STAT

struction resulting from repeated action, the corresponding equation reads

$$J = \gamma_1 (a_{sbl} - a_{kr})\frac{\gamma}{\Delta L} , \tag{32}$$

where η is a fraction whose numerator is equal to the number of repeated actions leading to destruction.

For molecular interaction, the intensity of wear is expressed in the following manner:

$$J = (a_{sbl} + \delta_{ql} - a_{kr})\frac{\gamma}{\Delta L} ,$$

where δ is the magnitude of depth leveling, measured from the line of penetration.

An exact analytical examination of destruction conditions in osculating roughnesses represents a mixed problem of the theories of elasticity and plasticity,
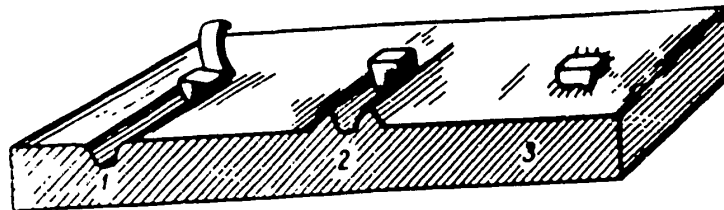
Fig.19 - Nature of Destruction as a Function of the Depth of Penetration

1 - Gouging; 2 - Repeated deformation; 3 - Elastic rebound

which has not yet been solved. However, even a rough examination of the problem furnishes an explanation of the basic rules observed during wear.

An analysis of eq.(32) shows that a decrease in intensity of wear may be accomplished in the following ways:

1) Decreasing the magnitude of mutual penetration (a_{sbl}) characterizing the deformation zone, which can be done by increasing the hardness of the friction surface and creating conditions under which sufficient smoothness of surface is

STAT

retained.

2) Increasing a_{kr}, i.e., the deformation leading to a given form of destruc-tion. The greater the magnitude a_{kr} during high deformation values, the more possi-ble is interaction without destruction. Increasing the value a_{kr} for different types of destruction is accomplished in various ways.

For example, in the case of gouging it is essential to increase the radius of curvature of the penetrating elements; to provide a durable connection separating
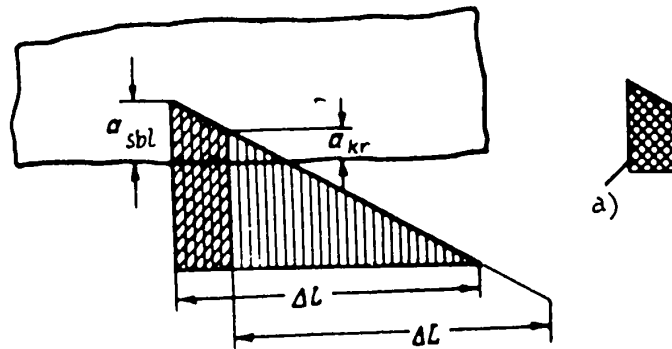

Fig.20 - Interaction of Rough Surface with Smooth Surface (Geometric Diagram)

a) Worn material

the clean film surfaces from the basic metal; to create conditions for rapid recov-ery of destroyed film. Simultaneously with this, the film must be less durable than the basic metal.

3) Decreasing the value of η_{up} which is a coefficient, evaluating the fatigue limit of material under conditions of repeated plastic deformations. The coeffi-cient η_{up} may be reduced by regulating the mechanical properties of the material and likewise by creating conditions under which the cold-hardening sharply increases the value η_{up}.

All this explains the use of materials whose recrystallization point is lower than the temperature in a friction unit, in friction units.

4) During molecular interaction, decreased wear may be obtained by lowering

STAT

the magnitude of depth tearing δ_{gl}, by creating conditions under which δ_{gl} will be-

come zero, i.e., conditions under which destruction occurs according to the point of

interaction. In the case of destruction according to the point of interaction, the

intensity of wear may be practically equal to zero since molecular interaction is

not dependent on penetration.

Such a phenomenon occurs during polishing, pulverized wear.

Destruction at tne place of interaction occurs most easily when the

surfaces are coated by oxides or chemical films whose durability is inferior to that

of the basic material.

Naturally a lubricating film is the simplest means of localizing destruction

in an interaction zone.

The use of metals with unmachined surfaces and capable of cold-working during

plastic deformation may render the resultant gripping joint more durable than the

underlying layers and may result in the formation of sections with depth tearing.

Raising the temperature during contact to prevent cold-working in this case may be

extremely effective as far as decrease in wear is concerned. However, raising the

temperature during contact in materials with poor heat resistance may lead to char-

ring of the material which, accordingly, would increase the wear.

Therefore, the very same procedure in different cases may lead to entirely

different results.

However, in all cases the wear is decreased if the above two laws, applicable

to mechanical molecular interaction, are observed.

In the first case such mutual penetration of contacting bodies requires that

the surfaces retain their connection with the basic mass of material.

This may be accomplished by decreasing the magnitude of penetration (principle

of maximum rigidity) or by creating conditions that ensure repeated deformation

without destruction (principle of maximum pliability).

In the second case, the molecular connection formed between the surfaces must

53

STAT

be less durable than the underlying material.

The result of the combined effect of loading and speed during braking is heat. Let us analyze how each of these factors affects friction and wear.

Effect of Pressure

The dependence of the intensity of wear on pressure has a functional correlation which is illustrated by the curves in Fig.21. The curves show that, with an
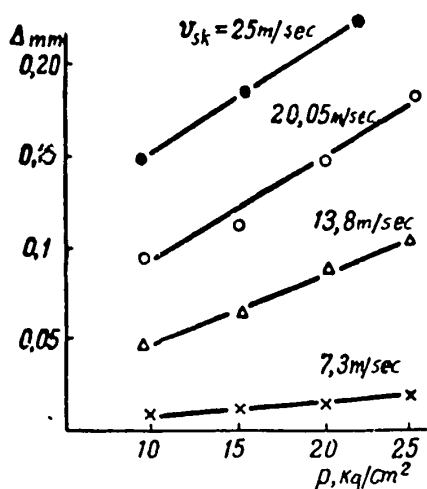

Fig.21 - Intensity of Wear Δ as a Function of the Pressure p:
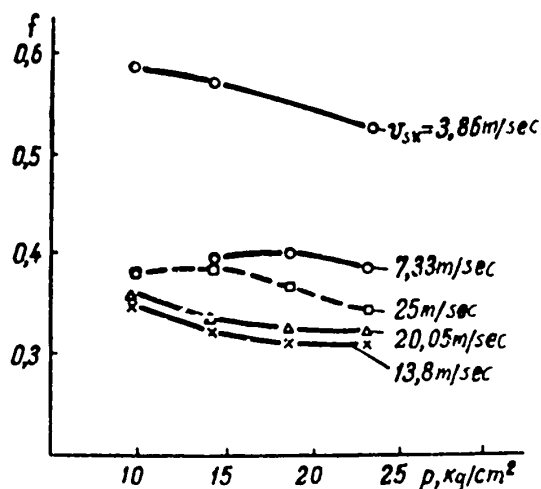
Plastic No.22 - Cast Iron ChNMKh; θ = 260°

Fig.22 - Coefficient of Friction f as a Function of the Pressure p:

Plastic No.22 - Cast Iron ChNMKh; θ = 260°

increase in pressure, the intensity of wear grows gradually with no tendency toward extreme values. This is natural since an increase in load leads to an increase in the number of contacting sections, while preserving the type of destruction in each of them.

The coefficient of friction is related to the load by a more complicated ratio. The coefficient is given by the nature of the curve of the supporting

54

STAT

surface. However, as indicated by the curves in Fig.22, the coefficient of friction changes gradually and does not suddenly greatly increase or decrease with variations in pressure within sufficiently small limits.

As a result of a pressure rise within the limits applicable to brake pairs, the mechanical properties of the materials change only insignificantly.

Effect of Speed

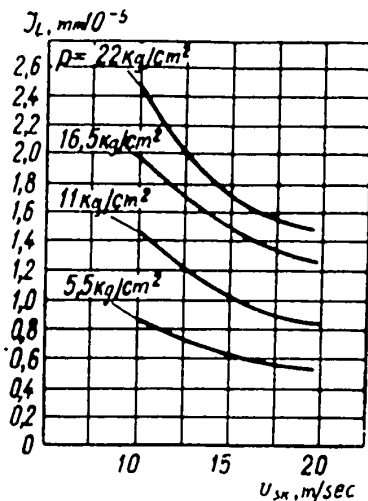The dependence of the intensity of wear on the sliding speed is shown in Fig.23.

Fig.23 - Intensity of Wear J_L as
a Function of the Sliding Speed v_{sk}
for Material KF-3 (According to
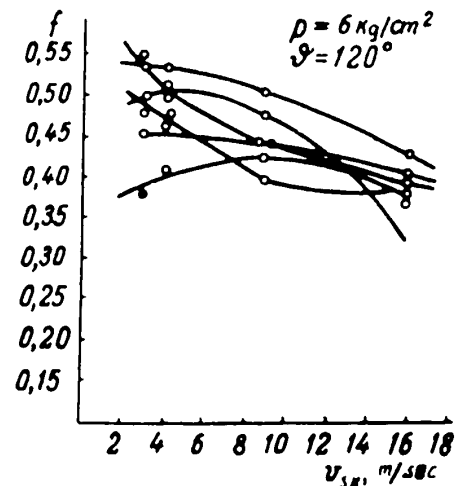Data by A.A.Gryzlov)

Fig.24 - Coefficient of Friction f
of Frictional Plastic Materials Used
for Automobile Brakes, with Gray Iron,
as a Function of the Sliding Speed v_{sk}
(According to Data by S.G.Borisov)

As indicated by these graphs, the intensity of wear decreases by a smooth curve with an increase in speed at constant pressures and temperature within the volume of the frictional material.

As shown in Fig.24, the coefficient of friction passes a maximum or decreases

55

STAT

with increasing speed. Again it should be noted that the change in the coefficient of friction is gradual. This is explained by the fact that the mechanical properties of the materials depend very little on the sliding speed, i.e., on the rate of
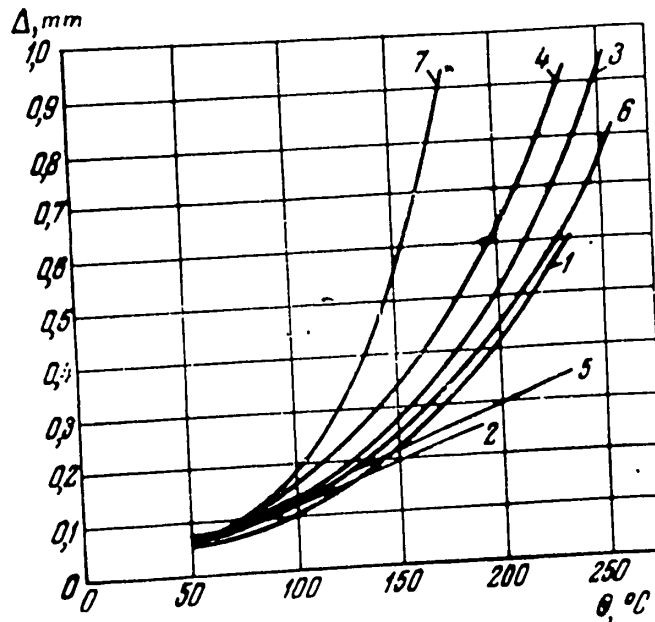

Fig.25 — Linear Wear Δ of Frictional Materials as a Function of the Temperature θ after 5000 Brakings (M.P.Aleksandrov)

1 — Rolled strips; 2 — Cermets; 3 — Frictional Brake Material of the Automobile GAZ-AA; 4 — Frictional Brake Material of the Automobile ZIS-150; 5 — Frictional Material for Brake Shoes of Subway Cars; 6 — Frictional Brake Material of the Automobile ZIS-6; 7 — Strip of Type "A"

deformation in the friction zone.

Effect of Temperature

Temperature has the greatest influence on the intensity of wear and the coefficient of friction.
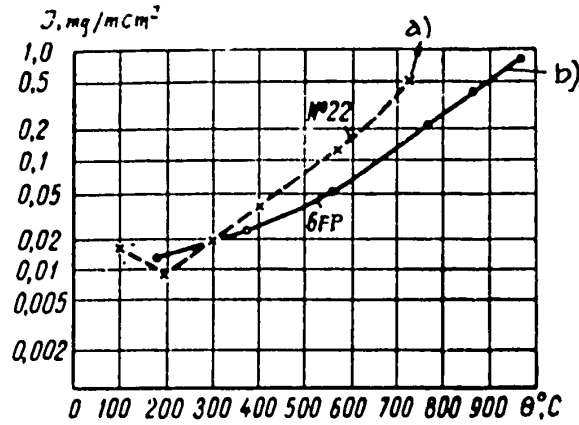
STAT

Fig.26 – Intensity of Wear J as a Function of the Temperature θ for

Plastic No.22 and 6FP with Cast Iron ChNMKh (Experiment on Machine I-47);

θ = Temperature of Cast Iron Model at a Depth of 1 mm from the Friction

Surface

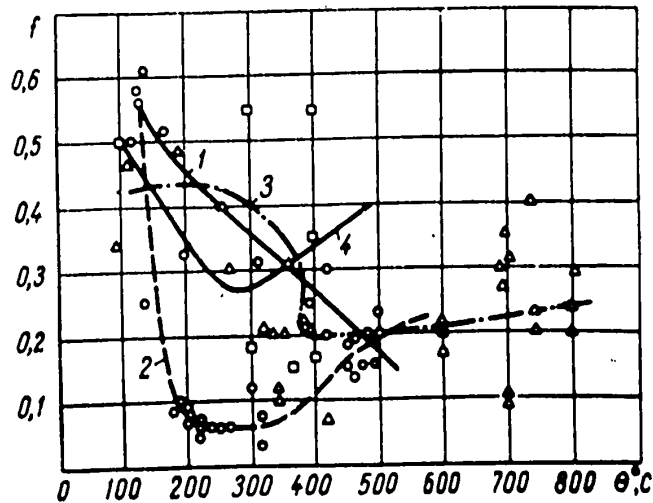a) Charring and destruction of model; b) Considerable wear, no charring

or destruction

Fig.27 – Coefficient of Friction f for Cast Iron, as a Function of the

Temperature θ (θ = Temperature of the Cast Iron Model at a Depth of 1 mm)

1 – Plastic 6KKh-1; 2 – Plastic PA-2; 3 – Plastic "M"; 4 – Plastic 7KF-31

STAT

The intensity of wear changes sharply (usually increases) with an increase in temperature (Figs.25 and 26) and, on reaching a certain critical temperature, becomes catastrophic for many frictional materials (Bibl.19).

Any change in temperature significantly affects the coefficient of friction. A temperature rise in a friction unit causes a significant drop in the coefficient of friction in most frictional materials. During this time, at certain temperature values, the coefficient of friction changes sharply (Fig.27). For certain frictional materials, after a rather gradual decrease in the coefficient of friction, a sharp increase is noted after reaching a sufficiently high temperature. This is explained by the fact that the surface of the material becomes charred.

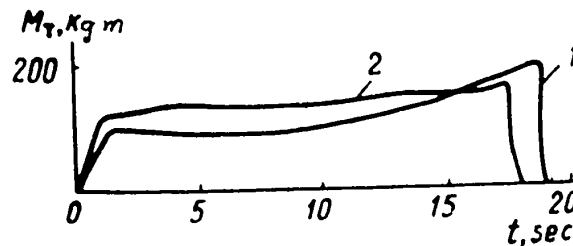The temperature gradient which changes in accordance with the conditions of

Fig.28 —.Brake Moment M_T in a Chamber Brake of a Wheel 660 × 160 as a

Function of Heat Liberation

1 - Braking without air blasting; 2 - With blasting

heat emission, significantly affects the frictional properties of friction pairs.

Figure 28 gives data on the brake moment of the plastic No.22 in a wheel 660 × 160: without air scavenging of the brake during braking and with air blast.

The change in frictional characteristics, depending on the above parameters, is connected with a change in the mechanical properties of materials which are mainly affected by temperature.

The variation in the ultimate strength of pure iron and chromium cast iron

58

STAT

(Bibl.20) caused by heat is shown in Fig.29, and in frictional plastic 6KF-32 and Ts-17-52 in Fig.30. As seen from these curves, the ultimate strength of metals and plastics drops considerably with increase in temperature.

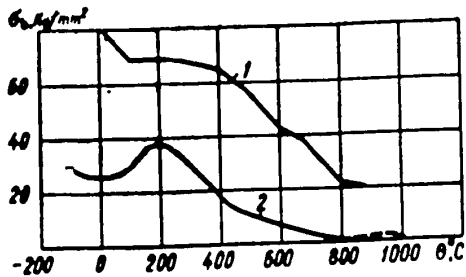In Fig.31 the curves show the temperature distribution and ultimate strength of

Fig.29 — Change in Ultimate Strength σ_b of Chromium Cast Iron (Curve 1) and Pure Iron (Curve 2) Due to Temperature θ
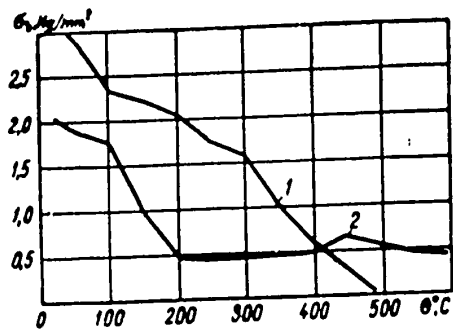
Fig.30 — Change in Ultimate Strength σ_b of Frictional Plastic 6KF-32 (Curve 1) and Ts-17-52 (Curve 2) Due to Temperature θ

a cast-iron brake drum, according to depth. As indicated by these curves, the ultimate strength of the metal according to variations in depth during the friction process, changes from a minimum value in the rubbing surfaces to a maximum value in the remote depth layers.

The temperature gradient produces, within the drum material, a gradient in the mechanical qualities, which decisively affects the wear and functional qualities of the drum. The same applies to the coatings of brake shoes.

The magnitude of temperature on a friction surface and the temperature gradient depend on the performance of the brake pair as well as on the material and construction of the drum. The temperature gradient in the layers of the pair bordering the friction surface plays an especially large role in thermal tensions and durability of the frictional pairs.

STAT

When the friction surface layer of the drum is affected by heat, it tends to expand; however, this expansion is prevented from taking place by the outer layers of the drum which have not yet warmed up. Therefore, the layer bordering the friction surface is subject to compression strains which, in turn, cause expansion
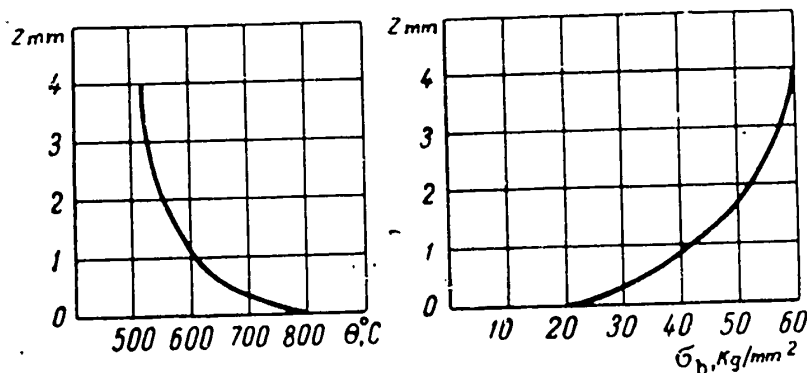

Fig.31 — Change in Temperature θ and Mechanical Properties σ According to Depth z in a Cast Iron Brake Drum

stresses in the inner layers of the drum. Stresses in the surface friction layer do not cause damage as long as they do not exceed the yield point. If, however, during heating, the metal at the inside is subjected to compressions greater than the ultimate strength, then, during cooling, the inner compressed drum surface tends to retain a smaller inside diameter than the original one. Since the surface, compressed beyond the ultimate strength, is part of the drum, it cannot remain at a smaller diameter without causing a loaded diameter. As a result, the inner drum surface undergoes expansion stresses and the outer surface compression strains.

If the inner surface of the drum material does not perform well during the expansion, as for example, cast iron, cracks will form during cooling; this happens in actual practice and also explains the systematic decrease in the inside diameter of steel drums, from braking to braking, during operation.

Temperature also greatly affects the properties of surface layers, causing for-

STAT

mation of oxides and various chemical compounds whose mechanical properties differ from the properties of the material itself. As a result, the nature of interaction and destruction changes. In addition, a large temperature gradient creates the phenomenon of diffusion, which leads to a change in the mechanical properties of materials.

In cases in which the mechanical properties of a material do not depend on temperature changes, the coefficient of friction retains a stable value in the same range of temperature variations (Bibl.21 and 22).

Therefore, summarizing the above, the following conclusion can be drawn: Any change in the frictional characteristics is directly connected with a change in the mechanical properties of materials of the rubbing pair. Of the three factors: pressure, sliding speed, and temperature, the latter affects mechanical properties most and thus also the frictional characteristics.

Since, in friction, the expended work A distributed throughout the masses drawn into the deformation of the materials of the rubbing bodies, is converted into heat in all the elemental volumes of these masses; therefore, in each pair member a spatial field of is created, which leads to a definite temperature field in the volume of a given material.

It is well to bear in mind that the area occupied by the thermal flow considerably exceeds the area drawn into the deformation. The temperature field is of interest in the deformation area as well as in the contiguous layers of the material, where the temperature may reach high values.

Therefore, the temperature field of rubbing bodies cannot be characterized only by absolute temperature values on the friction surface or at some point in the volume. It is also necessary to know the temperature gradient according to the depth of a given material in order to obtain a full characterization of the temperature field and to clarify the connection between heat generation and friction.

Therefore, to fully characterize the temperature field of a coupled friction

61

STAT

pair, it is necessary to examine three characteristic values for each element of a pair:

1) Surface temperature;

2) Volume temperature;

3) Temperature gradient according to depth.

In connection with the above, the appraisal of various designs of experimental machines and testing methods from the viewpoint of miniature-scale temperature testing on small models, is of exceptional interest.

All this is connected with calculating temperature fields in friction pairs, which in itself is a sufficiently difficult problem.

62

STAT

REVIEW OF WRITINGS AND RESEARCH ON CALCULATING TEMPERATURES DURING FRICTION

As established earlier, the behavior of frictional material is mainly determined by three temperature characteristics: surface temperature θ_S, volume temperature θ_V, and temperature gradient $\frac{\partial \theta}{\partial n}$ = grad θ.

Surface temperature θ_S is dependent on the friction work and is generated on the actual contact surface. Volume temperature θ_V is produced by the heating of the mass of rubbing bodies which result from an accumulation of heat due to the work of sliding friction. The temperature gradient $\frac{\partial \theta}{\partial n}$ = grad θ determines the type of temperature field, according to depth, in the frictional material.

Let us examine the existing methods for mathematical calculations of heat processes and let us attempt to establish to what extent they permit determining the temperature characteristics indicated above.

Problem of Heat Conductivity

The problem of the theory of heat conductivity is to determine the temperature at separate points of the body at any instant of time (Bibl.23). In mathematical terms, the problem is reduced to finding the temperature distribution in a body in the form of a continuous and differentiated function:

$$\theta = f(x, y, z, t) \tag{33}$$

As in many other problems of mathematical physics, the indicated dependence in the heat-conductivity theory is first expressed by a differential equation

STAT

$$\frac{\partial \theta}{\partial t} = a^2 \left(\frac{\partial^2 \theta}{\partial x^2} + \frac{\partial^2 \theta}{\partial y^2} + \frac{\partial^2 \theta}{\partial z^2} \right), \qquad (34)$$

where x, y, z = coordinates of a point of a uniform and isotropic heat-conducting

medium;

$a = \frac{\lambda}{\gamma c}$ = coefficient of heat conductivity (λ = heat conductivity, γ = density,

c = heat capacity);

t = coordinate of time.

In the practical application of the theory of heat conductivity, various problems occur which can be subdivided into three main groups:

1) Transfer of heat during established heat conditions;

2) Continuous heating or cooling of bodies;

3) Periodic heating and cooling of bodies.

It is necessary to know the initial and boundary conditions of a problem in order to integrate a differential equation.

Initial Conditions. The initial temperature distribution in a body may vary widely. For example, during heating or cooling a body may have, at the initial instant of time, the same temperature in all its mass

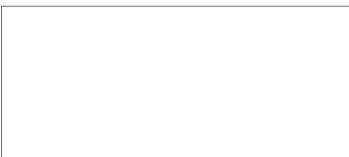$$\theta (x,\, y,\, z) = \theta_0 = \text{const.} \qquad (35)$$

In other cases, the initial temperature in the body may be expressed by the equation

$$\theta_0 = \theta (x,\, y,\, z). \qquad (35')$$

Boundary Conditions. Three types of boundary conditions are possible*.

1) the temperature distribution over the body surface is given only as a

*Note: Other boundary conditions are combinations of these three types of boundary conditions.

64

STAT

function of time θ_s = f(t) for any given instant of time. Such a case is possible during heating or cooling of bodies by means of a heat source with a constant temperature.

2) On the surface of the body, at different positions, the specific thermal flow q_{tp} is given for any instant of time. According to Fourier's hypothesis, the assignment of a specific q_{tp} is equivalent to the assignment of a derivative of the temperature, according to the inner normal to the interface. Therefore, the indicated boundary conditions may be expressed by the function $\frac{\partial \theta}{\partial n}$ = f(t) on the surface S.

3) The temperature of the medium surrounding the body is given, and also the law of heat transfer of the surface

$$\frac{\partial \theta}{\partial n} = \sigma \left(\theta - \theta_a \right),$$

where σ = coefficient of heat transfer;

θ_a = temperature of the surrounding medium.

A great number of domestic as well as foreign publications (M.V.Kirpichev, G.M. Kondrat'yev, A.V.Lykov, M.A.Mikheyev, S.N.Shorin, Kh.S.Karslou, J.C. Jaeger and others) were devoted to solving the various problems of the heat-transfer theory and are based on the generally accepted premises of the theory of heat conductivity.

Therefore, from the general solution of the heat conductivity equation it is necessary to extract a quotient solution which would satisfy eq.(34), the initial conditions (35,35'), and one of the boundary conditions stated above. In this case, it must be remembered that the function θ (x, y, z, t) expressing the equation does not necessarily have to assume a value f(t) on the surface S, but the following condition must always be satisfied:

$$\lim 0 \left(x,\; y,\; z,\; t\right) = f\left(t\right),$$

when we take the point M(x, y, z) $\rightarrow$ M_0(S).

STAT
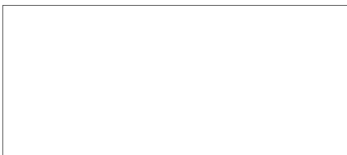
The researchers mentioned above and many others studied bodies of various configurations: parallelepipeds, cylinders, spheres, and similar bodies. In each separate case, various problems were solved in various ways with the help of the most convenient Cartesian, cylindrical, spherical, or some other coordinates in any given concrete case.

As applied to friction problems, the general theory has disregarded the following questions:

1. In what manner is the source formed during friction;

2. What is the nature of the heat source in terms of geometric size and its distribution along the surface;

3. What temperature is developed by the heat source during a given friction work at any instant of time, at any point of a given boundary friction zone.

Without examining these questions, the heat problem of friction cannot be solved by applying the heat conductivity theory stated above, since the boundary conditions are unknown in this case.

Therefore, the generally accepted heat-conductivity theory (assuming that somehow the function answering these questions is given) makes it possible to determine two temperature characteristics out of three - volume temperature θ_V and temperature gradient according to depth of material

$$\frac{\partial \theta}{\partial n} = \text{grad } \theta.$$

Naturally, in recent years works have appeared devoted to the problem of determining temperatures on a friction surface. Let us examine the main premises on which these works have been based.

Determining the Source of Heat during Friction and the Problem of Temperature Determination on the Friction Surface

Numerous research studies were made for clarifying the boundary conditions as

STAT

well as the physical nature of heat sources during friction. Some researchers (Bibl.24,25) studied heat formation on macrocontact and others (Bibl.26,27,28) on microcontact.

The attempt by Bowden (Bibl.24) to determine the temperature of a long cylindrical rod whose end abuts a disk, during friction, does not fully solve the problem. In this study, the actual area of contact is assumed equal to the nominal (this circumstance was noted by Ya.M.Frenkel). In addition, the method of the study is useful only for a quiescent contact. Bowden does not explain, in his papers, the means by which he attained sufficiently uniform pressure on the support. Under these conditions Bowden's method at best determines only a certain neutralized temperature on the surface and only for a given type of reciprocal contact of the element of the rubbing pair. The same shortcomings are also inherent in the paper by M.P.Levitskiy (Bibl.25).

The papers by Block (Bibl.26,27) and Iyeger (Jaeger) (Bibl.28,29) are quite free of the shortcomings mentioned, but the results of these studies have a limited practical application because of the smallness and isolation of the single microcontact examined in them.

A few words should be said about the works of Iyeger and P.Khol'm. Iyeger managed to create a considerably more orderly and rigid mathematical scheme (as compared to Block) for determining the maximum and mean temperatures of the microcontacts on a unit strip and unit square.

Complicated initial equations derived for determining temperatures with the aid of Bessel and Newman function are reduced to simple solutions which are correct during certain intervals of a dimensionless coefficient

$$L = \frac{l_1 v_{sk}}{2a} ,$$

where l = width of a strip and square source;

v_{sk} = sliding speed;

67

STAT
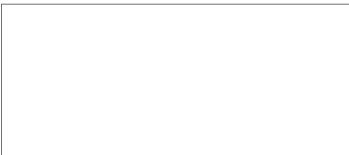
a = coefficient of heat conductivity.

For example, for mean temperatures on a single contact at a small L (L $\leq$ 0.1), we have

$$\theta_{sp} = \frac{0.236\, a_1^{1/2}\, Jf p_{ud} v_{sk}}{l\,(\lambda_1 + \lambda_2)}\; ; \tag{36}$$

and at a large L (L > 5),

$$\theta_{sp} = \frac{0.266 a_1^{1/2}\, Jf p_{ud} v_{sk}}{l\,[1.125\lambda_2 a_1^{1/2} + \lambda\,(lv_{sk})^{1/2}]}\; . \tag{37}$$

Both these formulas are derived for a case when friction is achieved according to the diagram shown in Fig.32.

Iyeger's eq.(37) for large L may be simplified and applied to orienting calculations. When cases of sliding friction during high speeds v_{sk}, assuming that $\lambda_1 \gg$ $\gg \lambda_2$, are considered, this equation can be written in the following manner, without particular miscalculation

$$\theta = \frac{f p_{ud} \sqrt{lv_{sk} a_1}}{\lambda_1}\; . \tag{38}$$

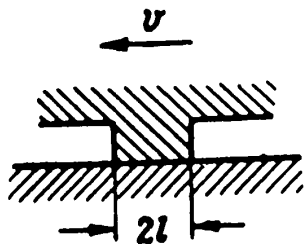In this formula, the subscript "l" refers to the smooth semispace.

The parameters most difficult to determine in this formula are the terms and p_{ud}.

Let us calculate the surface temperature of a cast-iron brake drum, during braking with shoes made of plastic No.22. Let us assume the following parameter values:

Fig.32 - Diagram of a Sliding Single Isolated Contact (According to Iyeger)

$v_{sk} = 20$ m/sec $= 2 \times 10^3$ cm/sec; $2l = 1.5 \times 10^{-2}$ cm; $\lambda_1 = 2.6$ kg - cm/cm sec °C; $a_1 = 0.08$ cm^2/sec; $\lambda_2 = 0.05$ kg - cm/cm sec °C; $p_{ud} = 4 \times 10^3$ kg/cm$^2 = 2H_B$ on con-

68

STAT

tact (here H_B is the hardness of plastic No.22); $f = 0.5$.

Here $\lambda_1 \gg \lambda_2$, since $2.6 \gg 0.05$.

With these values, eq.(38) gives the mean temperature for an elementary contact

$$\theta_{sp} = \frac{0,5 \cdot 4 \cdot 10^3 \cdot 0,75 \cdot 10^3 \cdot 2 \cdot 10^3 \cdot 0,08}{2,6} = 843°.$$

For intermediate magnitudes of L, Iyeger gives a graph according to which the correction coefficients are determined.

R.Khol'm bases his work (Bibl.30) on the conclusions by Jaeger, but he simplifies all the computations considerably by using graph plotting. In addition, he also examined the case of an oval heat source.

Here it should be again emphasized that the work by Block and the work by Jaeger and R.Khol'm make it possible to determine only the temperature of a single and isolated microcontact, without taking into account the previous temperature of the volume of the body. This temperature is therefore actually a temperature rise. However, the conclusions given in these papers can be fully utilized for some individual temperature problems. A.I.Petrusevich (Bibl.31) who developed and first used the surface temperature problem in an engineering calculation of gears, proved this assumption.

Because of the practical importance of the heat problem in friction, attempts to solve it naturally lead to generalizing both methods.

Solution of the Heat Problem in Friction According to V.S.Shchedrov

The research study conducted by V.S.Shchedrov is the most outstanding work on the solution of this rather complicated problem. This work is free of the above-mentioned shortcoming, i.e., of considerations of the reciprocal effect of the great number of elementary heat sources or, in other words, microcontacts.

Let us here examine the physical aspect of this work only, omitting all intermediate mathematical computations because of their considerable complexity.

STAT

Let the given nominal contact be of the size $S_{H} = 4h_1 h_2$. Let us assume that this contact slides over any kind of surface*. As a result of waviness, the touching surfaces on the friction surface have areas of contact or, in other words, macrocontacts giving $S_{real'n}$.

It is known that the actual contact area is the total of many small actual contacts. Here the actual area of touching is confined to the area earlier referred to as an actual area of contact. The area of actual contact comprises only an insignificant part of S_{II} and fluctuates within the following limits:

$$S_H \approx 0,0001 S_n \text{ to } 0,1 S_n.$$

During friction, these tiny actual contacts turn into elementary heat sources.

Some researchers (P.Ye.D'yachenko, M.M.Khrushchov, and others) point out that it is necessary to distinguish between the longitudinal and lateral roughness in its relation to the displacement of the rubbing bodies. Here the linear problem is also examined.

On making an imaginary division of the nominal contact along the line AB (axis x), it will be found that the elementary heat sources (Fig.33) are distributed chaotically along this axis. Let this distribution of elementary heat sources create a definite temperature field (Fig.34). Let us imagine that, along the same axis (Fig.34), heat dipoles are distributed in some definite order which create the same kind of temperature field as the actual chaotically distributed elementary heat sources. Let the time of action of the elementary heat dipole be τ, its arm $d\xi$, and let it be located at the point m with a coordinate ξ.

With these data, the elementary heat dipole can be characterized by the moment:

$$M = q(\xi, \tau) d\xi.$$

Let us take any point along the axis x; for example, point n with the coordi-

*In physics, the term surface means the boundary of a physical body.

STAT

nate x. As a result of the presence of certain temperatures at this arbitrary point n, the constant of the elementary heat dipole at the point m will generate quite a definite temperature. However, at the arbitrary point n there is also an
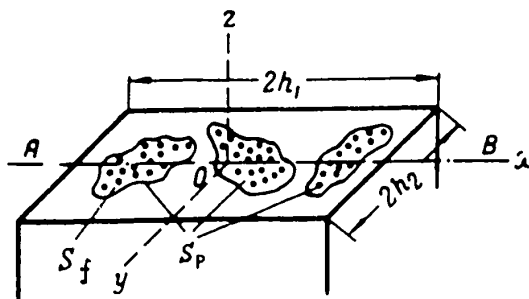

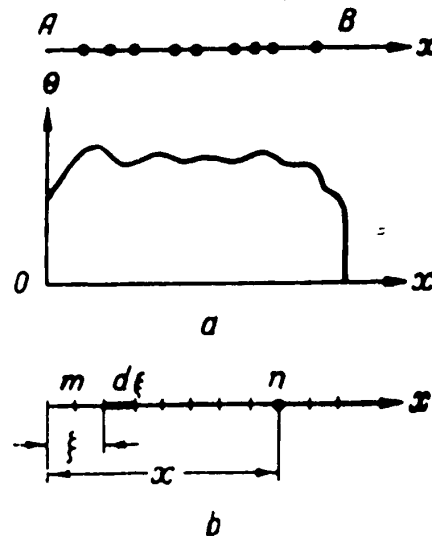Fig.33 – Distribution of Elementary Heat Sources on a Sliding Contact

Fig.34 – Temperature Distribution Curve Along the Axis "x"

elementary heat dipole which, in turn, affects the temperature at the point m and at all other points located along the axis x.

Therefore, the mutual effect of two, three, four, etc. elementary heat dipoles (sources) must be examined.

Mathematical processes where the reciprocal effect of definite parameters is taken into account are described by special integral equations. The structural scheme of such equations, on the whole, is as follows:

If f(x) is the unknown function, and R(x, ξ) the given function, called the core of the equation, then to find the unknown function f(x) one can form the following integral equation:

$$f(x) = A \int_a^b f(\xi) R(x, \xi) \, d\xi + c \ldots \qquad (39)$$

71

STAT
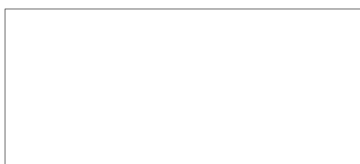
A characteristic sign of such an integral equation is that the unknown function in the given case of $f(x)$ is also contained in the subintegral expression in the form of $f(\xi)$.

In examining a case of friction of two rough bodies, V.S.Shchedrov formed the following integral equation:

$$q(x, t) = \sum_{n=1}^{n=2} \frac{A_n}{16\,\pi^{\prime\prime}a_n^{\prime\prime}} \int_0^{t+h_1} \int_{-h_1} q(\xi, l) \frac{(x-\xi-vt)}{(t-\tau)^{\prime\prime}} \exp \times$$
$$\times \left[-\frac{(x-\xi-vt)^2}{4a_n(t-\tau)}\right] d\xi \cdot d\tau + kq_0. \qquad (40)$$

In this equation, known as an integral equation of the Fredholm type, the unknown function is q(x,t) which is the general quantity of heat formed by all elementary heat sources on the nominal macrocontact (from $-h_1$ to $+h_1$) at any instant of time t.

The core of the equation or, in other words, the function of the effect here is the expression

$$R(x, \xi, t) = \frac{x-\xi-vt}{(t-\tau)^{\prime\prime}} \exp\left[-\frac{(x-\xi-vt)^2}{4a_n(t-\tau)}\right].$$

The sum symbol $\sum_{n=1}^{n=2}$ takes into account the general quantity of heat on a given nominal contact formed in a given boundary zone on one and on other surfaces belonging to the respective materials of the friction pair.

By means of complex computations, eq.(40) is reduced to the following form:

$$q^*(\omega, t) = hq_0^* \sum_{n=1}^{n=2} \frac{A_n}{16\,\pi^{\prime\prime}a_n^{\prime\prime}} \int_0^t e^{i\omega vt}q^*(\omega, t) \times$$
$$\times \int_{x+h_1-vt}^{x-h_1-vt} e^{i\omega z - \frac{z^2}{4a_n(t-\tau)}} \frac{z}{(t-\tau)^{\prime\prime}} dz\, d\tau, \qquad (41)$$

STAT

where

$$z = x - \xi - vt; \quad q^{\bullet}(\omega, t) = \int_{-h_1}^{+h_1} q(x,t) e^{i\omega x}\, dx,$$

$$q_0^{\bullet} = \int_{-h_1}^{+h_1} q_0 e^{i\omega x}\, dx, \quad -1 \leqslant \omega \leqslant +1;$$

ω being an independent variant.

From eq.(41) the following integral is derived:

$$J = \int_0^t \int_{x+h_1-vt}^{x-h_1-vt} \exp\left[i\omega z - \frac{z^2}{4a_n(t-\tau)} \right] \cdot \frac{z}{(t-\tau)^{5/2}}\, dz\, d\tau. \tag{42}$$

Integral (42) can be calculated approximately, and therefore the quantity J can be treated as a known function. After corresponding reductions, eq.(41) appears in its final form as follows:

$$q(x, t) = 8\pi^{1/2} k \int_{-1}^{+1} \frac{q_0^{\bullet}(\omega) e^{-i\omega x}}{16\pi^{3/2} + \sum_{n=1}^{n=2} \frac{A_n}{a_n^{3/2}} J e^{i\omega t}}\, d\omega, \tag{43}$$

where, as a result of the factor $e^{-i\omega}$, the integrand is an actual quantity.

Let us return to a study of Fig.33. If we make a division of the nominal macrocontact by means of the plane xz, we will have a profile diagram of the friction surface, having a definite degree of roughness. This roughness is correlated with the definite curve of the supporting surface (Fig.35) which may be replaced by a straight line in its working part without noticeable miscalculations.

If we assume, as a base, the curve of the supporting surface, which in some definite proportional dependence gives the actual contact area, the following equation of heat balance for a boundary friction zone is derived, when all the friction

73

STAT

work is converted into heat:

$$\int_0^{t+h_1} \int_{-h_1}^{t+h_1} q\,(x,\ t)\,dx\,dt = Apf v_{sk} t_0,$$

(44)

where A is the heat equivalent of mechanical work and t_0 the net time of friction

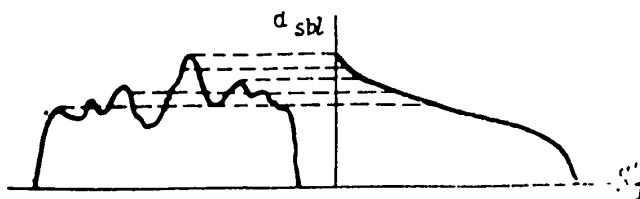Fig.35 - Supporting Surface Curve

work; in the general case, $t_0 \neq t$.

In eq.(44) let us substitute the value q(x,t), derived earlier in eq.(43),

$$\int_0^{t_0+h_1} \int_{-h_1}^{t+h_1} \left[8\pi^{1/2} k \int_{-1}^{+1} \frac{q_0^{\bullet}(\omega)\,e^{-i\omega x}}{16\,\pi^{3/2} + \sum_{n=1}^{n-2} \frac{A_n}{a_n}\cdot Je^{-i\omega vt}}\,d\omega \right] dx\,dt = A pf v_{sk} t_0.$$

(45)

When the friction pair consists of one material, the expression (45) is considerably simplified

$$\int_0^{t_0+h_1} \int_{-h_1}^{t+h_1} \left[8\pi^{1/2} a^{1/2} k \int_{-1}^{+1} \frac{q_0^{\bullet}(\omega)}{J}\,e^{i\omega\,(x-vt)}\,d\omega \right] dx\,dt = Apf v_{sk} t_0.$$

(46)

On the left-hand side of eq.(46) let us extract the integral

$$J^{\bullet} = \int_0^{t_0+h_1} \int_{-h_1}^{t+h_1} \left[\int_{-1}^{+1} \frac{q_0^{\bullet}(\omega)}{J}\,e^{i\omega\,(x-vt)}\,d\omega \right] dx\,dt$$

(47)

74

STAT

which will finally yield the following equation for heat balance in a friction pair made of one material:

$$8\pi^{1/2}a^{1/2}kJ^{\bullet} = pfv_{sk}t_0. \qquad (48)$$

From eq.(48) it is easy to determine the coefficient k

$$k = \frac{fpv_{sk}t_0}{8\pi^{1/2}a^{1/2}J^{\bullet}}. \qquad (49)$$

Then, knowing k, one can write the final expression for determining the general quantity of heat given off in a friction case where the two materials are the same:

$$q(x, t) = \frac{fpv_{sk}t_0}{J^{\bullet}a} \int_{-1}^{1} \frac{q_0^{\bullet}(\omega)}{J} \cdot e^{i\omega(x-vt)} d\omega. \qquad (50)$$

The result obtained depends on q_o (see expression 50), which makes it possible to explain, in the following manner, the physical nature of the quantities k and q_o, which have entered the initial integral equation (40). Let us turn again to the supporting surface curve (Fig.35). It can be assumed that the magnitude of mutual surface penetration a_{sbl} is directly proportional to the load:

$$a_{sbl} = k_1 p. \qquad (51)$$

On the other hand, the temperature effects on the friction surface and in particular the reciprocal effect of elementary heat sources are not at all dependent on their physical natures.

Block, Jaeger and R.Khol'm, for example, took advantage of this circumstance in their research studies, in which some results were obtained without examining the nature of the heat sources themselves. Therefore, the quantity q_o, which on the basis of the initial equation (40) appears as a definite quantity of heat, can be attributed to the previous distribution of friction heat sources. In this case,

75

STAT

q_0 must be proportional to the load. Consequently,

$$q_0 = k_2 p. \tag{52}$$

Expressing the quantity p from eq.(52) and substituting its value in eq.(51) we get

$$a_{sbl} = \frac{k_1}{k_2} q_0 = k_3 q_0. \tag{53}$$

However, the condition has already been assumed above that, for the straight-line part of the supporting curve, we have

$$a_{sbl} = k_4 S_f'. \tag{54}$$

In adjusting the right-hand sides of eqs.(53) and (54) we get

$$q_0 = \frac{k_4}{k_3} S_f' = k S_f'. \tag{55}$$

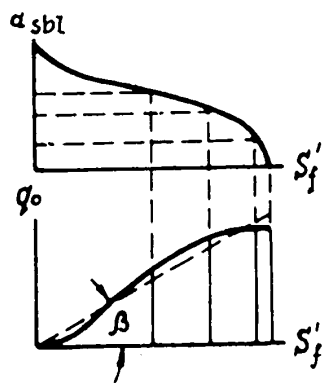Therefore, it is clear that coefficient k = tan β represents the initial distribution of elementary heat sources, while q_0 represents the reserve quantity of heat in a given mass up to the moment of recording the friction process (Fig.36).

The above research study by V.S. Shchedrov permits a sufficiently accurate determination of the boundary conditions for solving the heat problem of friction, on the basis of the heat conductivity theory. To find the temperature value of a given element of a rubbing pair at any point and at any instant of time, it is necessary to substitute the value dq, found in expression (50),

Fig.36 - Graphic Plotting of the Distribution Characteristics of Heat Sources

STAT
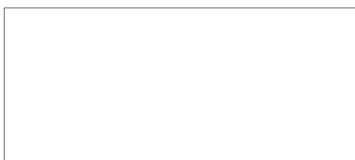
$$d\theta = \frac{2\,dq}{4\pi a\gamma st} \cdot e^{\frac{-r^2}{4at}} \tag{56}$$

in the general theory of heat conductivity (where r is the radius vector of an indicated point).

In conclusion, it should be mentioned that the described method is easily extended to three-dimensional problems; however, for determining q_0 and k this would make it necessary to replace the profile diagrams which give the supporting surface by topograms which reflect the surface contour and give the supporting surface. However, the available data on friction and wear do not yet include the means for quantitative refinement of experimental results in this field.

STAT

CALCULATION OF TEMPERATURE CONDITIONS IN FRICTION TESTING MACHINES

All experimental friction machines can be arranged in a definite sequence depending on the macrogeometry of the reciprocal contact of the tested pair. The extreme limits of this sequence will be the "miniature" machine and the friction machine with complete reciprocal contact overlap. All other testing machines occupy some intermediate position in this sequence.

Proceeding on this basis, we calculated the temperature operating conditions in a "miniature" friction machine as well as in a ring friction machine with complete overlap.

"Miniature" Friction Machine

The development of temperature operating conditions in the "miniature" machine may be reduced to the solution of the following mathematical problem.

Let us examine the friction pair shown in Fig.37. We have a right-angled parallelepiped sliding along the supporting surface represented by the plane xy. The parallelepiped has the edges h_1, h_2, h_3; its rubbing side is $z = 0$.

Let this rubbing side have a mean contact temperature θ^*, while on all other sides a heat exchange with the outer medium whose temperature is equal to zero $(\theta_a = 0)$ takes place, which somewhat simplifies the mathematical computations.

Let us assume that the initial temperature of the parallelepiped is equal to θ_o. With these assumptions, the mathematical problem is reduced to the solution of the equation for heat conductivity (34):

78

STAT

$$\frac{\partial\theta}{\partial t} = a\left(\frac{\partial^2\theta}{\partial x^2} + \frac{\partial^2\theta}{\partial y^2} + \frac{\partial\theta}{\partial z^2}\right).$$

Initial conditions:

$$t = 0; \quad \theta = \theta_0. \tag{57}$$

Boundary conditions:

$$\left. \begin{aligned}
-\frac{\partial\theta}{\partial x} + \sigma\theta = 0 \ \text{ at } \ x = 0; \ \ \frac{\partial\theta}{\partial x} + \sigma\theta = 0 \ \text{ at } \ x = h_1 \\
-\frac{\partial\theta}{\partial y} + \sigma\theta = 0 \ \text{ » } \ y = 0; \ \ \frac{\partial\theta}{\partial y} + \sigma\theta = 0 \ \text{ » } \ y = h_2 \\
\theta = \theta^\bullet \qquad\qquad \text{ » } \ z = 0; \ \ \frac{\partial\theta}{\partial z} + \sigma\theta = 0 \ \text{ » } \ z = h_3
\end{aligned} \right\} \tag{58}$$

We consider the temperature of the outer medium to be independent of time, i.e., θ_a = const = 0, and we reduce our problem to examining two simpler problems.
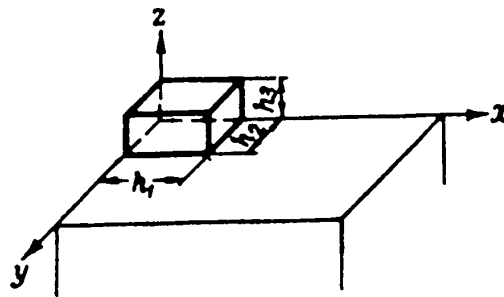

Fig.37 - Friction in a Right-Angled Parallelepipedon Along
the Surface of a Semibound Body

One pertains to the case of a steady distribution of temperatures, i.e., to stationary heat conditions, and the other to the case of an unsteady distribution of temperatures, i.e., to nonstationary heat conditions.

Let us assume that

STAT

$$\theta = \theta' + \theta'',\qquad(59)$$

where θ' is the function of the coordinates of a point only, i.e., $\theta' = \theta'(x, y, z)$, and θ'' is the function of the coordinates of a point and time, i.e., $\theta'' = \theta''(x, y, z, t)$.

For stationary conditions we have

$$\frac{\partial^2\theta'}{\partial x^2} + \frac{\partial^2\theta}{\partial y^2} + \frac{\partial^2\theta}{\partial z^2} = 0.\qquad(60)$$

This equation is actually for the volume inside the parallelepiped with boundary conditions:

$$\left.\begin{array}{ll} -\dfrac{\partial\theta'}{\partial x} + \sigma\theta' = 0 \quad\text{at}\quad x = 0; \quad \dfrac{\partial\theta'}{\partial x} + \sigma\theta' = 0 \ \text{at} \quad x = h_1 \\[2mm] -\dfrac{\partial\theta'}{\partial y} + \sigma\theta' = 0 \quad\text{»}\quad y = 0; \quad \dfrac{\partial\theta'}{\partial y} + \sigma\theta' = 0 \quad\text{»}\quad y = h_2 \\[2mm] \theta' = \theta^\circ f(x, y) \quad\text{»}\quad z = 0; \quad \dfrac{\partial\theta'}{\partial z} + \sigma\theta = 0 \quad\text{»}\quad z = h_3 \end{array}\right\}\qquad(61)$$

For nonstationary conditions we accordingly get the equation

$$\frac{\partial\theta''}{\partial t} = a\left(\frac{\partial^2\theta''}{\partial x^2} + \frac{\partial^2\theta''}{\partial y^2} + \frac{\partial^2\theta''}{\partial z^2}\right).\qquad(62)$$

This equation is likewise valid for the volume inside the parallelepipedon, for the initial condition

$$\theta'' = \theta_0 - \theta' \quad\text{at}\quad t = 0\qquad(63)$$

and for boundary conditions

$$-\frac{\partial\theta''}{\partial x} + \sigma\theta'' = 0 \quad\text{at}\quad x = 0; \quad \frac{\partial\theta''}{\partial x} + \sigma\theta'' = 0 \quad\text{at}\quad x = h_1 \left.\right|\left.\right|$$

80

STAT

$$-\frac{\partial \theta''}{\partial y} + \sigma\theta'' = 0 \quad \text{at} \quad y = 0; \frac{\partial \theta''}{\partial y} + \sigma\theta'' = 0 \quad \text{at} \quad y = h_2 \left. \right\}$$
$$\theta'' = 0 \qquad \text{»} \quad z = 0; \frac{\partial \theta''}{\partial z} + \sigma\theta'' = 0 \quad \text{»} \quad z = h_3 \left. \right\} \qquad (64)$$

Therefore eq.(60) and conditions (61) characterize the stationary temperature distribution in a right-angled parallelepiped, while eq.(62), together with conditions (63) and (64), characterizes an unsteady temperature distribution.

Let us solve each equation separately.

Solution of a Differential Equation of Stationary Temperature Conditions

Let us express the particular solution of eq.(60) in the following form:

$$U = XYf(z), \qquad (65)$$

where

$$X = \cos ix + \frac{\sigma}{l} \sin lx, \qquad (66)$$

$$Y = \cos my + \frac{\sigma}{m} \sin my, \qquad (67)$$

and f(z) is the unknown function which has to be determined in a corresponding manner.

On substituting expressions (66) and (67) in eq.(60) we obtain, after corresponding reductions, the following expression:

$$-l^2 f(z) - m^2 f(z) + f^2(z) = 0 \qquad (68)$$

and denoting

$$n^2 = l^2 + m^2,$$

we finally obtain

STAT

$$f''(z) - n^2 f(z) = 0. \qquad (69)$$

We will write the solution of differential equation (69) in the following form:

$$f(z) = C' e^{nz} + C'' e^{-nz}, \qquad (70)$$

where C' and C'' are arbitrary invariables.

It is apparent that the function

$$\theta' = \sum_{i=0}^{\infty} \sum_{j=0}^{\infty} X_i Y_j \left(C'_{i,j} e^{n_{i,j} z} + C''_{i,j} e^{-n_{i,j} z} \right) A_i A_j \qquad (71)$$

is also the solution for eq.(69) and for eq.(60).

Let us compute the invariables $C'_{i,j}$ and $C''_{i,j}$ so as to satisfy the boundary conditions (61). For this, we will substitute expression (71) in the equation

$$\theta' = \theta^* f(x, y) \quad \text{at} \quad z = 0.$$

Then, we get

$$\sum_{i=0}^{\infty} \sum_{j=0}^{\infty} X_i Y_j \left(C'_{i,j} + C''_{i,j} \right) A_i A_j = \theta^* f(x, y). \qquad (72)$$

It is clear from expression (72) that the total of $C'_{i,j} + C''_{i,j}$ does not depend on the function $f(x,y)$ so that we can write

$$C'_{i,j} + C''_{i,j} = \theta^*. \qquad (73)$$

The remaining parts of expression (72) show that the function $f(x,y)$ is expanded into several forms:

$$f(x, y) = \sum_{i=0}^{\infty} \sum_{j=0}^{\infty} A_i A_j X_i Y_j. \qquad (74)$$

STAT

On substituting expression (71) in another equation of boundary condition (61),

namely in the equation

$$\frac{\partial \theta'}{\partial z} + \sigma \theta' = 0 \quad \text{at} \quad z = h_3,$$

we get

$$C'_{i,j}(n_{i,j} + \sigma)e^{n_{i,j}h_3} - C''_{i,j}(n_{i,j} - \sigma)e^{-n_{i,j}h_3} = 0. \tag{75}$$

From expressions (73) and (75), solving them both together, we find the arbitrary invariables

$$C'_{i,j} = \theta^* \frac{(n_{i,j} - \sigma) e^{-n_{i,j}h_3}}{(n_{i,j} + \sigma) e^{n_{i,j}h_3} + (n_{i,j} - \sigma) e^{-n_{i,j}h_3}};$$

$$C''_{i,j} = \theta^* \frac{(n_{i,j} + \sigma) e^{n_{i,j}h_3}}{(n_{i,j} + \sigma) e^{n_{i,j}h_3} + (n_{i,j} - \sigma) e^{-n_{i,j}h_3}}.$$

Using expression (70) and knowing the quantities $C'_{i,j}$ and $C''_{i,j}$ we determine the function $f(z)$:

$$f(z) = \theta^* \frac{(n_{i,j} - \sigma) e^{-n_{i,j}(h_3-z)} + (n_{i,j} + \sigma) e^{n_{i,j}(h_3-z)}}{(n_{i,j} - \sigma) e^{-n_{i,j}h_3} + (n_{i,j} + \sigma) e^{n_{i,j}h_3}}, \tag{76}$$

Now if we substitute the value of the function $f(z)$, i.e., eq.(76), in expression (71), then the solution of the differential equation (61) for a stationary process is written in the following form:

$$\theta = \sum_{i=0}^{\infty}{}' \sum_{j=0}^{\infty} \theta^* \frac{(n_{i,j} - \sigma) e^{-n_{i,j}(h_3-z)} + (n_{i,j} + \sigma) e^{n_{i,j}(h_3-z)}}{(n_{i,j} - \sigma) e^{-n_{i,j}h_3} + (n_{i,j} + \sigma) e^{n_{i,j}h_3}} \times$$
$$\times X_i Y_j A_i A_j. \tag{77}$$

How easily convinced one can be that the solution of equation (77) also satis-

83

STAT

fies the boundary conditions. (61) at $x = 0$ and $y = 0$.

Next, we will determine the value $n_{i,j}$, i.e., l_i and m_j in order to satisfy the boundary conditions (61) at $x = h_1$ and $y = h_2$.

For this, we substitute expression (65), together with the calculations of eqs.(66) and (67), in the equation

$$\frac{\partial \theta'}{\partial x} + \sigma \theta' = 0 \qquad \text{at} \quad x = h_1;$$

and

$$\frac{\partial \theta'}{\partial y} + \sigma \theta' = 0 \qquad \text{at} \quad y = h_2.$$

After substitution, we obtain

$$2\sigma \cos l_i h_1 + \left(\frac{\sigma^2}{l_i} - l_i\right) \sin l_i h_1 = 0;$$

$$2\sigma \cos m_j h_2 + \left(\frac{\sigma^2}{m_j} - m_j\right) \sin m_j h_2 = 0.$$

After the corresponding reductions, we have

$$\text{tg } l_i h_1 = \frac{2l_i \sigma}{l_i^2 - \sigma^2} \; ; \quad \text{tg } m_j h_2 = \frac{2m_j \sigma}{m_j^2 - \sigma} \cdot \qquad (78)$$

In analyzing eq.(78) it becomes obvious that l_i and m_j must be the positive roots of the equations. Besides, these equations have no imaginary roots of the type $l = l_i'$ and $m = m_i'$, since in this case they would have a position of equality

$$\text{th } l'l + \frac{2\sigma l'}{l'^2 + \sigma^2} = 0; \quad \text{th } m'm + \frac{2\sigma m'}{m'^2 + \sigma^2} = 0,$$

which is impossible since both members of each equation have the same symbol.

It is likewise easy to show that eqs.(78) have no complex roots of the type $a + bi$. If they had such roots, we would have such functions as X_1, X_2, Y_1, and Y_2

STAT

which would satisfy the conditions

$$\int_0^l X_1 X_2 dx = 0; \quad \int_0^m Y_1 Y_2 dy = 0.$$

If we separate the real and imaginary parts in these functions we would have

$$X_1 X_2 = (A + Bi)(A - Bi) = A^2 + B^2 > 0$$

and

$$Y_1 Y_2 = (C + Di)(C - Di) = C^2 + D^2 > 0,$$

which would lead to the impossible ratios

$$\int_0^l (A^2 + B^2)\, dx = 0 \text{ и } \int_0^m (C^2 + D^2)\, dx = 0.$$

Assuming the following symbols in the system of equations (78):
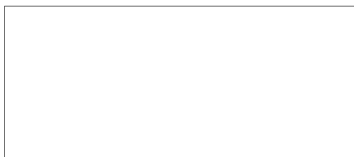
$$l_i h_1 = x, \quad l_i = \frac{x}{h_1}$$

and, reducing the equation, after substituting the symbols, we have

$$\operatorname{tg} l_i h_i = \frac{2\sigma \frac{x}{h_1}}{\frac{x^2}{h_1^2} - \sigma} = \frac{2}{\frac{x}{h_1\sigma} - \frac{h_1\sigma}{x}} = \frac{2}{y},$$

where

$$y = \frac{x}{h_1\sigma} - \frac{h_1\sigma}{x}.$$

Therefore, all roots of eqs.(78) are determined by abscissas of the points of intersection on the curves:

85

STAT

$$y_1 = \frac{x_1}{h_1 \sigma} - \frac{\sigma h_1}{x_1} \text{ and } y_1 = \frac{2}{\operatorname{tg} x_1};$$

$$y_2 = \frac{x_2}{h_2 \sigma} - \frac{\sigma h_2}{x_2} \text{ and } y_2 = \frac{2}{\operatorname{tg} x_2}.$$

(79)

Hence it is obvious that the equations have no multiple roots and the positive roots x_{1_i}, x_{2_j}, as was established earlier, are included in the integrals:

$$0 < x_{1_i} < \pi; \quad \pi < x_{1_i} < 2\pi;$$

$$0 < x_{2_j} < \pi; \quad \pi < x_{2_j} < 2\pi;$$

where i, j = 0, 1, 2, 3.

Let us suppose that the arbitrary function f(x), examined earlier, is expanded to x in a Fourier series with terms of the type, x_1, x_2, ..., and that the coefficients of such a series

$$f(x) = \sum_{i=1}^{\infty} A_i X_i$$

are computed by the formulas

$$A_{2k} = 0; \quad A_{2k} = \frac{4\sigma}{h_1 (l_i^2 + \sigma^2) + 2\sigma};$$

(80)

if analagous conditions are assumed for the variable y, then the particular solution (65)

$$U = XYf(z)$$

leads to the general solution which satisfies the same conditions.

Therefore, after substituting the coefficient values of A_i and A_j, eq.(77) is now written as

STAT

$$\theta' = 16\sigma^2\theta^\bullet \sum_i \sum_j \frac{(n_{ij} - \sigma)\,e^{-n_{ij}(h_s-z)} + (n_{ij} + \sigma)\,e^{n_{ij}(h_s-z)}}{(n_{ij} - \sigma)\,e^{-n_{ij}h_s} + (n_{ij} + \sigma)\,e^{n_{ij}h_s}} \times$$

$$\times \frac{X_{2i+1}}{h_1\,(c_{2i+1}^2 + \sigma^2) + 2\sigma} \cdot \frac{Y_{2j+1}}{h_2\,(m_{2j+1}^2 + \sigma^2) + 2\sigma}. \qquad (81)$$

Expression (81) is the solution of the differential equation for stationary temperature conditions (60) with the boundary conditions (61).

Solution of a Differential Equation for Nonstationary Temperature Conditions

Let us look for a particular solution of eq.(62) in the form

$$u' = A_1 XY \sin p_\kappa z e^{-a(l^2+m^2+p^2)t}, \qquad (82)$$

where X and Y are the functions computed from eqs.(66) and (67).

The solution in this form, as easily proved by substitution, satisfies eq.(62) and the boundary conditions of eq.(64).

Therefore, the general solution which also satisfies the initial condition (63) has the form

$$\theta' = \sum_i \sum_j \sum_k A_{l,m,p}\, X_{2i+1}\, Y_{2j+1} \sin p_\kappa z e^{-a\left(l_{2i+1}^2 + m_{2j+1}^2 + p_\kappa^2\right)t}, \qquad (83)$$

where

$$A_{l,m,p} = \frac{8 l_{2i+1}^2 m_{2j+1}^2 \left(p_\kappa^2 + \sigma^2\right)}{\left[h_1(l_{2i+1}^2 + \sigma^2) + 2\sigma\right]\left[h_2\left(m_{2j+1}^2 + \sigma^2\right) + 2\sigma\right]\left[h_3 p_\kappa^2 + \sigma(1 + \sigma h_3)\right]} \times$$

$$\times \int_0^{h_3} \int_0^{h_2} \int_0^{h_1} (\theta_0 - \theta'_{(x,y,z)}) \left(\cos l_{2i+1}x + \frac{\sigma}{l_{2i+1}} \sin l_{2i+1}x\right) \times$$

$$\times \left(\cos m_{2j+1}y + \frac{\sigma}{m_{2j+1}} \sin m_{2j+1}y\right)\sin p_\kappa z\, dx\, dy\, dz. \qquad (84)$$

STAT

Substituting the value of the coefficient $\mathrm{A}l,\mathrm{m,p}$ in expression (83) we get

$$
\theta'' = \sum_i \sum_j \sum_k X_{2i+1} Y_{2j+1} \sin p_{\kappa} z \, e^{-a\left(l^2_{2i+1} + m^2_{2j+1} + p^2_{\kappa} \right) t} \times
$$

$$
\times \left\{ \frac{8\theta_0 l^2_{2i+1} m^2_{2j+1} \left(p^2_{\kappa} + \sigma^2 \right)}{\left[h_1 \left(l^2_{2i+1} + \sigma^2 \right) + 2\sigma \right] \left[h_2 \left(m^2_{2j+1} + \sigma^2 \right) + 2\sigma \right] \left[h_3 p^2_{\kappa} + \sigma \left(1 + \sigma h_3 \right) \right]} \times \right.
$$

$$
\times \int_0^{h_3} \int_0^{h_2} \int_0^{h_1} X_{2i+1} Y_{2j+1} \sin p_{\kappa} z \, dx \, dy \, dz -
$$

$$
- \frac{8 l^2_{2i+1} m^2_{2j+1} \left(p^2_{\kappa} + \sigma^2 \right)}{\left[h_1 \left(l^2_{2i+1} + \sigma^2 \right) + 2\sigma \right] \left[h_2 \left(m^2_{2j+1} + \sigma^2 \right) + 2\sigma \right] \left[h_3 p^2_{\kappa} + \sigma \left(1 + \sigma h_3 \right) \right]} \times
$$

$$
\left. \times \int_0^{h_3} \int_0^{h_2} \int_0^{h_1} \theta'_{(x,y,z)} X_{2i+1} Y_{2j+1} \sin p_{\kappa} z \, dx \, dy \, dz \right\} \qquad (85)
$$

and further, after completing certain computations,

$$
\theta'' = \sum_i \sum_j \sum_k X_{2i+1} Y_{2j+1} \sin p_{\kappa} z \, e^{-a\left(l^2_{2i+1} + m^2_{2j+1} + p^2_{\kappa} \right) t} \times
$$

$$
\times \left\{ \frac{64\theta_0 \sigma^3 \left(p^2_{\kappa} + \sigma^2 \right) \sin^2 \dfrac{p_{\kappa} h_3}{2}}{p_{\kappa} \left[h_1 \left(l^2_{2i+1} + \sigma^2 \right) + 2\sigma \right] \left[h_2 \left(m^2_{2j+1} + \sigma^2 \right) + 2\sigma \right] \left[h_3 p^2_{\kappa} + \sigma \left(1 + \sigma h_3 \right) \right]} - \right.
$$

$$
- \frac{8 l^2_{2i+1} m^2_{2j+1} \cdot \left(p^2_{\kappa} + \sigma^2 \right)}{\left[h_1 \left(l^2_{2i+1} + \sigma^2 \right) + 2\sigma \right] \left[h_2 \left(m^2_{2j+1} + \sigma^2 \right) + 2\sigma \right] \left[h_3 p^3_{\kappa} + \sigma \left(1 + \sigma h_3 \right) \right]} \times
$$

$$
\left. \times \int_0^{h_3} \int_0^{h_2} \int_0^{h_1} \theta'_{(x,y,z)} X_{2i+1} Y_{2j+1} \sin p_{\kappa} z \, dx \, dy \, dz \right\}, \qquad (86)
$$

where $\theta'_{(x,y,z)}$, is the established temperature determined by eq.(81), and p_k is the positive root of the system of equations, determined by analogy with l and m from the boundary conditions (64):

$$
y = \mathrm{ctg} \, p_{\kappa} h_3 \quad \text{и} \quad y = - \frac{\sigma}{p_{\kappa}}. \qquad (86')
$$

88

STAT

Then, knowing the values of θ' and θ'' and adding them, we get the solution of the general differential equation (34) with the initial and boundary conditions (58), as follows:

$$\theta = 16\sigma^2\theta^* \sum_i \sum_j \frac{(n_{ij}-\sigma)e^{-n_{ij}(h_3-z)} + (n_{ij}+\sigma)\,e^{n_{ij}(h_3-z)}}{(n_{ij}-\sigma)\,e^{-n_{ij}h_3} + (n_{ij}+\sigma)\,e^{n_{ij}h_3}} \times$$

$$\times \frac{X_{2i+1}}{h_1(l^2_{2i+1}+\sigma^2)+2\sigma} \cdot \frac{Y_{2j+1}}{h_2(m^2_{2j+1}+\sigma^2)+2\sigma} +$$

$$+ \sum_i \sum_j \sum_k X_{2i+1}Y_{2j+1} \sin p_\kappa z \, e^{-a(l^2_{2i+1}+m^2_{2j+1}+p^2_\kappa)t} \times$$

$$\times \left\{ \frac{64\theta_0\sigma^2\,(p^2_\kappa+\sigma^2)\sin^2\dfrac{p_\kappa h_3}{2} \cdot}{p_\kappa[h_1(l^2_{2i+1}+\sigma^2)+2\sigma][h_2(m^2_{2j+1}+\sigma^2)+2\sigma][h_3 p^2_\kappa+\sigma(1+\sigma h_3)]} - \right.$$

$$- \frac{8l^2_{2i+1}m^2_{2j+1}\,(p^2_\kappa+\sigma^2)}{[h_1(l^2_{2i+1}+\sigma^2)+2\sigma][h_2(m^2_{2j+1}+\sigma^2)+2\sigma][h_3 p^2_\kappa+\sigma(1+\sigma h_3)]} \times$$

$$\left. \times \int_0^{h_3}\int_0^{h_2}\int_0^{h_1} \theta'_{(x,y,z)}X_{2i+1}Y_{2j+1} \sin p_\kappa z \, dx\, dy\, dz \right\}. \qquad (87)$$

When $t \to \infty$, the expression (87) determines the stationary temperature distribution which does not depend on θ_0.

Equation (87) makes it possible to determine the mean temperature of contact θ^* during set friction conditions, i.e., after the lapse of an adequate length of time from the instant the friction process started. Let us assume the following condition namely, that the general quantity of heat generated at the expense of the work of the friction forces is subdivided into a definite ratio between the parallelepiped and the supporting surface (Fig.37). Let the quantity of heat, flowing through the parallelepiped per second, be

$$Q' = Jfpv_{S\kappa}(1 - \alpha_{TP}), \qquad (88)$$

89

STAT

where J = heat equivalent of mechanical work;

f = coefficient of friction;

p = load;

v_{sk} = sliding speed;

$(1-\alpha_{TP})$ = factor always smaller than unity, which determines the quantity of heat branching into the parallelepiped.

The quantity of heat that has entered the parallelepiped during steady heat conditions flows into the surrounding space through a side surface of the parallelepiped and through its top side

$$Q' = \sigma'\left(2\int_0^{h_2}\int_0^{h_3}\theta\,dy\,dz + 2\int_0^{h_1}\int_0^{h_3}\theta\,dx\,dz + \int_0^{h_1}\int_0^{h_2}\theta\,dx\,dy\right),\ (89)$$

where σ' is the coefficient of outer heat emission of the parallelepiped material.

Adjusting the right-hand terms of eqs.(88) and (89) and substituting the value θ from eq.(87), we get the following relationship:

$$Jfpv_{sk}(1-\alpha_{TP}) = 32\sigma^2\theta^\circ\sigma'\sum_{i=0}^\infty\sum_{j=0}^\infty \times$$

$$\times \frac{X_{2i+1}}{\left[(n_{i,j}-\sigma)e^{-n_{i,j}h_3}+(n_{i,j}+\sigma)e^{n_{i,j}h_3}\right]\times} \rightarrow$$

$$\rightarrow \frac{X_{2i+1}}{\times[h_1(l_{2i+1}^2+\sigma^2)+2\sigma][h_2(m_{2j+1}^2+\sigma^2)+2\sigma]} \times$$

$$\times \int_0^{h_2}\int_0^{h_3}[(n_{i,j}-\sigma)e^{-n_{i,j}(h_3-z)}+(n_{i,j}+\sigma)e^{n_{i,j}(h_3-z)} \times$$

$$\times [\cos m_{2j+1}y + \frac{\sigma}{m_{2j+1}}\sin m_{2j+1}y]\,dy\,dz + 32\sigma^2\theta^\circ\sigma' \times$$

$$\times \sum_{i=0}^\infty\sum_{j=0}^\infty \frac{Y_{2j+1}}{\left[(n_{i,j}-\sigma)e^{-n_{i,j}h_3}+(n_{i,j}+\sigma)e^{n_{i,j}h_3}\right]\times} \rightarrow$$

90

STAT

$$\rightarrow \frac{Y_{2j+1}}{\times \left[h_1\left(l^2_{2i+1}+\sigma^2\right)+2\sigma\right]\left[h_2\left(m^2_{2j+1}+\sigma^2\right)+2\sigma\right]} \times$$

$$\times \int_0^{h_1}\int_0^{h_2} \left[(n_{i,j}-\sigma)\,e^{-n_{i,j}(h_2-z)}+(n+\sigma)\,e^{n_{i,j}(h_2-z)}\right] \times$$

$$\times \left[\cos l_{2i+1}x + \frac{\sigma}{l_{2i+1}}\sin l_{2i+1}x\right]dx\,dz + 16\sigma^2\theta^{\circ}\sigma' \times$$

$$\times \sum_{i=0}^{\infty}\sum_{j=0}^{\infty} \frac{(n_{i,j}-\sigma)\,e^{-n_{i,j}(h_2-z)}+(n_{i,j}+\sigma)\,e^{n_{i,j}(h_2-z)}}{\left[(n_{i,j}-\sigma)\,e^{-n_{i,j}h_2}+(n_{i,j}+\sigma)\,e^{n_{i,j}h_2}\right]\times} \rightarrow$$

$$\rightarrow \frac{(n_{i,j}-\sigma)\,e^{-n_{i,j}(h_2-z)}+(n_{i,j}+\sigma)\,e^{n_{i,j}(h_2-z)}}{\times \left[h_1\left(l^2_{2i+1}+\sigma^2\right)+2\sigma\right]\left[h_2\left(m^2_{2j+1}+\sigma^2\right)+2\sigma\right]} \times$$

$$\times \int_0^{h_1}\int_0^{h_2} X_{2i+1}Y_{2j+1}dx\,dy \ldots \qquad (90)$$

With the condition that z = 0, we calculate the integrals appearing in eq.(90); then

$$A_{y_{ji}} = \left[\frac{n_{ij}-\sigma}{n_{ij}}\left(1-e^{-n_{ij}h_2}\right)-\frac{u_{ij}+\sigma}{n_{ij}}\left(1-e^{n_{ij}h_2}\right)\right] \times$$

$$\times \frac{1}{m_{2j+1}}\left(\sin m_{2j+1}h_2 + \frac{2\sigma}{m_{2j+1}}\sin^2\frac{m_{2j+1}h_2}{2}\right); \qquad (91)$$

$$B_{x_{ij}} = \left[\frac{n_{ij}-\sigma}{n_{ij}}\left(1-e^{-n_{ij}h_2}\right)-\frac{n_{ij}+\sigma}{n_{ij}}\left(1-e^{n_{ij}h_2}\right)\right] \times$$

$$\times \frac{1}{l_{2i+1}}\left(\sin l_{2i+1}h_1 + \frac{2\sigma}{l_{2i+1}}\sin^2\frac{l_{2i+1}h_1}{2}\right); \qquad (92)$$

$$L_{ij} = \left[(n_{ij}-\sigma)e^{-n_{ij}h_2}+(n_{ij}+\sigma)\,e^{n_{ij}h_2}\right]\left[h_1\left(l^2_{2i+1}+\sigma^2\right)+2\sigma\right] \times$$

$$\times \left[h_2\left(m^2_{2j+1}+\sigma^2\right)+2\sigma\right]; \qquad (93)$$

$$N_{ij} = \left[h_1\left(l^2_{2i+1}+\sigma^2\right)+2\sigma\right]\left[h_2\left(m^2_{2j+1}+\sigma^2\right)+2\sigma\right]. \qquad (94)$$

91

STAT

Now, taking into account eqs.(91) - (94) we can write eq.(90) in the following manner:

$$Jfpv_{\text{SK}}(1 - \alpha_{\text{TP}}) = 32\sigma^2\sigma\theta^* \sum_i \sum_j \times$$

$$\times \frac{A_{y_{i,j}}X_{2i+1} + B_{x_{ij}}Y_{2j+1}}{L_{ij}} + 16\sigma^2\sigma\theta^* \times$$

$$\times \sum_i \sum_j \frac{\left(\sin l_{2i+1}h_1 + \frac{2\sigma}{l_{2i+1}}\sin^2\frac{l_{2i+1}h_1}{2}\right) \times}{N'_{ij}} \rightarrow$$

$$\rightarrow \frac{\times \left(\sin m_{2j+1}h_2 + \frac{2\sigma}{m_{2j+1}}\sin^2\frac{m_{2j+1}h_2}{2}\right)}{N_{ij}} . \qquad (95)$$

It is easy to obtain the temperature distribution along the surface of a right-angled contact from eq.(95)

$$\theta^* = (1 - \alpha_{\text{TP}}) \frac{Jfpv_{\text{SK}}}{16\sigma^2\sigma' \sum_{i=0}^{\infty} \sum_{j=0}^{\infty} \left(2\dfrac{A_{y_{i,j}}X_{2i+1} + B_{x_{i,j}}Y_{2j+1}}{L_{i,j}} + \dfrac{X^*_{2i+1}Y^*_{2j+1}}{N_{i,j}}\right)} , \qquad (96)$$

where

$$X^*_{2i+1} = \sin l_{2i+1}h_1 + \frac{2\sigma}{l_{2i+1}}\sin^2\frac{l_{2i+1}h_1}{2} ; \qquad (97)$$

$$Y^*_{2j+1} = \sin m_{2j+1}h_2 + \frac{2\sigma}{m_{2j+1}}\sin^2\frac{m_{2j+1}h_2}{2} . \qquad (98)$$

Summarizing all above statements, the following conclusion can be drawn:

Equation (96) makes it possible to compute the mean temperature of a friction surface of a right-angled parallelepiped while sliding along a semibound body, which practically maintains a constant temperature because of its unlimited great

92

STAT

heat capacity.

When friction of quite commensurate bodies takes place, for example if the supporting body is also a right-angled parallelepiped with edges h_1', h_2' and h_3', whose material is characterized by the thermal parameters of λ_1 and σ_1', a solution is possible, under the condition that the incomplete overlapping of rubbing bases at each instant of time is disregarded, i.e., when $h_1' \approx h_1$ and $h_2' \approx h_2$:

$$\theta_1^* = \alpha_{TP} \frac{J f p v_{SH}}{16\sigma_1^2 \sigma_1' \displaystyle\sum_{i=0}^{\infty} \sum_{j=0}^{\infty} \left(2\frac{A_{v_{i,j}}' X_{2i+1}' + B_{x_{i,j}}' Y_{2j+1}'}{L_{i,j}'} + \frac{X_{2i+1}^{*'} Y_{2j+1}^{*'}}{N_{i,j}'} \right)} \cdot \tag{99}$$

Solutions of eqs.(96) and (99) are found for a case of stabilized temperature distribution. This case might play an especially important role in studying the effects of the temperature influence on the mechanical as well as the frictional properties of materials in the rubbing pair in various test setups.

If we accept the condition of the absence of temperature discontinuities along the friction surface at $\theta^* = \theta_1^*$, we can determine the coefficient of distribution of the quantity of heat between the elements of the rubbing pair. To do this, we adjust the right-hand terms of eqs.(96) and (99) and solve the resulting equation pertaining to α_{Tp}; then, we have

$$\alpha_{TP} = \frac{\sigma_1^2 \sigma_1' \displaystyle\sum_{i\ 0}^{\infty} \sum_{j\ 0}^{\infty} \left(2\frac{A_{v_{i,j}}' X_{2i+1}' + B_{x_{i,j}}' Y_{2j+1}'}{L_{i,j}'} + \frac{X_{2i+1}^{*'} Y_{2j+1}^{*'}}{N_{i,j}'} \right)}{\sigma^2 \sigma' \displaystyle\sum_{i=0}^{\infty} \sum_{j=0}^{\infty} \left(2\frac{A_{v_{i,j}} X_{2i+1} + B_{x_{i,j}} Y_{2j+1}}{L_{i,j}} + \frac{X_{2i+1}^{*} Y_{2j+1}^{*}}{N_{i,j}} \right) + } \longrightarrow$$

$$\longrightarrow \frac{\sigma_1^2 \sigma_1' \displaystyle\sum_{i\ 0}^{\infty} \sum_{j=0}^{\infty} \left(2\frac{A_{v_{i,j}}' X_{2i+1}' + B_{x_{i,j}}' Y_{2j+1}'}{L_{i,j}'} + \frac{X_{2i-1}^{*'} Y_{2j+1}^{*'}}{N_{i,j}'} \right)}{+ \sigma_1^2 \sigma_1' \displaystyle\sum_{i=0}^{\infty} \sum_{j=0}^{\infty} \left(2\frac{A_{v_{i,j}}' X_{2i+1} + B_{x_{i,j}}' Y_{2j+1}'}{L_{i,j}'} + \frac{X_{2i+1}^{*'} Y_{2j+1}^{*''}}{N_{i,j}'} \right)} \cdot \tag{100}$$

Equation (100) permits the very important conclusion that the coefficient α_{Tp}, in first approximation, does not depend on the sliding speed and is only a function of the thermal parameters and geometric dimensions which characterize the elements of the rubbing pair.

Then, substituting the value α_{Tp} from eq.(100) into eq.(99), we finally obtain the value of the mean temperature on a friction surface:

$$\theta = \cfrac{J f p v_{sk}}{16 \left[\sigma^2 \sigma' \sum_{i=0}^{\infty} \sum_{j=0}^{\infty} \left(2 \cfrac{A_{\nu_{i,j}} X_{2i+1} + B_{x_{i,j}} Y_{2j+1}}{L_{i,j}} + \cfrac{X_{2i+1}^{*} X_{2j+1}^{*}}{N_{i,j}} \right) + \right.} \longrightarrow$$

$$\longrightarrow \cfrac{J f p v_{sk}}{\left. + \sigma_1^2 \sigma_1' \sum_{i=0}^{\infty} \sum_{j=0}^{\infty} \left(2 \cfrac{A'_{\nu_{i,j}} X'_{2i+1} + B'_{x_{i,j}} Y'_{2j+1}}{L'_{i,j}} + \cfrac{X_{2i+1}^{*'} Y_{2j+1}^{*'}}{N'_{i,j}} \right) \right]} \qquad .(101)$$

Here it should be noted that, for an element of a counterbody, $z < 0$.

Therefore eqs.(96), (99), and (100) permit determining one of the unknown temperature characteristics, namely, the mean temperature of a friction surface.

To find the other temperature characteristic – the temperature gradient $\dfrac{\partial \theta}{\partial z}$ – – eq.(90) can be used, from which θ must be determined with a corresponding differentiation of the left- and right-hand terms of this equation according to ∂z, $\dfrac{\partial \theta}{\partial z}$. However, this method is too cumbersome and requires excessive time for computing the numerical values of the gradients.

For our concrete study of a parallelepiped, sliding along the surface xy or along the surface of another parallelepiped commensurate in dimensions, it can be stated, that, along the axis of symmetry parallel to (or coinciding with) the axis z, the heat flow is linear. If we accept this condition, it is easier to determine the temperature gradient $\dfrac{\partial \theta}{\partial z}$ along this axis, for stationary heat conditions.

For this case, the general equation for heat conductivity assumes, as is generally known, the following particular form:

STAT
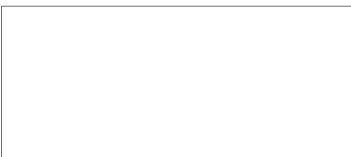
$$\frac{\partial^2 \theta}{\partial z^2} - b^2 \theta = 0, \tag{102}$$

so that the integral of eq.(102) can be written as

$$\theta = C_1 e^{bz} + C_2 e^{-bz}, \tag{103}$$

where

$$b = \sqrt{\frac{2(h_1 + h_2)\sigma'}{\lambda h_1 h_2}} = \sqrt{\frac{2(h_1 + h_2)\sigma}{h_1 h_2}}. \tag{104}$$

Here $\sigma = \dfrac{\sigma'}{\lambda}$, where σ' is the coefficient of heat emission and λ is the coefficient of heat conductivity.

Since the studied parallelepiped has limited dimensions in the direction of the axis z, the boundary condition for determining the arbitrary invariables C_1 and C_2, at $z = h_3$, will be

$$\sigma \theta_{h_3} = -\lambda \left| \frac{\partial \theta}{\partial z} \right|_{z=h_3}. \tag{105}$$

In eq.(105) let us substitute the value θ from the general solution (103) and, after reducing it somewhat, obtain

$$C_1 e^{bh_3}(b\lambda + \sigma') = C_2 e^{-bh_3}(b\lambda - \sigma')$$

or in other words,

$$C_1 e^{bh_3}(b + \sigma) = C_2 e^{-bh_3}(b - \sigma). \tag{106}$$

The other boundary condition for determining arbitrary invariables is the condition of heat balance:

$$(1 - \alpha_{TP}) J/pv_{SK} = 2(h_1 + h_2)\sigma' \left[C_1 \int_0^{h_3} e^{bz} dz + C_2 \int_0^{h_3} e^{-bz} dz \right] +$$

95

STAT

$$+ h_1 h_2 \mathfrak{z}' (C_1 e^{bh_3} + C_2 e^{-bh_3}) \ldots, \qquad (107)$$

where the quantities α_{Tp}, J, f, p, v_{sk} are the same as before.

Solving eqs.(106) and (107) together we find

$$\left.\begin{array}{l}
C_1 = \dfrac{(1 - \alpha_{TP}) J f p v_{SK} b e^{-bh_3} (b - \sigma)}{2\sigma' \{(h_1 + h_2)[e^{bh_3}(b+\sigma) + e^{-bh_3}(b-\sigma) - 2\sigma] + h_1 h_2 b^2\}}, \\[2ex]
C_2 = \dfrac{(1 - \alpha_{TP}) J f p v_{SK} b e^{bh_3} (b + \sigma)}{2\sigma' \{(h_1 + h_2)[e^{bh_3}(b+\sigma) + e^{-bh_3}(b-\sigma) - 2\sigma] + h_1 h_2 b^2\}}.
\end{array}\right\} \quad (108)$$

Treating the quantities C_1 and C_2 as numbers it is easy to determine the temperature gradient

$$\frac{\partial \theta}{\partial z} = b (C_1 e^{bz} - C_2 e^{-bz}) \qquad (109)$$

or

$$\frac{\partial \theta}{\partial z} = \sqrt{\frac{2(h_1 + h_2)\sigma}{h_1 h_2}} \left(C_1 e^{\sqrt{\frac{2(h_1+h_2)\sigma}{h_1 h_2}} z} - C_2 e^{-\sqrt{\frac{2(h_1+h_2)}{h_1 h_2}} z} \right). \qquad (109')$$

Therefore, summarizing all above statements, it is possible to draw a basic conclusion on the principles of testing brake materials.

In order to obtain the actual values for the temperature characteristics in testing small samples of brake materials (elements of the friction pair), it is necessary to have in the small power testing setups the same values of the coefficient α_{Tp} which would sufficiently correspond to the values α_{Tp} in the actual friction units.

On this basis, the coefficient α_{Tp} can be considered a certain criterion of similarity in friction processes.

Ring Friction Machine with Complete Reciprocal Overlapping

It is more convenient to study the conditions of heat generation in the opera-

STAT

tion of a friction machine with complete reciprocal contact overlap, in terms of cylindrical coordinates. Figure 38 shows a friction pair of interest to us.

In cylindrical coordinates, the position of any point M in space is determined by the coordinates r, φ, z, where

$$x = r \cos \varphi,$$
$$y = r \sin \varphi,$$
$$z = z.$$
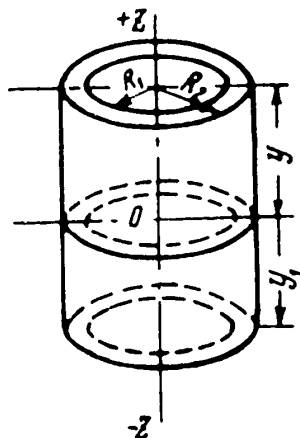
In this case, the general differential equation of heat conductivity (34), written earlier for Cartesian coordinates, now assumes the form

$$\frac{\partial \theta}{\partial t} = a \left(\frac{\partial^2 \theta}{\partial r^2} + \frac{1}{r} \frac{\partial \theta}{\partial r} + \frac{1}{r^2} \frac{\partial^2 \theta}{\partial r^2} + \frac{\partial^2 \theta}{\partial z^2} \right).$$

$$(110)$$

Fig.38 – Friction of Butting Ends in Ring Cylinder

For a concrete case (Fig.38) of a symmetrical axis problem of friction at the ends of two cylindrical rings, eq.(110) is somewhat simplified and assumes the following form for the inside volume of cylindrical rings:

$$\frac{\partial \theta}{\partial t} = a \left(\frac{\partial^2 \theta}{\partial r^2} + \frac{1}{r} \frac{\partial \theta}{\partial r} + \frac{\partial^2 \theta}{\partial z^2} \right),$$

$$(111)$$

where initial conditions, at

$$t = 0; \quad \theta = \theta_0$$

$$(112)$$

and the boundary conditions

$$-\frac{\partial \theta}{\partial r} + \sigma \theta = 0 \quad \text{at} \quad r = R_1;$$
$$\frac{\partial \theta}{\partial r} + \sigma \theta = 0 \quad \text{at} \quad r = R_2;$$
$$\theta = \theta^* \quad \text{at} \quad z = 0 \text{ and } \frac{\partial \theta}{\partial z} + \sigma \theta = 0 \quad \text{at} \quad z = h,$$

$$(113)$$

97

STAT

where R_1 = inner radius of a cylindrical ring;

R_2 = outer radius of a cylindrical ring;

h = height of a circular cylinder.

Of course, the height h of one or another element of the friction pair may be different, i.e., $h \neq h'$.

Just as was done earlier in the case of the "miniature" machine, we will consider two separate problems: stationary and nonstationary heat conditions. In this case,

$$\theta = \theta' + \theta'',\qquad (114)$$

where $\theta' = \theta'$ (r,z) and $\theta'' = \theta''$ $(r,\ z,\ t)$.

The general differential equation (111) for stationary conditions assumes the form

$$\frac{\partial^2 \theta'}{\partial r^2} + \frac{1}{r}\frac{\partial \theta'}{\partial r} + \frac{\partial^2 \theta'}{\partial z} = 0 \qquad (115)$$

with the boundary conditions

$$\left. \begin{array}{ll} -\dfrac{\partial \theta'}{\partial r} + \sigma\theta' = 0 & \text{at} \quad r = R_1; \\[2mm] +\dfrac{\partial \theta'}{\partial r} + \sigma\theta' = 0 & \text{at} \quad r = R_2; \\[2mm] \theta' = \theta^* \quad \text{at} \quad z = 0 \ \text{and} \ \dfrac{\partial \theta'}{\partial z} + \sigma\theta' = 0 & \text{at} \quad z = h. \end{array} \right\} \qquad (116)$$

Nonstationary heat conditions are characterized by the equation

$$\frac{\partial \theta''}{\partial t} = a\left(\frac{\partial^2 \theta''}{\partial r^2} + \frac{1}{r}\frac{\partial \theta''}{\partial r} + \frac{\partial^2 \theta''}{\partial z^2}\right); \qquad (117)$$

with the initial condition

$$\theta'' = \theta_0 - \theta' \quad \text{at} \quad t = 0 \qquad (118)$$

98

STAT

and the boundary conditions

$$-\frac{\partial \theta''}{\partial r} + \sigma\theta'' = 0 \quad \text{at} \quad r = R_1; \quad \frac{\partial \theta''}{\partial r} + \sigma\theta'' = 0 \quad \text{at} \quad r = R_2, \\ \theta'' = 0 \quad \text{at} \quad z = 0; \quad \frac{\partial \theta''}{\partial r} + \sigma\theta'' = 0 \quad \text{at} \quad z = h, \tag{119}$$

where θ_0 is the initial temperature distribution in a circular cylinder.

Let us solve each problem separately.

Solution of a Differential Equation for Stationary Heat Conditions

Solving eq.(115) by the Fourier method, we assume that

$$\theta' = RZ. \tag{120}$$

After substituting expression (120) in eq.(115) we get

$$ZR'' + \frac{1}{r} ZR' + RZ'' = 0$$

or, dividing the left and right-hand terms by RZ,

$$\frac{R''}{R} + \frac{1}{r}\frac{R'}{R} + \frac{Z''}{Z} = 0. \tag{121}$$

This equality is possible only when

$$+ \left(\frac{R''}{R} + \frac{1}{r}\frac{R'}{R} \right) = \rho^2 \tag{122}$$

and

$$\frac{Z''}{Z} = -\rho^2. \tag{123}$$

We solve eqs.(122) and (123) separately and then write eq.(122) in the following manner:

$$\frac{d^2R}{dr^2} + \frac{1}{r}\frac{dR}{dr} - \rho^2 R = 0. \tag{124}$$

STAT

Equation (124) is a canonical Bessel equation. The solution of this equation has the form (Bibl.26) of

$$R_1 = C_1 J_0 (\rho r) + C_2 Y_0 (\rho r),\qquad (125)$$

where $J_0(\rho r)$ is a Bessel function of zero order of the first kind; $Y_0(\rho r)$ is a Bessel function of zero order of the second kind.

To solve eq.(123), let us write it in the following form:

$$Z'' + \rho^2 Z = 0. \qquad (126)$$

The solution of eq.(126) may be presented in the following manner:

$$Z = C_3 \cos \rho (z + z_0). \qquad (127)$$

Therefore, the partial solution for eq.(115) can then be written as

$$\theta'_{part} = C_3 \cos \rho (z + z_0) [C_1 J_0 (\rho r) + C_2 Y_0 (\rho r)].$$

Placing the arbitrary invariable C_3 into parentheses we get

$$\theta'_{part} = \cos \rho (z + z_0) [C' J_0 (\rho r) + C'' Y_0 (\rho r)].$$

The general solution will then be

$$\theta' = \sum_i \cos \rho_i (z + z_0) [C'_i J_0 (\rho_i r) + C''_i Y_0 (\rho_i r)], \qquad (128)$$

which also satisfies eq.(115) and the boundary conditions of eq.(116). At z = 0, we have $\theta' = \theta*$. Therefore,

$$\theta* = \sum_i \cos \rho_i z_0 [C'_i J_0 (\rho_i r) + C''_i Y_0 (\rho_i r)]. \qquad (129)$$

Using an artificial way of multiplying both sides by (1 + 1) and expanding the left-hand side into the following series:

100

STAT

$$1 + 1 = B_1 J_0(\rho_i r) + B_2 J_0(\rho_i r) \; \vdots \; \ldots + B_1' Y_0(\rho_i r) +$$

$$+ B_2' Y_0(\rho_i r) + \ldots = \sum_i B_i J_0(\rho_i r) + \sum_i B_i' Y_0(\rho_i r). \quad (130)$$

Then, expression (129) may be written as follows:

$$\theta^\bullet \sum_i [B_i J_0(\rho_i r) + B_i' Y_0(\rho_i r)] = \sum_i 2 \cos \rho_i z_0 \, [C_i' J_0(\rho_i r) +$$

$$+ C_i'' Y_0(\rho_i r)], \quad (131)$$

from which we find C_i' and C_i'';

$$C_i' = \frac{B_i \theta^\bullet}{2 \cos \rho_i z_0} \; ; \quad (132)$$

$$C_i'' = \frac{B_i' \theta^\bullet}{2 \cos \rho_i z_0} \, . \quad (133)$$

At $z = h$, the boundary conditions of eq.(116) yield

$$[- \rho_i \sin \rho_i (h + z_0) + \sigma \cos \rho_i (h + z_0)] \, [C_i J_0(\rho_i r) +$$

$$+ C_i' Y_0(\rho_i r)] \, r = 0. \quad (134)$$

In expression (134), only the first parentheses can be equal to zero, so that

$$\operatorname{tg} \rho_i (h + z_0) = \frac{\sigma}{\rho_i} \; ; \quad (135)$$

$$z_0 = \frac{\operatorname{arc\,tg} \dfrac{\sigma}{\rho_i} - \rho_i h}{\rho_i} = \frac{\operatorname{arc\,tg} \dfrac{\sigma}{\rho_i}}{\rho_i} - h. \quad (136)$$

From the boundary conditions (116), at $r = R_1$ and $r = R_2$, we find

$$C_i' [\rho_i J_0'(\rho_i R_1) - \sigma J_0(\rho_i R_1)] + C_i'' [\rho_i Y_0'(\rho_i R_1) -$$

$$- \sigma Y_0(\rho_i R_1)] = 0; \quad (137)$$

STAT

$$C_i' [\rho_i J_0' (\rho_i R_2) + \sigma J_0 (\rho_i R_2)] + C_i'' [\rho_i Y_0' (\rho_i R_2) + \\ + \sigma Y_0 (\rho_i R_2)] = 0. \tag{138}$$

It is clear that this is possible only when each of the terms in eqs.(137) and (138) in parentheses is equal to zero, i.e.,

$$\rho_i J_0' (\rho_i R_1) - \sigma J_0 (\rho_i R_1) = 0; \tag{139}$$

$$\rho_i J_0' (\rho_i R_2) + \sigma J_0 (\rho_i R_2) = 0; \tag{140}$$

$$\rho_i Y_0' (\rho_i R_1) - \sigma Y_0 (\rho_i R_1) = 0; \tag{141}$$

$$\rho_i Y_0' (\rho_i R_2) + \sigma Y_0 (\rho_i R_2) = 0. \tag{142}$$

The relationships of (139) - (142) are possible when ρ_i is the root of the corresponding equation.

From the general theory of the Bessel function (Bibl.32, 33) it is known that

$$\int_0^R r J_n^2 (\rho r)\, dr = \frac{R^2}{2} \left[J_n'^2 (\rho R) + \left(1 - \frac{n^2}{R^2 \rho^2} \right) J_n^2 (\rho R) \right]. \tag{143}$$

If ρ is the root of the equations, then

$$\rho J_n' (\rho R) \pm \sigma J_n (\rho R) = 0 \tag{144}$$

and eq.(143) is simplified and assumes the form

$$\int_0^R r J_n^2 (\rho r)\, dr = \frac{1}{2\rho^2} [R^2 (\sigma^2 + \rho^2) - n^2] J_n^2 (\rho R). \tag{145}$$

In our concrete case, when ρ is the root of eqs.(139) - (142) and the order of the Bessel functions is n = 0, eq.(145) is written in the following manner:

$$\int_0^R r J_0^2 (\rho_i r)\, dr = \frac{R^2}{2\rho^2} (\sigma^2 + \rho^2) J_0^2 (\rho R). \tag{146}$$

STAT

To find the coefficients B_i and B_i', let us take advantage of the expansions of eq.(130):

$$1 = \sum_i B_i J_0(\rho_i r); \qquad (147)$$

$$1 = \sum_i B_i' Y_0(\rho_i r). \qquad (148)$$

Multiplying the left and right-hand terms of the expansion (147) by $rJ_0(\rho_i r)dr$, then integrating within the limits of R_1 to R_2, and considering expression (146) we get

$$\int_{R_1}^{R_2} rJ_0(\rho_i r)\, dr = \sum_i \frac{(\sigma^2 + \rho_i^2)}{2\rho_i^2} \left[R_2^2 J_0^2(\rho_i R_2) - R_1^2 J_0^2(\rho_i R_1) \right] B_i'. \qquad (149)$$

Similarly, we obtain

$$\int_{R_1}^{R_2} rJ_0(\rho_i r)\, dr = \sum_i \frac{(\sigma^2 + \rho_i^2)}{2\rho_i^2} \left[R_2^2 Y_0^2(\rho_i R_2) - R_1^2 Y_0^2(\rho_i R_1) \right] B_i'. \qquad (150)$$

From eqs.(149) and (150) it is easy to compute the coefficients B_i and B_i':

$$B_i = \sum_i \frac{A \cdot 2\rho_i^2}{D}; \qquad (151)$$

$$B_i' = \sum_i \frac{A' 2\rho_i^2}{D'}, \qquad (152)$$

where

$$A = \int_{R_1}^{R_2} rJ_0(\rho_i r)\, dr; \qquad (153)$$

103

STAT

$$A' = \int\limits_{R_1}^{R_2} r Y_0\left(\rho_i r\right) dr; \qquad (154)$$

$$D = [R_2^2 J_0^2\left(\rho_i R_2\right) - R_1^2 J_0^2\left(\rho_i R_1\right)]\left(\sigma^2 + \rho_i^2\right); \qquad (155)$$

$$D' = [R_2^2 Y_0^2\left(\rho_i R_2\right) - R_1^2 Y_0^2\left(\rho_i R_1\right)]\left(\sigma^2 + \rho_i^2\right). \qquad (156)$$

Considering eqs.(151), (152), and (136), the expressions (132) and (133) will yield.

$$C_i' = \sum_i \frac{\theta^\bullet A \rho_i^2}{D \cos\rho_i \left(\dfrac{\operatorname{arc\ tg}\ \sigma/\rho_i}{\rho_i} - h\right)}; \qquad (157)$$

$$C_i'' = \sum_i \frac{\theta^\bullet A' \rho_i^2}{D' \cos\rho_i \left(\dfrac{\operatorname{arc\ tg}\ \sigma/\rho_i}{\rho_i} - h\right)}. \qquad (158)$$

Therefore, the final general solution of the differential equation (115) for stationary heat conditions with the boundary conditions (116) is written as follows:

$$\theta' = \theta^\bullet \sum_i \rho_i^2 \frac{\cos\rho_i \left[z + \left(\dfrac{\operatorname{arc\ tg}\ \sigma/\rho_i}{\rho_i} - h\right)\right]}{\cos\rho_i \left(\dfrac{\operatorname{arc\ tg}\ \sigma/\rho_i}{\rho_i} - h\right)} \times$$
$$\times \left[\frac{A}{D} J_0\left(\rho_i r\right) + \frac{A'}{D'} Y_0\left(\rho_i r\right)\right]. \qquad (159)$$

Equation (159) is a function of the coordinates z and r and the parameters σ and ρ_i. The parameter σ, again as before, represents the thermal characteristic of the material of the pair element ($\sigma = \dfrac{\sigma'}{\lambda}$, where σ' is the coefficient of heat emission and λ the coefficient of heat conductivity).

The basic parameter ρ_i of eq.(159) is easiest to compute by a graphic solution

104

STAT

of the equation systems (139) – (142).

For this, we introduce the substitutions

$$\begin{aligned} \rho_i R_1 &= x_{1i} \\ \rho_i R_2 &= x_{2i} \end{aligned}\Bigg\} \qquad (160)$$

Substituting these in eqs.(139) and (140) we get

$$\frac{x_{1i}}{R_1} J_0'(x_{1i}) = \sigma J_0(x_{1i})$$

or, otherwise,

$$x_{1i} J_0'(x_{1i}) = \sigma R_1 J_0(x_{1i}).$$

Let

$$y_1' = x_{1i} J_0'(x_{1i}), \qquad (161)$$

$$y_2' = \sigma R_1 J_0(x_{1i}) \qquad (162)$$

and by analogy

$$y_1'' = x_{2i} J_0'(x_{2i}); \qquad (163)$$

$$y_2'' = \sigma R_2 J_0(x_{2i}). \qquad (164)$$

The curves of lines y_1' and y_2' and also of lines y_1'' and y_2'' intersect at defi-
nite points x_{1i} and x_{2i}.

To compute the parameter ρ_i we reduce eqs.(139) and (140), substituting there
the values of the found series x_{1i} and x_{2i}; this yields

$$\rho_i = \frac{\sigma [J_0(x_{1i}) - J_0(x_{2i})]}{J_0'(x_{1i}) + J_0'(x_{2i})}, \qquad (165)$$

where i = 1, 2, 3, ... n.

105

STAT

In this way, the parameter of the general solution of the differential equation (159) is computed; this parameter, resulting from eqs.(139) and (140), is a function of the thermal parameters and geometric dimensions of the elements of the friction pair.

To study the performance of a friction machine with complete reciprocal contact overlap, eq.(159) which characterizes stationary heat conditions is quite adequate.

It should be noted that the differential equation of nonstationary processes (117) with the initial and boundary conditions (118) and (119) is solved in a similar way. The general solution of eq.(117) is sought in the form of

$$\theta'' = ZRT, \qquad (166)$$

which, by analogy with the preceding, assumes the form of

$$\theta' = \sum_i \sum_j e^{-a\left(\nu_i^2 + \beta_j^2\right)t} \times$$
$$\times \cos \beta_j (z + z_0) \left[C' J_0 (\mu_i r) + C'' Y_0 (\mu_i r)\right]. \qquad (167)$$

Substituting the general solution (167) in the initial and boundary conditions (118) and (119), we obtain a system of equations, as follows

$$\left.\begin{aligned}
\theta_0 - \theta' &= \sum_i \sum_j \sin \beta_j z \left[C' J_0 (\mu_i r) + C'' Y_0 (\mu_i r)\right], \\
0 &= \sum_i \sum_j e^{-a\left(\nu_i^2 + \beta_j^2\right)t} \sin \beta_j z \left\{C' \left[\mu_i J_0' (\mu_i R_1) - \right.\right. \\
&\quad - \sigma J_0 (\mu_i R_1)\bigr] + C'' \left[\mu_i Y_0' (\mu_i R_1) - \sigma Y_0 (\mu_i R_1)\right]\bigr\}, \\
0 &= \sum_i \sum_j e^{-a\left(\mu_i^2 + \beta_j^2\right)t} \sin \beta_j z \left\{C' \left[\mu_i J_0' (\mu_i R_2) + \right.\right. \\
&\quad + \sigma J_0 (\mu_i R_2)\bigr] + C'' \left[\mu_i Y_0' (\mu_i R_2) + \sigma Y_0 (\mu_i R_2)\right]\bigr\}, \\
0 &= \sum_i \sum_j e^{-a\left(\nu_i^2 + \beta_j^2\right)t} \left[C' J_0 (\mu_i r) + C'' Y_0 (\mu_i r)\right] \times \\
&\quad \times \left(\beta_j \cos \beta_j h_3 + \sigma \sin \beta_j h_3\right).
\end{aligned}\right\} \qquad (168)$$

STAT

The arbitrary invariables C', C'', z_0 and the parameters μ_i and β_j are computed from the system of equations (168).

By analogy with eq.(88), we derive an expression for characterizing the quantity of heat flowing per second through the material of one of the ring cylinders,

$$Q' = Jfpv_{sK}(1 - \alpha_{TP}), \qquad (169)$$

where $(1 - \alpha_{Tp})$ is the coefficient indicating what part of the general quantity of heat is branched into a given ring cylinder. At stabilized heat conditions, this quantity of heat passes into the surrounding medium through the inner, outer, and free end surfaces of the ring cylinder, so that

$$Q' = \sigma' \left[2\pi R_1 \int_0^h \vartheta' dz + 2\pi R_2 \int_0^h \vartheta' dz + \frac{\pi}{4}(R_2^2 - R_1^2) \int_{R_1}^{R_2} \vartheta' dr \right]. \qquad (170)$$

Adjusting the right-hand terms of eqs.(169) and (170) and making the reductions, we obtain

$$Jfpv_{sK}(1 - \alpha_{TP}) = 2\pi\sigma'\vartheta^{\bullet}(R_1 + R_2) \sum_i \rho_i^2 \times$$

$$\times \frac{\left[\frac{A}{D} J_0(\rho_i r) + \frac{A'}{D'} J_0(\rho_i r) \right]_h}{\cos\rho_i \left(\frac{\text{arc tg } \sigma/\rho_i}{\rho_i} - h \right)} \int_0^h \cos\rho_i \left[z + \left(\frac{\text{arc tg } \sigma \cdot \rho_i}{\rho_i} - h \right) \right] dz +$$

$$+ \frac{\pi}{4} \sigma'\vartheta^{\bullet}(R_2^2 - R_1^2) \sum_i \rho_i^3 \frac{\cos\rho_i \left[z + \left(\frac{\text{arc tg } \sigma \cdot \rho_i}{\rho_i} - h \right) \right]}{\cos\rho_i \left(\frac{\text{arc tg } \sigma/\rho_i}{\rho_i} - h \right)} \times$$

$$\times \int_{R_1}^{R_2} \left[\frac{A}{D} J_0(\rho_i r) + \frac{A'}{D'} Y_0(\rho_i r) \right] dr. \qquad (171)$$

We reduce eq.(171) under the condition that $z = 0$. In this case,

107

STAT

$$J/p v_{sK} (1 - \alpha_{TP}) = 4\pi\sigma'\theta^\bullet (R_1 + R_2) \sum_i \rho_i \times$$

$$\times \frac{\left[\dfrac{A}{D} J_0(\rho_i r) + \dfrac{A'}{D'} Y_0(\rho_i r)\right]\cos\rho_i \left|\dfrac{\mathrm{arc\ tg}\ \sigma/\rho_i}{\rho_i} - \dfrac{h}{2}\right| \sin\rho_i \dfrac{h}{2}}{\cos\rho_i \left[\dfrac{\mathrm{arc\ tg}\ \sigma/\rho_i}{\rho_i} - h\right]} +$$

$$+ \frac{\pi}{4}\sigma'\theta^\bullet (R_2^2 - R_1^2) \sum_i \rho_i \left\{\frac{A}{D}\left[J_0^2(\rho_i R_2) - J_0^2(\rho_i R_1)\right] + \frac{A'}{D'} \times\right.$$

$$\left. \times \left[Y_0^2(\rho_i R_2) Y_0^2(\rho_i R_1)\right]\right\}. \tag{172}$$

Using the following symbols:

$$z_K = \mathrm{arc\ tg}\ \sigma/\rho_i, \tag{173}$$

$$M = \frac{A}{D}[J_0^2(\rho_i R_2) - J_0^2(\rho_i R_1)], \tag{174}$$

$$N = \frac{A'}{D'}[Y_0^2(\rho_i R_2) - Y_0^2(\rho_i R_1)], \tag{175}$$

where

$$i = 1,\ 2,\ 3,\ \ldots\ n,$$

we finally get

$$J/p v_{sK}(1 - \alpha_{TP}) = 4\pi\sigma'\theta^\bullet (R_1 + R_2)\cdot \sum_i \rho_i \times$$

$$\times \frac{\left[\dfrac{A}{D}J_0(\rho_i r) + \dfrac{A'}{D'}J_0(\rho_i r)\right]\cos\left(z_K - \rho_i\dfrac{h}{2}\right)\sin\rho_i\dfrac{h}{2}}{\cos(z_K - \rho_i h)} +$$

$$+ \frac{\pi}{4}\sigma'\theta^\bullet (R_2^2 - R_1^2)\sum_i \rho_i (M + N). \tag{176}$$

From expression (176) it is easy to obtain temperature distribution on the sur-

108 STAT

face of a ring contact

$$\eta^{\bullet} = \frac{Jfpv_{SK}(1-\alpha_{TP})}{4\pi\sigma'(R_1+R_2)\cdot\sum_i \rho_i}$$

$$\rightarrow \frac{Jfpv_{SK}(1-\alpha_{TP})}{\times\left\{\frac{\left[\dfrac{A}{D}J_0(\rho_i r)+\dfrac{A'}{D'}J_0(\rho_i r)\right]\cos\left(z_K-\rho_i\dfrac{h}{2}\right)\sin\rho_i\dfrac{h}{2}}{\cos(z_K-\rho_i h)}+\right.}$$

$$\left.-\frac{Jfpv_{SK}(1-\alpha_{TP})}{+\dfrac{(R_2+R_1)(M+N)}{16}}\right\} \tag{177}$$

By analogy with the preceding [see eq.(99)], the other element of the friction pair can be expressed by

$$\eta_1^{\bullet} = \frac{Jfpv_{SK}\alpha_{TP}}{4\pi\sigma_1'(R_1+R_2)\sum_i \rho_i'}$$

$$-\frac{Jfpv_{SK}\alpha_{TP}}{\times\left\{\frac{\left[\dfrac{A_1}{D_1}J_0(\rho_i' r)+\dfrac{A_1'}{D_1'}Y_0(\rho_i' r)\right]\cos\left(z_K'-\rho_i'\dfrac{h'}{2}\right)\sin\rho_i'\dfrac{h'}{2}}{\cos(z_K'-\rho_i' h')}+\right.}$$

$$\left.-\frac{Jfpv_{SK}\alpha_{TP}}{+\dfrac{(R_2+R_1)(M_1+N_1)}{16}}\right\} \tag{178}$$

where σ_1' = coefficient of heat transfer of the material in this pair element;

  h' = height of a circular cylinder;

and for the coefficient of heat distribution α_{Tp}:

$$\alpha_{TP} = \frac{\dot{U}_{ts}'}{U_{ts}+U_{ts}'}, \tag{179}$$

where

109

STAT

$$U_{ts} = \sigma' \sum_i \rho_i \left\{ \frac{\left[\frac{A}{D} J_0(\rho_i r) + \frac{A'}{D'} Y_0(\rho_i r)\right] \cos\left(z_{\text{к}} - \rho_i \frac{h}{2}\right) \sin \rho_i \frac{h}{2}}{\cos(z_{\text{к}} - \rho_i h)} + \right.$$
$$\left. + \frac{(R_2 + R_1)(M + N)}{16} \right\}, \tag{180}$$

$$U'_{ts} = \sigma_1 \sum_i \rho_i' \left\{ \frac{\left[\frac{A_1}{D_1} J_0(\rho_i' r) + \frac{A_1'}{D_1} Y_0(\rho_i' r)\right] \cos\left(z_{\text{к}}' - \rho_i' \frac{h'}{2}\right) \sin \rho_i' \frac{h'}{2}}{\cos(z_{\text{к}}' - \rho_i' h')} + \right.$$
$$\left. + \frac{(R_2 + R_1)(M_1 + N_1)}{16} \right\}. \tag{181}$$

From eq.(179) it is clear that, in the case of a friction machine with complete reciprocal contact overlap, the coefficient of heat distribution between the elements of the friction pair α_{Tp} does not depend, in first approximation, on the sliding speed and is a function of the thermal parameters and geometric dimensions.

This result, indicating the independence of α_{Tp} of the sliding speed under non-stationary heat conditions, has been experimentally established by F.Sharon (Bibl.34) in a large series of experiments on friction in cylindrical disks.

Cylindrical disks of the same diameter and height and of the same as well as different materials were heated by friction in a special setup for several seconds, i.e., under unstable temperature conditions.

Since the magnitude of the friction work made no difference in the experiment, the specimens were pressed together by the hand of the experimenter. The heat produced by the hand in the specimen was eliminated by its heat insulation.

The quantity of heat absorbed by each sample is computed by means of a water calorimeter.

The experiments described were conducted for dry friction as well as for friction with boundary films of viscous fluids.

The results of most of these experiments essentially confirm that α_{Tp} is inde-

STAT

pendent of the speed and lead to the following equation for the distribution of heat flow:

$$\frac{q_1}{q_2} = \frac{V\overline{c_1\gamma_1\lambda_1}}{V\overline{c_2\gamma_2\lambda_2}} , \qquad (182)$$

where q is the heat flow, and the subscripts 1 and 2 refer to different rubbing specimens. The other quantities in this equation are the same as above.

However, the experimental results include data which do not confirm the described dependence. For example, in testing one of the rubbing pairs, the ratio of heat flow was equal to

$$\frac{q_1}{q_2} = 1,88,$$

at a ratio of

$$\frac{V\overline{c_1\gamma_1\lambda_1}}{V\overline{c_2\gamma_2\lambda_2}} = 3,79.$$

This deviation from the assumed dependence has not been thoroughly explained. It can only be presumed that the reason lies in miscalculations during the experiment, one of which must be that the experimenter disregarded external heat emission. However, apparently in the other cases the physical laws were preserved since the described ratios in some experiments had values of 1.59; 1.52 and 1.51; 1.52.

Let us return to eq.(177). Substituting eq.(179) in eq.(177) we finally get the value of the mean temperature on the surface of a ring contact:

$$\theta^{\bullet} = \theta_1^{\bullet} = \frac{Jfpv_{s\kappa}}{4\pi(R_1 + R_2)(U_{ts} + U_{ts}')} . \qquad (183)$$

When the friction pair is made of the same material and the height of the ring

STAT

cylinders is the same ($h = h'$), then eq.(183) is somewhat simplified and assumes the form of

$$q^\bullet = \frac{J f p v_{sk}}{8\pi (R_1 + R_2) \sigma' \sum_i \rho_i \times} -$$

$$\to -\frac{J f p v_{sk}}{\times \left\{ \frac{\left[\dfrac{A}{D} J_0(\rho_i r) + \dfrac{A'}{D'} Y_0(\rho_i z)\right] \cos\left(z_k - \rho_i \dfrac{h}{2}\right) \sin \rho_i \dfrac{h}{2}}{\cos(z_k - \rho_i h)} + } \to$$

$$\to \frac{J f p v_{sk}}{+ \dfrac{(R_2 + R_1)(M + N)}{16}} \right\} \cdot \tag{184}$$

In this case,

$$\alpha_{TP} = 0{,}5.$$

As described earlier, during complete reciprocal contact overlap and for unstable heat conditions, α_{Tp} does not depend on the sliding speed and is a function of only the physical parameters of the material making up the friction pair elements.

However, in the experiments by Sharon, only linear distribution of heat was presumed.

Let us point out several reasons which make it permissible to use the equation for heat conductivity and, without integrating it, to draw a conclusion on the distribution of any three-dimensional heat flow between rubbing bodies for unstable heat conditions, during complete reciprocal contact overlap.

As is generally known, the Fourier equation for heat conductivity at nonstationary conditions reads as follows:

$$\frac{\partial \theta}{\partial t} = a \left(\frac{\partial^2 \theta}{\partial x^2} + \frac{\partial^2 \theta}{\partial y^2} + \frac{\partial^2 \theta}{\partial z^2} \right) . \tag{184'}$$

Let us turn to the new variables ν, η, ξ which are determined by the ratios

112

STAT

$$\nu = \frac{x}{\sqrt{a}}; \quad \eta = \frac{y}{\sqrt{a}}; \quad \xi = \frac{z}{\sqrt{a}}, \tag{185}$$

from which it follows that:

$$\frac{\partial^2}{\partial x^2} \rightarrow \frac{1}{a}\frac{\partial^2}{\partial \nu^2}, \quad \frac{\partial^2}{\partial y^2} \rightarrow \frac{1}{a}\frac{\partial^2}{\partial \eta^2}, \quad \frac{\partial^2}{\partial z^2} \rightarrow \frac{1}{a}\frac{\partial^2}{\partial \xi^2}$$

and, further,

$$\frac{\partial \theta}{\partial t} = \frac{\partial^2 \theta}{\partial \nu^2} + \frac{\partial^2 \theta}{\partial \eta^2} + \frac{\partial^2 \theta}{\partial \xi^2}. \tag{186}$$

Equation (186) does not contain the thermal parameters of the elements of the friction pair in a clear form and the temperature is a function of only the new co-ordinates ν, η, ξ.

Any three-dimensional heat flow in each element of the pair may be represented by the sum

$$\begin{aligned} q_1 &= q_{1x} + q_{1y} + q_{1z} = \lambda_1 \left(\frac{\partial \theta}{\partial x_1} + \frac{\partial \theta}{\partial y_1} + \frac{\partial \theta}{\partial z_1} \right) \\ q_2 &= q_{2x} + q_{2y} + q_{2z} = \lambda_2 \left(\frac{\partial \theta}{\partial x_2} + \frac{\partial \theta}{\partial y_2} + \frac{\partial \theta}{\partial z_2} \right) \end{aligned} \tag{187}$$

From eq.(186) it becomes clear that, at the same values of ν, η, and ξ at any points in the elements of the pair, the temperature is equal since

$$\frac{x_1}{\sqrt{a_1}} = \frac{x_2}{\sqrt{a_2}}; \quad \frac{y_1}{\sqrt{a_1}} = \frac{y_2}{\sqrt{a_2}}; \quad \frac{z_1}{\sqrt{a_1}} = \frac{z_2}{\sqrt{a_2}}$$

or, in other words,

$$\begin{aligned} x_1 &= x_2 \sqrt{\frac{a_1}{a_2}} \\ y_1 &= y_2 \sqrt{\frac{a_1}{a_2}} \end{aligned} \tag{188}$$

113

STAT

$$z_1 = z_2 \sqrt{\frac{a_1}{a_2}} \Bigg]$$

Taking eq.(188) into consideration, eq.(187) will yield

$$\left. \begin{aligned} q_1 &= \lambda_1 d i r_2{}^{()} \sqrt{\frac{a_2}{a_1}} \\ q_2 &= \lambda_2 d i r_2{}^{()} \end{aligned} \right\}. \tag{189}$$

From eq.(189) it is easy to compute the coefficient α_{Tp}:

$$\alpha_{tp} = \frac{q_1}{q_2} = \frac{\lambda_1 \sqrt{\dfrac{a_2}{a_1}}}{\lambda_1} = \sqrt{\frac{\lambda_1 \gamma_1 c_1}{\lambda_2 \gamma_2 c_2}}. \tag{190}$$

Therefore eq.(182), derived for the case of linear heat flow, is valid for any three-dimensional heat flow in friction pairs under nonstationary conditions.

To compute the temperature gradient at any points in the elements of the friction pair on a machine with complete reciprocal contact overlap, let us turn to eq.(171) which, when differentiated, yields

$$O = K (R_1 + R_2) \frac{\partial \theta^\bullet}{\partial z} + L \frac{\partial \theta^\bullet}{\partial z} (R_1^2 - R_1^2) \cos [\rho_i z + (z_\kappa - \rho_i h)] - \\ - L \theta^\bullet (R_2^2 - R_1^2) \rho_i \sin [\rho_i z + (z_\kappa - \rho_i h)], \tag{191}$$

where

$$K = 2\pi \sigma' \sum_i{}' \rho_i^2 \frac{\left[\dfrac{A}{D} J_0(\rho_i r) + \dfrac{A'}{D'} Y_0(\rho_i r)\right]}{\cos (z_\kappa - \rho_i h)} \int_0^h \cos [\rho_i z + (z_\kappa - \rho_i h)] \, dz; \tag{192}$$

$$L = \frac{\pi}{4} \sigma' \sum_i \rho_i^2 \frac{\displaystyle\int_{R_1}^{R_2} \left[\dfrac{A}{D} J_0(\rho_i r) + \dfrac{A'}{D'} Y_0(\rho_i r)\right] dr}{\cos (z_\kappa - \rho_i h)}. \tag{193}$$

STAT

From eq.(191) we obtain

$$\frac{\partial \theta^{\bullet}}{\partial z} = \frac{L\,(R_2 - R_1)\,\rho_i \sin\,[\rho_i z + (z_{\scriptscriptstyle K} - \rho_i h)]}{K + L\,(R_2 - R_1)\,\cos\,[\rho_i z + (z_{\scriptscriptstyle K} - \rho_i h)]} \cdot \theta^{\bullet}. \qquad (194)$$

Using the accepted symbols in eqs.(192) and (193) for θ^{*}, we get the following

expression:

$$\theta^{\bullet} = \frac{J f p v_{s\kappa}\,(1 - \alpha_{\scriptscriptstyle TP})}{K\,(R_1 + R_2) + L\,(R_2^2 - R_1^2)\,\cos\,[\rho_i z + (z_{\scriptscriptstyle K} - \rho_i h)]}, \qquad (195)$$

which we substitute in eq.(194); this will yield the following equation for the tem-

perature gradient:

$$\frac{\partial \theta^{\bullet}}{\partial z} = \frac{L\,(R_2 - R_1)\,\rho_i \sin\,[\rho_i z + (z_{\scriptscriptstyle K} - \rho_i h)]}{(R_1 + R_2)\,\{K + L\,(R_2 - R_1)\,\cos\,[\rho_i z + (z_{\scriptscriptstyle K} - \rho_i h)]\}^2} \times \qquad (196)$$
$$\times\, J f p v_{s\kappa}\,(1 - \alpha_{\scriptscriptstyle TP}).$$

From eq.(194) it becomes clear that the higher the temperature gradient in the

elements of the friction pair, the greater will be the temperature upon contact.

Equation (196) shows that the gradient is a function of the coefficient α_{Tp}.

Any increase in the coefficient α_{Tp} leads to a decrease in the temperature gradient.

The temperature gradient, at symmetric points in the elements of the pair, can be

the same only in the case when the friction pair is made of the same material and

its elements have the same geometric dimensions.

Maintaining Certain Conditions in Testing Small Specimens

So that the results of experiments on heating of rubbing bodies are sufficient-

ly universal as far as their transfer from one model to another or practical appli-

cation is concerned, certain conditions must be maintained.

Generally, as proved by the theory of similitude of physical phenomena, the

STAT

uniformity of certain criteria must be preserved (for example, Fourier's, Reynolds, Strouhal's, Euler's, Pekle, etc. numbers).

The similarity of heat phenomena can be preserved if one or several criteria of similitude (Bibl.23) are maintained.

In particular, similarity of heat flows, which is sufficiently accurate in practice for a stationary temperature field of rubbing bodies, is ensured by the constancy of the coefficient α_{Tp} which is computed from eqs.(100) and (179). However, in view of the complexity of these equations for a preliminary clarification of the conditions of similitude, the solution of Fourier's equation for linear heat flow* can be used.

The solution for linear heat flow has the form of

$$\theta = \frac{(1 - \alpha_{TP}) J f p v_{s\kappa}}{\sqrt{\omega \sigma' \lambda S}}, \tag{197}$$

where ω = perimeter of nominal contact;

S = nominal area of contact.

All other symbols as earlier.

In particular, for prismatic specimens with contact dimensions of h_1 and h_2, we have

$$\omega = 2(h_1 + h_2), \quad S = h_1 h_2.$$

In this case, eq.(197) assumes the form

$$\theta = \frac{(1 - \alpha_{TP}) J f p v_{s\kappa}}{\sqrt{2(h_1 + h_2) h_1 h_2 \lambda \sigma'}}. \tag{198}$$

---

*See the article by V.S.Shchedrov, (Bibl.39) "Temperature on a Sliding Contact". Collection Friction and Wear in Machines, published by Kh.Izd., Academy of Sciences of the USSR, 1955.

STAT

If, for the second model, all terms in the equation are indicated by the same letters but with the addition of primes, we will have

$$\theta' = \frac{(1 - \alpha'_{Tp}) Jf'p'v'}{V\overline{2(h'_1 + h'_2) h'_1 h'_2 \lambda' \sigma'}}.$$ (199)

The similarity of the heat phenomena in the two described cases is equivalent to the condition

$$\theta' = \theta,$$ (200)

i.e.,

$$\frac{\beta'f'p'v'}{V\overline{(h'_1 + h'_2) h'_1 h'_2 \lambda' \sigma'}} = \frac{\beta fpv}{V\overline{(h_1 + h_2) h_1 h_2 \lambda \sigma'}},$$ (201)

where $\beta = 1 - \alpha_{Tp}$ and $\beta' = 1 - \alpha'_{Tp}$.

The equality (201) makes it possible to study the influence of different groups of parameters for two different models.

As an example, let us examine the influence of shape and area in a nominal contact.

For this, we presume the following:

1) Same materials of the rubbing bodies, $\lambda' = \lambda$;

2) Same sliding speeds, $v' = v$;

3) Load changes by n times, $p' = pn$;

4) Area of nominal contact changes, by n times:

case a - at a change in form of the nominal contact:

$$h'_1 = h_1, \quad h'_2 = h_2 n;$$

case b - at geometric similitude of form of the contact:

$$h'_1 = h_1 \sqrt{n} \text{ and } h'_2 = h_2 \sqrt{n}.$$

117

STAT

In case a, the equality (201) assumes the form

$$\frac{\beta f}{\sqrt{(h_1 + h_2)\,\sigma'}} = \frac{\beta' f'}{\sqrt{\left(\frac{h_1}{n} + h_2\right)\sigma''}}. \tag{202}$$

From here, we obtain the unknown ratio of βf and $\beta' f'$ which assumes equality of temperatures in both cases

$$\beta f = \beta' f' \frac{\sqrt{(h_1 + h_2)\,\sigma'}}{\sqrt{\left(\frac{h_1}{n} + h_2\right)\sigma''}}. \tag{203}$$

From this it follows that the ratio of similitude criteria $\frac{\beta f}{\beta' f'}$ depends not only on the area but also on the shape of the nominal contact.

In case b, the equality (201) assumes the form

$$\frac{\beta f}{\sqrt{\sigma'}} = \frac{\beta' f' \sqrt[4]{n}}{\sqrt{\sigma''}} \tag{204}$$

or

$$\beta f = \beta' f' \sqrt[4]{n}\, \sqrt{\frac{\sigma'}{\sigma''}}. \tag{205}$$

This ratio shows that, in geometrically similar nominal contacts, their dimensions do not at all affect the ratio of the similitude criteria.

In particular, if the coefficient of friction does not depend on pressure, we will have $f' = f$ for the same materials. If, in addition, the same conditions of heat exchange in the ambient medium are assumed, then $\sigma'' = \sigma'$. In this case, the equality (205) is considerably simplified:

$$\beta = \beta' \sqrt[4]{n}. \tag{206}$$

STAT

The correlation (206) shows that a change in load and area has little effect, since the quantity n appears in a ratio of 1/4. Therefore, the same conditions for heat exchange with the ambient medium are not the best for minature-scale operations of heat phenomena. It is easy to see that, if $\sigma'' = \sigma' \sqrt{n}$, the equality (206) will assume the form

$$\beta = \beta' \qquad (207)$$

or

$$\alpha_{TP} = \alpha'_{TP}. \qquad (208)$$

Therefore, the coefficient α_{TP} is a necessary and sufficient criterion of similitude.

The same results are obtained with $p' = p$, $v'_{sk} = v_{sk} n$, other conditions being equal.

Some studies for determining the criteria for miniature-scale operations were made by Parker (Bibl. 35), but the value of these studies is considerably reduced because he did not take into account the process of heat emission to the surrounding medium. In connection with this and also as a result of the admitted mathematical error, Parker's formula is not correct.

STAT

STUDY OF FRICTIONAL PROPERTIES OF MATERIALS ON RING

FRICTION MACHINE I-47

Existing standard friction machines (Fig. 39) give real values of specific pressure and sliding speed (criteria p_{ud} v_{sk}) but do not take into consideration the principles of heat in model operations, especially geometric similitude; this results in the fact that the friction temperatures, developed on these machines, are very limited ($175-200^\circ C$).

The following experiment shows the extent to which the ratio of friction areas affects heat conditions and consequently the intensity of wear. Samples of the friction material Ts-4-52, similar in volume and area of friction but different in geometric configuration, were tested on a "miniature" machine and on the friction machine I-47 with complete reciprocal contact overlap (for description of the machine see below). In both cases, friction was produced on brand ChNMKh cast iron. The sliding speed in both setups was $v_{sk} = 3.34$ m/sec and the pressure was p_{ud} 15 kg/cm^2. The test was conducted under stabilized temperature conditions. The results of the experiment are shown in Table 1.

From the data in Table 1 it is evident that the intensity of wear of the sample is about 30 times higher on the machine I-47 than on the "miniature" machine.

Figure 40 shows samples tested on the "miniature" machine (b) and a ring machine (a) under the same conditions, i.e., under the same values of p_{ud} and v_{sk}. In the first case, the friction surface absolutely was not damaged at all, while in the second case the samples showed intense wear.

120

STAT

Table 1

Type of Friction Machine	Ratio of Friction Areas	θ , $^\circ$C	Intensity of Wear $J_B \cdot 10^{-4}$ mg/m $\cdot$ cm^2
Standard "miniature" machine I-47 with complete reciprocal contact overlap	0.14 0.9	100 400	13.5 400

As is generally known, actual aircraft brakes work with nearly complete or sufficiently adequate reciprocal overlap of rubbing pairs. That is the reason why considerably higher temperatures are developed in these actual units than the temperatures developed under the same p_{ud} and v_{sk} on "miniature" friction machines. Therefore, test according to GOST 1786-42 on these machines used to give faulty results,
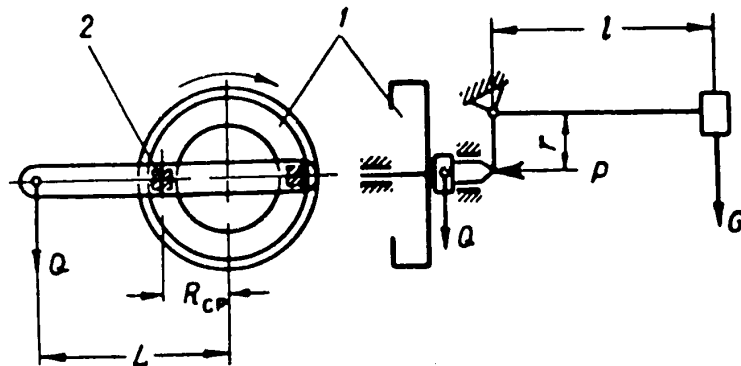
Fig. 39-Diagram of Standard Friction Machine

1 - Disk; 2 - "Miniature" samples

especially for frictional materials which had been intended for forced braking conditions when the temperature reaches 700-800 and even 1000°C (Bibl. 10).

The desire to obtain simultaneously on a friction machine the actual values of specific pressure, speed of sliding, and temperature is based on insufficient knowl-

121

STAT

ledge of small-scale modeling principles and results in extreme enlargement of the dimensions of the machine and the power of its drive. In the last analysis, such a laboratory machine for testing samples would grow to the dimensions of powerful inertia stands.
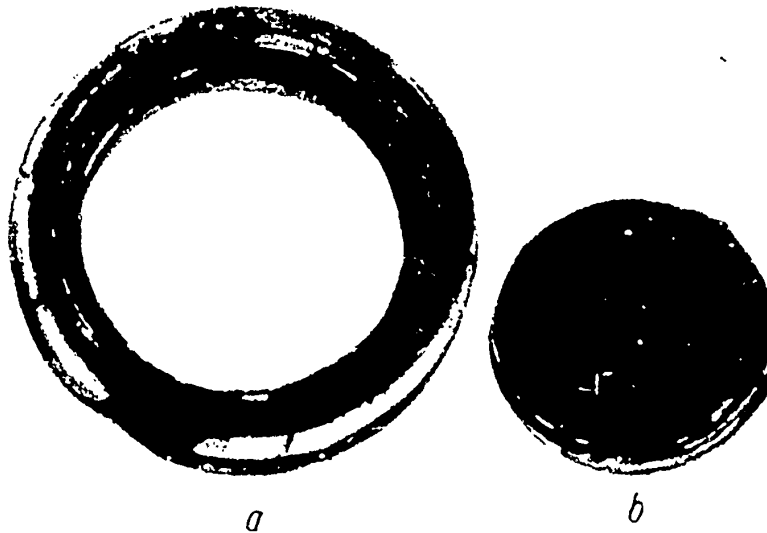
Fig. 40-Outer View of Friction Surface of Material

Ts-4-52 after Testing.

a - Tested on Ring Machine; b - Tested on "Miniature"Machine

Thus, to create a small power laboratory setup it is necessary to single out a basic parameter which can be considered essential and practically adequate for determining frictional characteristics of tested materials.

We assume temperature (Bibl. 36) as such a basic, controllable parameter.

Description of the Ring Friction Machine I-47

On the basis of these principles, the special friction machine I-47 was constructed in the Laboratory of Frictional Materials IMASh, Academy of Sciences, USSR, for testing small samples of experimental types of frictional materials. The friction machine I-47 is completely subject to the ratios derived above for the case of

122

STAT

friction of two ring cylinders osculating along their bases [see eqs. (179), (183), (196)]. Therefore, this machine simulates actual working conditions sufficiently
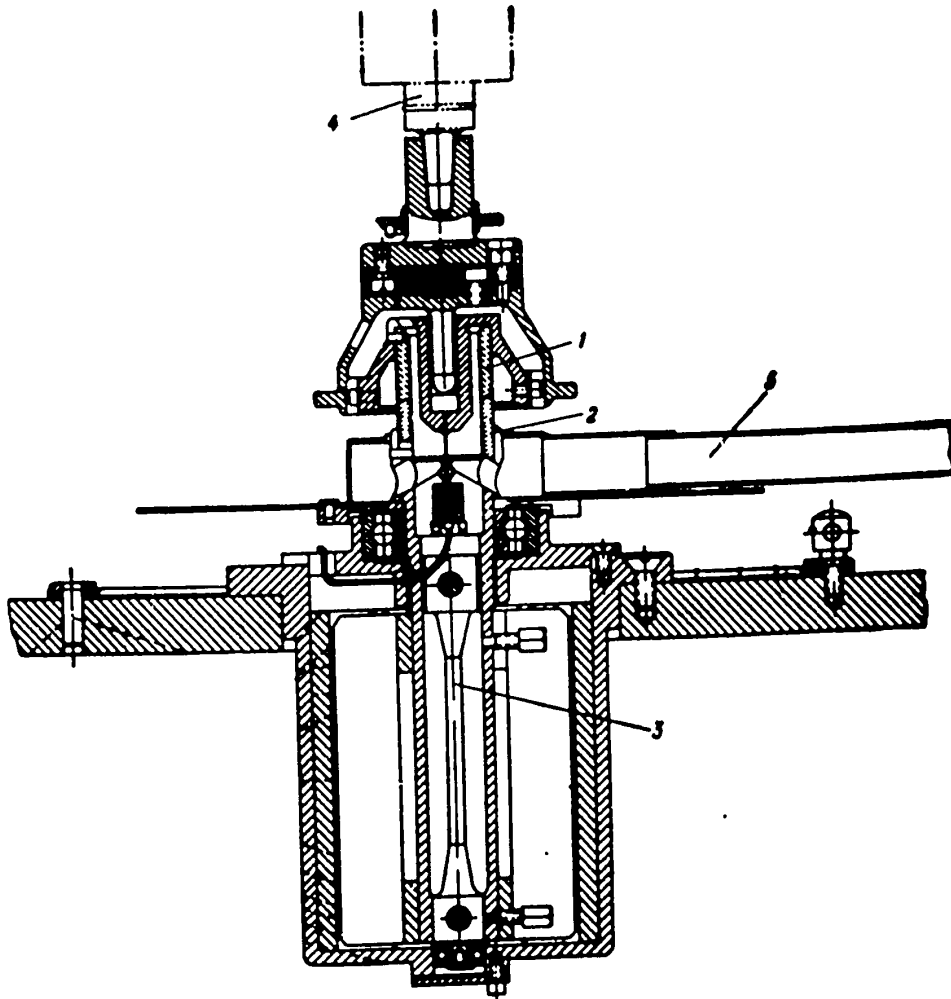
Fig. 41 — Design of Working Unit of Friction Machine I-47.

1,2 — Tested Samples, 3 — Torsion shaft, measuring

friction moment. 4 — Spindle turning the upper sample.

5 — Pipe for supply of air

closely, i.e., it creates an actual thermal field in the samples to be tested.

Figure 41 shows the design of the central assembly for the friction machine

I-47.

123

STAT

The friction machine I-47 is built on the base of a common drill press. The drive is furnished by a DC motor of 5 kw which, by means of a field rheostat in combination with removable drive pulleys, permits smooth variation of the number of revolutions of the spindle shaft within very broad limits (100-5000rpm).*

Pressure of the required magnitude on the test specimens is created by suspending a load from a lever over a cogwheel gear.

The oscillograph gives the values and records the brake moment produced by the torque of the calibrated brake shaft. The temperature is recorded by a galvanometer of one of the two therocouples built into the metal specimen at a depth of 1 mm from the friction surface.

The test specimens consist of ring cylinders with the standard dimensions of $2R_2 = 28$ mm, $2R_1 = 20$ mm, $h = 11 - 20$ mm. As can be seen from Fig. 41, the specimen ends are pressed together, resulting in complete overlap of the couple or overlap as required by the particular conditions.

The lower test sample is stationary and rigidly connected to the torsion shaft, whose angle of torsion determines the friction moment.

The upper test sample is fixed in a special spindle head which makes it possible to shift the load along the axis of rotation, thus causing the specimen to rotate together with the spindle.

Since the upper and lower samples have similar dimensions they are interchangeable, so that the tester if he wishes, can check the performance of the couple direct or reversed.

It should be specially emphasized here that tests are conducted on the machine I-47 of real friction pairs since both members of the pair are removable. This is not the case with a standard friction machine where usually one element of the friction pair (the metal disk) is permanently fixed.

---

* Removable pulleys are not necessary if the control is accomplished by a Leonard circuit.

The operating conditions of the actual aircraft brake, for which the test materials are intended, are usually known. The specific pressure and speed of sliding are also known but, most important, the temperatures and the ratio of friction areas are known. In other words, the reciprocal overlap, under which the tested materials should perform, is known.

For this reason, testing conditions are selected on laboratory friction machine I-47 which correspond to actual heat conditions.

Usually, the tests are conducted under constant specific pressure with an overlap corresponding to the actual unit, and at various gradually decreasing speeds of sliding (from 0.125 to 5 m/sec). Moreover, the duration of testing at every stage of speed is such that the heat conditions become practically stabilized.

Thus, each stage of speed gives a definite degree of temperature. Usually, the duration of an experiment at a given stage of speed is 15 min, since the heat conditions are practically stabilized within 3-4 min.

Accordingly, the oscillograph readings for the brake moment (and consequently for the friction coefficient) as well as the galvanometer readings for the temperature are taken every 5, 10, and 15 min after the start of the experiment, for a given stage of speed. If, at a given stage of temperature, no deformation of material takes place, then all three readings on the oscillograph tape are identical.

In this way, moving from one thermal stage to a higher one, we reach the temperatures which occur in the actual friction unit.*

Temperatures of the order of 400-600°C are usually reached at sliding speeds of v_{sk} = 1.6 - 2 m/sec. Higher temperatures (900-1000°C and higher) are formed in the tested samples at sliding speeds of v_{sk} = 3.5 - 5 m/sec.

---

* Before the basic tests, the specimens are fitted together at a low temperature so that the effect of the high temperatures on material properties is eliminated when friction takes place. The fitting is done approximately and is considered complete when the entire friction surface of the sample shows traces of wear.

125

STAT

The resistance of the test pair to wear is rated according to the wear of the samples in terms of weight. The specimens are weighed before and after each test. Knowing the length of the friction path traveled and the friction area of each element of the pair, it is easy to compute the intensity of wear J_B (mg/m . cm^2) as a function of temperature. Moreover, the linear intensity of wear J is sometimes computed.

To approximate the heat conditions of the experiment conducted with a laboratory setup (friction machine I-47) as closely as possible to the heat conditions of an actual brake (chamber or disk type), i.e., to get actual thermal gradients in materials of a pair - artificial electric heating or cooling by compressed air was used, or else conditions of heat transfer from the samples into the surrounding medium were varied by means of insulating gaskets and coatings.

All this work was conducted with small test samples to find the best types of frictional materials for brakes of high-speed jet aircraft. In the course of work on the machine I-47, there was an opportunity not only to rate materials according to a given index but to develop suggestions for making the friction materials themselves.

Results of Rating Certain Friction Materials on the Friction Machine I-47

In the past, about 70 friction materials of different types have been tested. Some materials were tested in several different ways.

All test materials can be divided into two basic groups: 1) nonmetallic friction materials and 2) cermet friction materials. Both these groups were tested in a pair of alloyed cast iron, type ChNMKh, which is used in manufacturing brake drums.

Tested nonmetal friction materials are divided according to their cohesive medium into asbestos-bakelite, asbestos-rubber, and resins.

Cermet friction test materials were made on copper and iron bases.

Plastic No. 22, which had also been tested on machine I-47, was the standard

STAT

for all·test materials.

Besides finding the thermostability of friction materials, i.e., the dependence of the friction coefficient and intensity of wear on the temperature during these
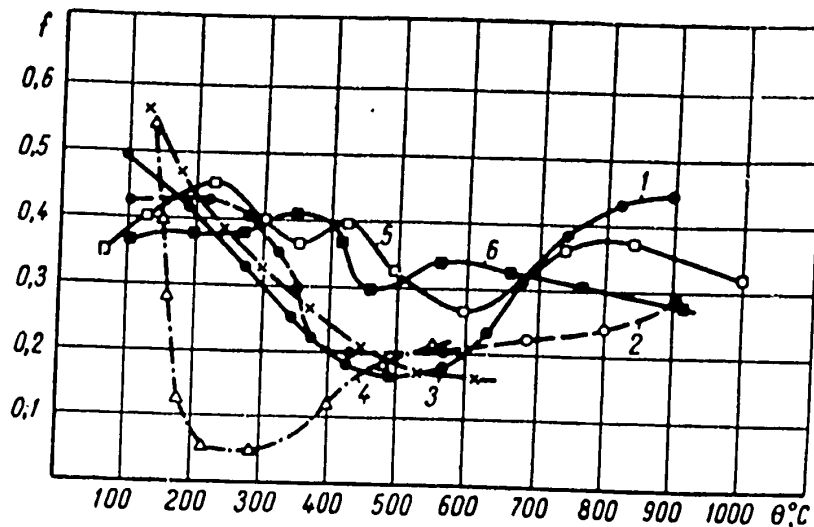
Fig. 42 - Friction Coefficient as a Function of Temperature for Various Plastics (the Temperature in the Cast Iron was Measured at a Depth of 1 mm from the Friction Surface)

1 - Plastic No. 22; 2- Plastic "TP"; 3 - Plastic 6 KKh-1;

4 - Plastic PA-2; 5 - Plastic 6FP; 6 - Plastic 6FS

tests, particular attention was paid to the quality of the friction surface and to the interaction of the individual elements of the pair, one another (phenomena of abrasion, fouling, folding over, etc.).

In the first stage of testing nonmetallic friction materials, attention was directed to the friction material Plastic "TP", taken from the brakes of an excavator hoist.

As can be seen from the graphs (Fig. 42 and 43), the Plastic "TP" retained a sufficiently high friction coefficient up to temperatures of 800-900°C, at which point its resistance to wear was considerably higher than the resistance of the serial friction material No. 22. While the Plastic No. 22, above temperatures of

STAT

127

600-700°C, showed very high wear and also, as in an actual chamber brake, first be-
came coated with the cast iron (Fig. 44) and then charred, the Plastic "T" at the
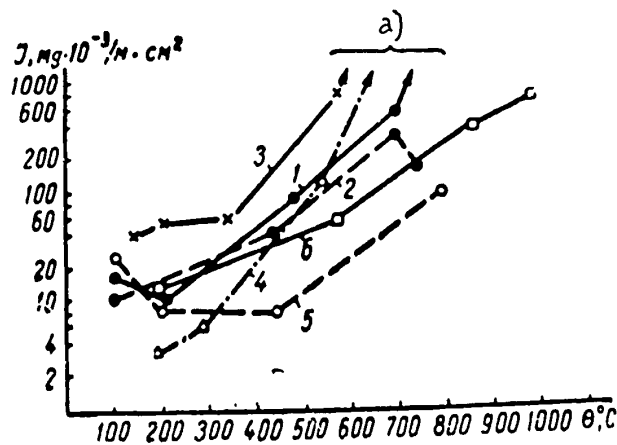
Fig. 43 - Wear Intensity as a Function of Temperature, for
Different Plastics (Temperature was Measured at a depth
of 1 mm from the Friction Surface) 1 - Plastic No. 22;
2 - Plastic "T"; 3 - Plastic 6KKh-1; 4 - Plastic PA-2;
5 - Plastic FK-24a; 6 - Plastic 6F a) Charring and
destruction

same temperatures became somewhat brittle, but did not char or disintegrate. It
was noted that the Plastic "T" displayed some tendency of becoming coated with the
cast iron.

On this basis, it was possible to recommend the Plastic "T" for actual tests on
an inertia stand in an actual brake.

Tests made on the machine I-47 and on an inertia stand permitted conclusions on
the following principles of manufacturing friction materials:

1) Friction materials should consist of components which change their mechan-
ical properties very little when used within broad temperature limits.

2) Friction materials should contain a component which prevents the appearance
of scratches and fold-over.

128

STAT

a

b

Fig. 44-Fold-Over of Cast Iron on Plastic No. 22

a),and Damage to a Brake Drum Made of Cast Iron

ChNMKh b),after Testing in a Chamber Brake

129

STAT

Simultaneously with tests of nonmetallic friction materials on the machine I-47, tests were conducted with different types of cermets. Very good results (Fig. 45, 46, curve 1) were obtained by one of the experimental versions of the cermet type
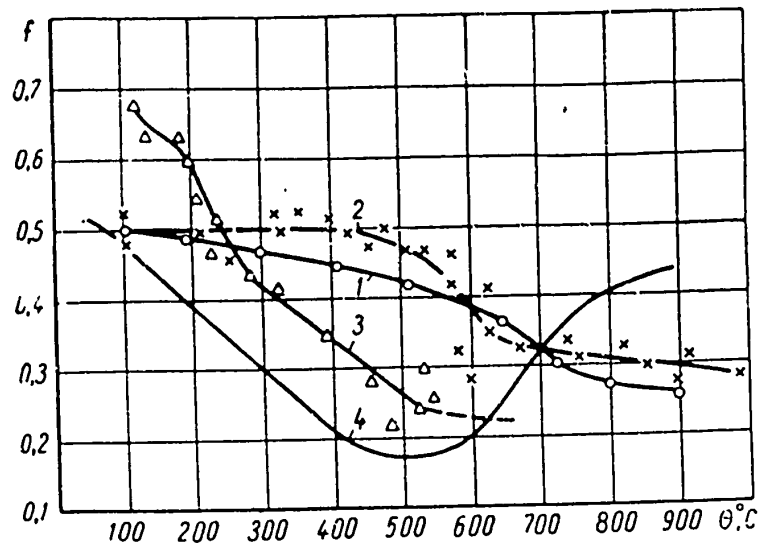
Fig. 45 - Friction Coefficient f as a Function of Temperature, for Different Experimental Variations of Cermets Coupled with Cast Iron ChNMKh (Temperature of Cast Iron Sample at a Depth of 1 mm from the Friction Surface). 1, 2, 3 - Cermet samples; 4 - Plastic No. 22

with an iron base. The other experimental versions of cermets with iron or copper bases merited less attention, since they showed greater wear and less mechanical strength, and some displayed a tendency to link with the cast iron. For some cermets very small linear wear with negative wear by weight was observed. It should be pointed out that for similar types of materials the transition from pilot-scale samples to full-scale lots of actual products presents considerable difficulties.

Therefore, particular attention should be given to working out technological processes when producing production lots.

New types of nonmetallic materials 6F and 3F were developed by workers in

130

STAT

research organizations, in cooperation with factory workers. In these materials, which have high resistance in the contact zone during the braking process, a special
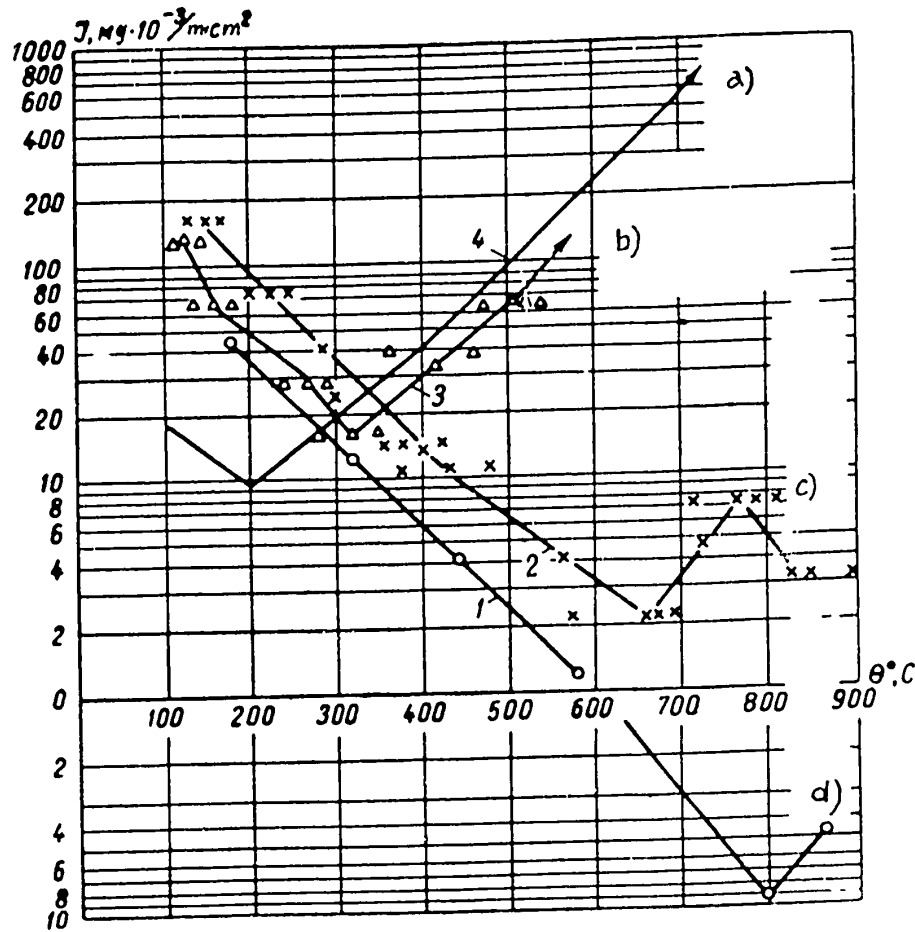
Fig. 46 — Intensity of Wear J_B as a Function of the Temperature θ for Different Experimental Versions of Cermets Coupled with Cast Iron ChNMKh (Temperature of Cast Iron Sample at a Depth of 1 mm from the Friction Surface) 1, 2, 3 — Cermet samples; 4 — Plastic No. 22 a) Start of considerable wear, charring, and destruction of sample; b) Start of considerable wear, abrasion of friction surface, and peeling; c) Smooth friction surfaces of a pair; d) Smooth friction surfaces of a pair

STAT

friction layer forms which has special properties, namely: increased capacity for secondary deformation and increase in strength of the material in this layer with increasing distance from the friction surface. The latter characteristic improves the quality of the friction surface and practically eliminates fold-over since the possibility of depth tearing is eliminated. The test results for the friction material variants 6F (6FP and 6FS) showed considerably better friction properties than the Plastic No. 22.
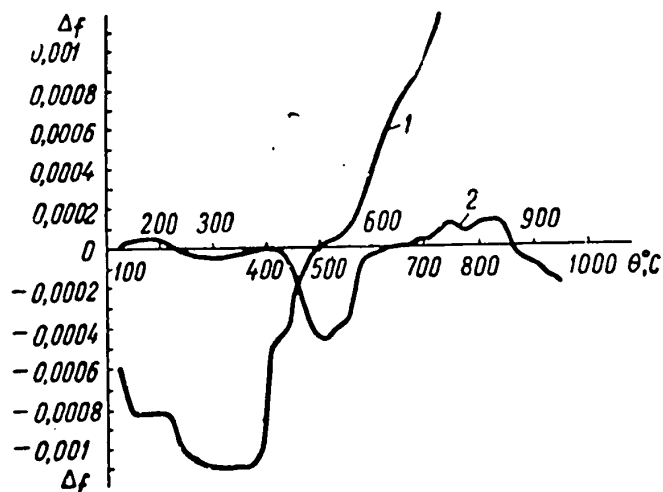
Fig. 47 - Temperature Coefficient of Friction, According to

G. I. Troyanovskiy for Plastics 6FP and No. 22

1 - Plastic No. 22; 2 - Plastic 6FP

The material 6F had a very high friction coefficient even at temperatures of $900-1000^\circ$C and high heat resistance. At high temperatures, the wear of the material 6F was less than the wear of the Plastic No. 22, and the phenomena of abrasion of the cast iron surface and its sliding over the plastic were absent. The material 6F did not char and was not destroyed. However, it showed an increase in brittleness.

As shown in the graphs (Fig. 47), the material 6FP had a considerably better temperature friction coefficient than the Plastic No. 22.

This was the reason for recommending the friction material 6F for actual tests.

132

STAT

The material "Retinax", which was developed later, belongs to this group.

Lately a number of new experimental cermet friction materials have been developed which satisfy the principles for making friction materials. These materials showed good results when tested on the machine I-47 and are recommended for full scale tests.

The experience of the Laboratory for Friction and Friction Materials IMASh, Academy of Sciences, USSR and of the basic research organizations of the country, working on the development of metal and nonmetal friction materials, makes it possible to recomment the ring friction machine I-47 for laboratory rating of various types of friction materials, in small sample lots.

Project for Methods of Rating Heat Resistance in Friction Materials on the Ring Friction Machine I-47

Tests were conducted on a machine of the type I-47, which has two structural variants for mounting the specimens and which allows samples to be tested:

1) when friction takes place between their bases at a different ratio of contact surfaces.

2) when friction takes place along the generatrix at a different ratio of contact surfaces.

For the first variant the shape of the specimens is shown in Fig. 48. In the lower specimen, usually metallic, narrow notches are cut to remove wear particles. The upper specimen may be provided with notches whose size is determined by the required ratio of contact surfaces. The sizes of samples for the first variant coincide with the dimensions of the inner sample for the second variant (Fig. 49).

For the second variant, in which the inner sample coincides in dimension with the specimens of the first variant, the outer specimen is built up of several separate small blocks; every block is subjected to the same pressure, produced by a hollow rubber chamber.

The lower specimen in the first variant and the outer specimen in the second

133

STAT

are mounted to the torsion shaft. The torsion angle of the shaft is used for computing the friction moment and consequently the friction coefficient.

a   *b*

Fig. 48 – Specimens for Testing on the Ring Friction Machine I-47

a – Upper specimen; b – Lower specimen

The upper specimen in the first variant and the inner specimen in the second are connected to the revolving spindle.

In the first variant, the spindle should move freely in the guides and produce the necessary pressure on the specimen. In the second variant, the spindle has no free axial movement, and to attain this the spindle is fixed by a special pin. The pressure on the specimens in the second variant is achieved by changing the inside pressure in the hollow rubber chamber (pressure controlled by a manometer).

Preparation of Specimens for Testing. For both variants, specimens are cut out of a finished lot of friction products.

For each test, not less than three specimens are cut from three different products of the same lot.

The metal counterpart body is made of the metal actually used in a given brake unit.

Before testing, the specimens are fitted (lapped) at small sliding speeds which provide for an increase in temperature in the friction unit of not more than

134

STAT

60-70°C. Lapping is considered completed when the entire friction surface shows traces of wear.

A thermocouple is built into the stationary specimen, with the cold junction located at a distance of 1 mm from the friction surface. The safe margin of linear wear is up to 0.5 mm, after which the thermocouple should be attached in a new place. The friction surface of the metal sample is cleaned before lapping.

Fig. 49 - Specimens for Testing on the Ring Friction Machine I-47.

1 - Inner specimen (connected with the revolving spindle);

2 - Outer specimen; 3 - Brake Chamber; 4 - Outside Head (Connected with the torsion shaft)

Technique for Conducting the Experiment

To determine the heat resistance in a friction pair to be tested, a load on a lever is used which provides specific pressure on the test specimens corresponding to the actual specific pressure of that friction unit for which the test pair is intended.

This specific pressure is maintained constant during the entire test. Also, the specimens are prepared for testing in such a way that, in the contact plane (contact is achieved by having the bases touch) reciprocal contact overlap of the specimens would be analagous (or close) to reciprocal contact overlap in the actual friction unit .

After this the specimens, which are under a given pressure, are made to slip relative to each other.

The sliding speed v_{sk} increases gradually by stages from 0.125 to 5 m/sec, and

135

STAT

at each stage a definite temperature is formed for the pair under test. Usually the test is conducted at 7 - 9 speed stages.

The duration of the experiment for each stage is 15 min. Normally, stabilization of the heat conditions is reached after three or four minutes. Therefore, the oscillograph reading for the friction moment and the galvanometer reading (or oscillograph reading) for temperature are made every 5, 10, and 15 min after starting the experiment at a given step.

If, at a given temperature, no changes occur in the materials of the friction pair then all three readings on the oscillograph tape are identical.

Thus, passing from one stage to another, temperatures as they exist in the actual friction unit are obtained. Usually, for many friction materials, temperatures of 400-600°C are reached at sliding speeds of v_{sk} = 1.6 - 2.4 m/sec. However, in general the testing of a given friction pair is not stopped at the actual temperature stage but is continued to determine the limits of friction properties in the test pair. On the friction machine I-47, testing can be conducted at a temperature of 1000°C and higher. Such temperatures are created in the samples when the sliding speeds reach v_{sk} = 4.0 - 5.0 m/sec.

The wear resistance of a friction test pair is rated according to the wear in terms of weight of the cooled specimens, which are weighed on analytical scales before and after each experiment at a given temperature stage. If, in some cases, it is more convenient to have a linear intensity of wear, several readings must be used for fixing a mean value for the difference in linear dimensions of specimens, after they have been in rubbing contact for fifteen minutes at a given temperature stage.

Basic changes (change in color, charring, sparking, fouling etc.) are usually recorded by the experimenter in his records. The dependence on temperature of both the friction coefficient and the intensity of wear are found as a mean value during the testing of three specimens.

The coefficient of friction f is calculated according to the following formula:

136

STAT

$$f = \frac{M}{rP}, \qquad (209)$$

where M = measured friction moment, in kg - cm;

r = mean radius of the specimen (1.2 cm) for the first variant;

for the second variant, r is the outside radius of the inner specimen

(1.4 cm);

p = total pressure on the sample in kg.

The intensity of wear J_B is calculated according to the formula*:

$$J_B = \frac{\Delta g}{SL}, \qquad (210)$$

where Δg = difference in weight, in mg;

S = area over which rubbing of the sample takes place, in cm^2.

It should be noted that, when the ratio of the touching surfaces is not equal to unity, the sizes of areas by which wear intensity is measured are different for the upper and lower specimens in the first variant and for the outer and inner specimens in the second variant.

L which denotes the friction path (in meters) in the first variant is determined from the mean diameter of the specimen d_{mean} = 0.024 m, and in the second variant from the outer diameter of the inner specimen d_{mean} = 0.028 m.

<u>Recommended Testing Conditions.</u> It is necessary to maintain different conditions for friction materials intended for different friction units.

Approximate mean values for these conditions are given in the following Table.

---

* Intensity of wear may also be found in accordance with the formula $J = \frac{\Delta g}{A_T}$, where A^T is the friction work produced at a given temperature stage.

STAT

Type of Materials	Specific Pressure kg/cm^2	Temperature $^{\circ}C$
For aircraft brakes	15 – 18	800 900
For drill hoists	6 – 10	600
For excavators type ESh-4/40	7 – 12	320 – 360
For automobile power brakes	5	250
For ordinary automobile brakes	3	170

138

STAT

LABORATORY TESTING OF FRICTIONAL PAIRS IN ACTUAL
BRAKES ON AN INERTIA STAND

Under nonstationary heat conditions, the rating of friction properties in small samples cannot give exact results. As a result of this, actual tests of brakes on an inertia stand operating under definitely nonstationary conditions because of decisive importance. These tests have the drawback in that they require much power and very powerful and bulky equipment.

Short Description of an Inertia Stand

The underlying principle of tests on an inertia stand is as follows: The flywheel and drum are set in motion and the speed is increased up to the required number of revolutions; in this manner, the energy of the flywheel masses is, stored. This energy is equal to the kinetic energy applied to the aircraft brake being tested, and it is absorbed and dissipated by braking the stand to which the test brake is mounted until the flywheel masses and drum come to a complete stop with the wheel pressing against the latter. Figure 50 shows a general view of an inertia stand and control panel. In the process of braking, any changes in the brake moment, the pressure in the brake, and the revolutions of the stand are automatically recorded according to the braking time.

The wheel is pressed against the drum with a force equal to the radial stress transmitted to the given wheel by the weight of the aircraft when at a standstill. The compressive force is controlled by contraction of the tire. Pressure is created

139

STAT
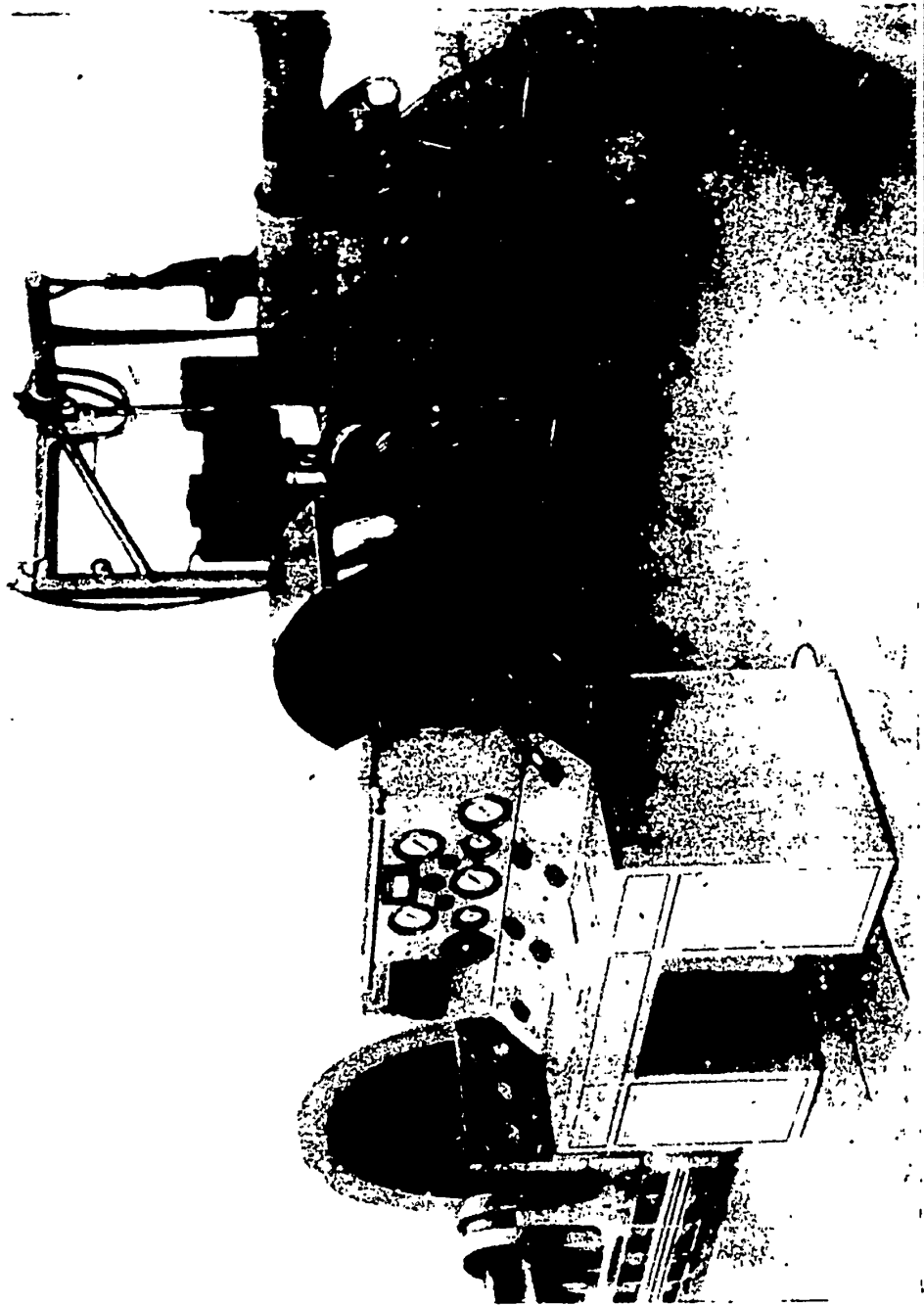
Fig. 50 – General View of Inertia Stand and Control Panel

140

in the test brake (by pneumatic or hydraulic means), with the magnitude of the pressure being so selected that the required brake moment is attained. In existing chamber brakes, a pressure of $p_T = 15$–40 kg/cm^2 is used. Multidisk brakes have pressures in the cylinders differing little in magnitude from the pressures in a chamber brake, while the pressure in a unidisk brake cylinder is considerably higher than the pressure in chamber and multidisk brakes. With some unidisk brakes cylinder, the pressure reaches 180 kg/cm^2 and more.

According to standards, the peripheral speed of the stand drum and therefore the speed of the wheel forced against it by the test brake, at incipient braking, should be

$$v_{per} = 0,8 v_{pos}. \qquad (211)$$

When testing a brake isolated from a wheel, the shaft revolutions should be equal to the wheel revolutions, guaranteeing a speed equal to 0.8 v_{pos}.

The number of flywheels connected to the stand shaft should be such that, at a given peripheral speed, the kinetic energy of the flywheels is equal to

$$A_T = 0,036 P_{ST} v_{pos}^2 + U, \qquad (212)$$

where A_T = kinetic energy, standardized for a given brake;

P_{st} = radial stationary stress on wheel;

v_{pos} = landing speed of the aircraft for which the given wheel and brake are intended;

U = energy loss in the stand due to overcoming friction in the shaft bearings, aerodynamic resistance to rotation of flywheel masses, and resistance to rolling of the wheel over the drum.

After the stand is stopped, the wheel is disengaged from the drum and cooled to room temperature. Then the cycle is repeated, i.e., the stand is brought to the required speed, the wheel is pressed to the drum, and the test brake is applied to bring the stand to a full stop.

141

STAT

The inertia stand (Fig. 51) consists of a shaft, a set of heavy flywheels (2) and a drum (3) installed on the stand shaft, an electric motor (5) connected to the end of the stand shaft, a brake (4) for stopping the stand in emergency cases, a pressure device (6), a device (1) for testing isolated brakes, and the base.

Basic Data of the Stand: Motor Pn-1320, N = 150 kw, n = 1500 rpm; maximum peripheral speed of drum v = 400 km/hr, inertia moments of revolving masses: $J_{max} = 211$ $kg/m-sec^2$, $J_{min} = 28$ $kg/m-sec^2$, maximum size of tested wheel 850 × 250, $P_{st} = 3800$ kg.

The Main Shaft of the stand, carrying the flywheels (2) and the drum (3), is set on four antifriction bearings, one on each side of the drum and two next to the flywheels. An electric motor is connected to the right end of the shaft over an elastic coupling. A brake drum for testing isolated brakes is connected to the left. Between the stand drum (3) and the flywheels, a special coupling is installed which makes it possible, when necessary, to disconnect the shaft and thus to disengage all flywheels at once. The shaft with the system of flywheels, drum and bearings, rests on supports set on a common solid frame of welded girders connected by anchor bolts to the base.

The Flywheels of the Stand are made in the form of solid steel disks of various thicknesses. Each flywheel can be easily connected to the shaft and, when necessary, disconnected. When flywheels have to be connected to the shaft, they are bolted to counterdisks which are rigidly connected to the shaft. Disconnected unused flywheels rest on special cylindrical footings fastened on supports. The number and weight of flywheels is selected so that, at a given peripheral speed v_{okr} the required kinetic energy can be obtained in a range from $A_{stand\ min}$ to $A_{stand\ max}$, with an accuracy of $\pm$ 5%.

The Drum of the stand (3) consists of a steel cylinder 600 mm wide and 1466 mm in diameter, welded to two ribbed steel disks which are connected with a hub, fitted tightly to the stand shaft.

The Emergency Brake (4) consists of a double chamber brake with a diameter of

STAT

Cross Section thr. A-B
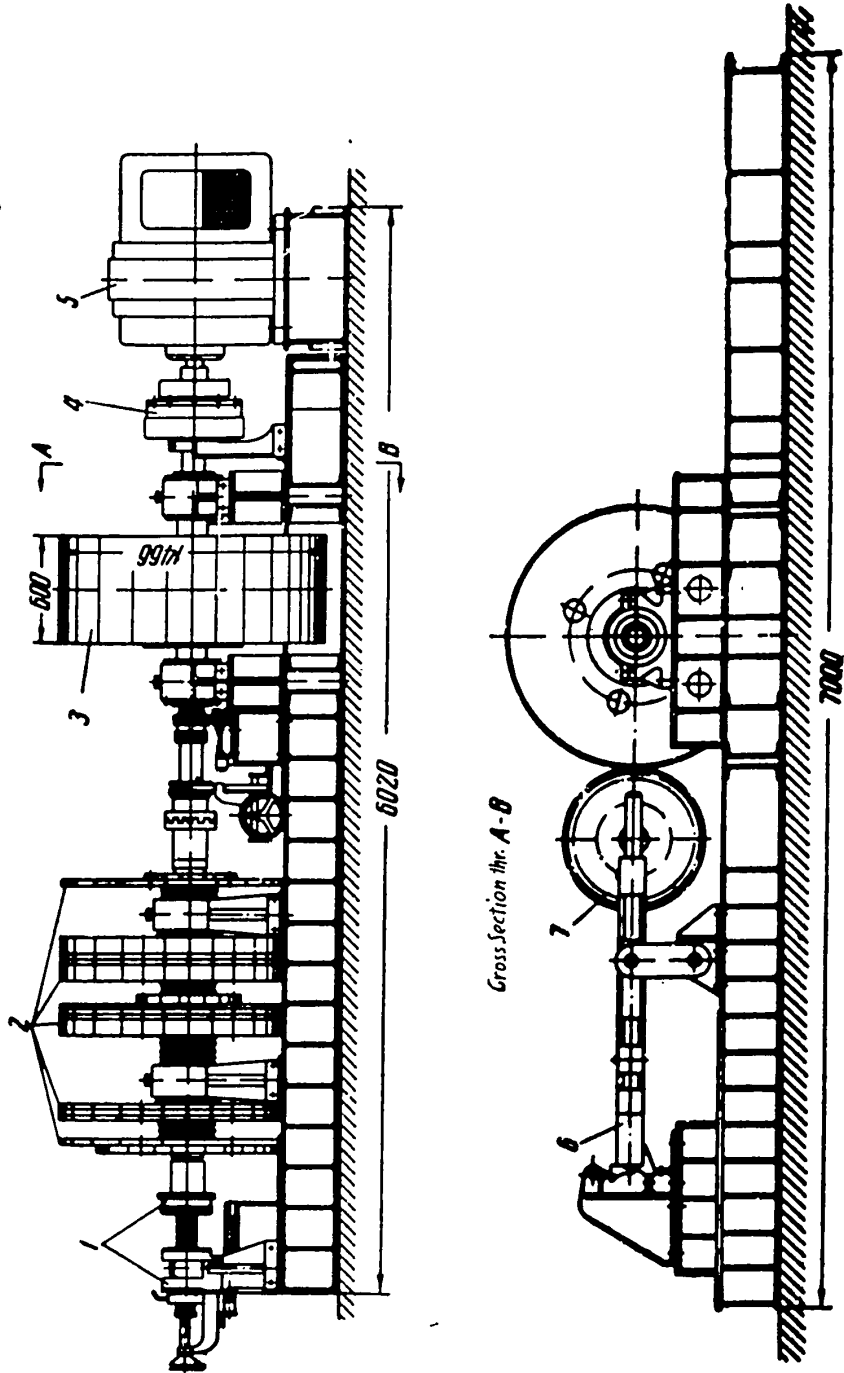
Fig. 51 - Diagram of Inertia Stand

1 - Assembly for testing isolated brakes; 2 - Flywheel masses; 3 - Drum;

4 - Emergency brake; 5 - Electric motor; 6 - Pressure device; 7 - Test wheel.

143

STAT

of 507 mm and a width of 140 mm, rigidly mounted to a bracket set on the stand base, and a steel brake drum connected to a flange solidly set on the main shaft. The weight of the brake drum of the emergency brake is so selected that, when the maximum energy of the stand is absorbed in emergency braking, its temperature reaches $500^\circ C$. The maximum brake moment of the emergency brake equals 250,000 kg/cm when $p_T = 17$ kg/cm^2. The brake stops the stand at a speed of $v_{okr} = 400$ km/hr in 6 sec. The emergency brake is switched on from the control panel.

The Electric DC Motor (5) of the stand is fed from a separate motorgenerator system. With all flywheels connected, the motor brings the machine to the maximum number of revolutions in 2 min. Starting and stopping and controlling the speed of the motor is done through the control panel.

The Pressure Device serves to press the wheel and the tested brake to the stand drum. It consists of two frames in one horizontal plane. The first of these frames is hinged to the stand frame; the second is fastened to the cylindrical guides of the first frame. The second frame can slide along guides of the first frame and so perform reciprocating motion under the action of the hydraulic cylinder. A wheel and its axle are set on the second frame. The wheel axle is rigidly fastened in clamps to the second frame.

The test brake is set freely on the wheel axle so that, under the action of the brake moment, it can easily turn around the axle center. A lever is fixed to the brake, with its free end resting on the piston of a hydraulic dynamometer which transfers the pressure along a pipe to a manometer recorder on the control panel.

The pressure device has a hydraulic system to help press the wheel against the drum and disengage it. The rate of pressing and the speed of disengaging are constant and are equal to 0.5 m/sec. The compressive force is regulated by a reduction valve switched into the line between pump and hydraulic cylinder and is controlled by the magnitude of radial contraction of the tire pressed to the drum of the wheel. Control of the hydraulic system of the pressure device is carried out from the control panel.

144

STAT

The Setup (1) for Isolated Test of brakes consists of a support to which the test brake is mounted. The setup has a dynamometer connected by a pipe to a recorder on the control panel; the free end of the brake lever rests on this dynamometer. A removable brake drum is connected rigidly to the end of the shaft and revolves together with the shaft.

The Base has a depth of 3.5 m. It is furnished with an iron trussing and anchor bolts which connect the stand frame to it. To eliminate vibrations, the area of support and the volume of the base are designed in such a manner that the amplitude of vertical vibrations of the base is less than its elastic contraction under active loads. At the same time, the frequency of the base vibrations, when the stand is operating, is 30% higher than the frequency of vibrations induced by the acting load.

The Control Panel for the stand has one vertical and one slanted panel. On the vertical panel are the manometer recorder and the manometers which show the air pressure in the storage balloon, reduced pressure, pressure in the test brake and pressure of the hydraulic system of the pressure device. In addition, the vertical panel carries an ammeter for the electric drive of the stand, a galvanometer to measure the temperature of the heated wheel and brake during testing, an electric tachometer showing the peripheral speed of the stand drum, and a system of signal lights used when the stand is being started.

The slanted panel carries pushbuttons and knobs for controlling the stand, the electric drive, the hydraulic system of the pressure device, the emergency brake, and a toggle switch for switching the tape recorder mechanism on and off. Above the machine-controlknob is a manometer to show the pressure in the emergency brake. The panels of the control panel are lighted by a fluorescent tube mounted to the top of the vertical panel. When tests are conducted, an operator standing at the control panel faces the test object. The control panel is 1300 mm high. This height was selected to permit the operator to watch not only the panel instruments but also the test object.

145

STAT

Power test on the stand were preceded by selective tests of friction materials on small samples. These tests had been conducted in the Laboratory for Friction and Frictional Materials of the Machine Studies Institute, Academy of Sciences, USSR.

Testing Conditions on an Inertia Stand

As mentioned above, after preliminary tests on small samples several types of new experimental frictional materials which have shown better properties when compared to the mass-produced friction plastic No. 22 were recommended for actual brake tests on the inertia stand. Let us see how the tests of these suggested materials were conducted.

The characteristics of these experimental frictional materials and mass-produced materials are shown in Table 2.

Tests were conducted on wheels, size 660×160, equipped with two brakes of basically different design. In one case, the wheel had a unidisk brake with a partially open and ventilated friction surface; in the other case, the wheel had a chamber brake whose friction surface was mostly covered.

The brake disk and brake drum of the wheel were made of ChNMKh cast iron.

The tests were conducted under the following conditions:

Radial stress on wheel p_{st}, kg – 2250:

Pressure in pneumatic tire p_o, kg/cm^2 – 7.5:

Stationary contraction of tire δ_{st}, mm – 40.

When tested on a disk brake, the peripheral speed of the stand drum was $v_{okr} = 0.8 v_{pos} = 160$ km/hr. This speed corresponded to the sliding speed of the disk brake pair

$$v_{sk}^{d} = 0{,}39\, v_{okr} = 17{,}3 \ m/sec. \qquad (213)$$

Tests with a chamber brake under calculated conditions were conducted at two speeds : $v_{okr} = 160$ km/hr and $v_{okr} = 300$ km/hr; this corresponded to sliding speeds of 21.1 and 39.6 m/sec, calculated by the formula

146

STAT

$$v_{sk}^{\kappa} = 0,475\, v_{okr}.$$

Under conditions of different pressures in the brake, tests were conducted at speeds of v_{okr} = 214, 254, and 300 km/hr. The weight of the brake disk was equal to half the calculated weight. Therefore, the kinetic energy of the flywheel masses of the stand, when tested on a disk brake, were assumed equal to one half of the energy normal for a wheel of 660 × 160: $\frac{\Delta_T}{2}$ = 125,000 kgm.

Table 2

Type of Friction Material	Composition	Cohesive Medium	Some Characteristics of the Materials		
			Specific Weight gm/m^3	Heat Conductivity kcal/m hr $^\circ$C	Heat Capacity kcal/kg $^\circ$C
No. 22	Asbestos-rubber composition	Rubber and dark factice	1.87	0.41	0.248
"M"	Unknown	Unknown	2.0	0.52	Unknown
6FS	Plastic Composition	Resins	3.05	1.1	0.345
6FP	Plastic Composition	Resins	2.97	1.2	0.327

Tests in a chamber brake were conducted with full kinetic energy A_T = 250,00 kg – m.

A pressure p_T = const was intermittently applied to the brakes and was maintained until the flywheel forces of the stand came to a complete stop. At the end of each individual braking, 15-20 sec after the wheel had been stopped, the temperature was measured by means of the thermocouple. This was the temperature of the brake drum (or brake disk when a disk brake was being tested).

The wear was figured by measuring the thickness of the brake lining before and

STAT

braking. Beam compasses served for measuring.

Before the tests, the test lining was fitted to the friction surface of the brake disk and the friction surface of the drum. The brakes were worked on until the selected magnitude of pressure in the brake resulted in a calculated magnitude of the brake moment $M_{T\ max}$, which was recorded at three consecutive brakings.

Considering that the landing speeds of jet aircraft are equal to 50-100 m/sec, the sliding speeds of a friction pair in wheel brakes of modern jet aircraft are made equal to v_{sk} = 25-50 m/sec.

The power absorbed by a brake is found from the formula

$$N_T = f p_{ud} S_T \frac{r_T}{r} v_{pos} = f p_{ud} S_T v_{sk},\qquad(215)$$

and this power characterizes the effectiveness of braking. The magnitude of the power N_T shows how effectively a given brake absorbs the given kinetic energy of an aircraft. The more kinetic energy is absorbed by a given brake in unit time, i.e., the higher (other conditions being equal) the mean power $N_{T\ mean}$ becomes, the more intensive will be the braking and the higher the brake efficiency. Equation (215) indicates that the power absorbed by a given brake depends not only on its geometric dimensions S_T, r_T, specific pressure p_{ud} and rate of sliding v_{sk}, but also on the magnitude of the friction coefficient f of the pair. Therefore, we may state that the more power is absorbed by a given brake at a given p_{ud} and v_{sk} the higher will be the efficiency of a given frictional brake pair. The specific powers used in modern brakes are in the range 30 - 70 kg/cm^2 sec.

The design of a brake has a noticeable effect on the performance of the brake lining. As shown by experiments, the friction plastics 6FP, 6FS, and "M" combined with cast iron ChMNKh and operating under conditions of a unidisk brake with a partially open friction surface, have a lower friction coefficient than when operating under conditions of a chamber brake. This is explained by the different heat conditions on the friction surfaces of chamber and disk brakes. This also explains the

STAT

fact that the efficiency of a pair, the stability of its friction coefficient at braking, and its resistance to wear are different for disk and chamber brakes.

Braking efficiency, stability of friction coefficient, and resistance to wear of the tested frictional pairs were studied as functions of the sliding speed v_{sk} and the pressure p_T in a brake whose size, in the case of chamber and unidisk types, was proportional to the specific pressure p_{ud}.

The kinetic energy of the stand in these tests was made constant and equal to the standardized kinetic energy for a given wheel. Additional tests were made with the plastic No. 22, combined with cast iron ChMNKh, in a chamber brake. This was done at calculated $M_{T\ max}$ and v_{okr}, i.e., at calculated N_T and for different magnitudes of kinetic energy. The dependence of the wear of the brake lining on the value of the kinetic energy was determined in these tests.

The speed of fitting of brake shoes is an important feature in braking. The best friction pair, other conditions being equal, is one which requires a minimum amount of braking for a calculated brake moment, under calculated pressure.

After mounting unidisk and chamber brakes, ten brakings were made for each plastic under calculated conditions which were the same for all tested plastics, i.e., at the same magnitudes of $M_{T\ max}$, v_{okr} and A_T. As long as these ten brakings for every sample were made at similar $M_{T\ max}$ and v_{okr}, it can be said that tests were made under similar maximum power

$$N_{T.\ max} = M_{T.\ max}\ \omega,\qquad\qquad (216)$$

where ω is the angular velocity of a wheel.

The mean value of the power $N_{T\ mean}$ in the process of braking depends on the value of the mean brake moment. Since various test plastics may have a different stability of the friction coefficient, the value of the mean specific brake power will be different for different materials. Moreover, in every one of the tested plastics the value of the absolute maximum friction coefficient differed from the absolute

149

STAT

value of the maximum friction coefficient of other plastics. Therefore the value of the pressure p_T in a brake was selected separately for each plastic to secure a calculated brake moment. Consequently, similarity of specific pressures for the tested plastics was not maintained.

Ten brakings for each plastic under calculated conditions of $v_{okr} = 160$ km/hr were conducted on disk and chamber brakes, for the plastics 6FP and No. 22. Besides this, five more brakings were conducted under the same calculated conditions on a chamber brake, but at speeds of $v_{okr} = 214$, 254, and 300 km/hr, i.e., at higher power and greater sliding speeds. All brakings, under calculated conditions, were conducted to determine the resistance to wear of each given pair and also to determine the general comparative evaluation of the friction characteristics of the tested pairs at various sliding speeds.

To determine the dependence of the braking efficiency and the stability of the friction coefficient of the tested plastics on the specific pressure and sliding speed in a unidisk brake at a speed of $v_{okr} = 160$ km/hr, two braking tests were made for each material at $p_T = 8$, 11, 12, 13, 16, 20, 24, 26, 28, and 30 kg/cm^2. Using a chamber brake, two brakings were made at speeds of $v_{okr} = 160$, 214, 254, and 300 km/hr with brake pressures of $p_T = 4$, 8, 10, 12, 15, 18, 20, 22, 25, and 28 kg/cm^2.

The results of the tests are shown in Table 3: The numerical values of the maximum calculated brake moment $M_{T\ max}$, of the mean brake moment $M_{T\ mean}$, of the length L of the brake path of the wheel, the time t of braking, and the linear wear Δ of the shoes for one braking - all were obtained as mean values of ten brakings operating under the calculated conditions shown above, at a speed of $v_{okr} = 160$ km/hr when tested on a unidisk brake and at speeds of $v_{okr} = 160$ and 300 km/hr when using a chamber brake.

Table 3 shows that when the braking is performed under the same calculated conditions for all tested pairs, at practically equal $M_{T\ max}$, A_T, and v_{okr}, the disk brake equipped with linings made of plastics "M" and 6FS guarantees a shorter brake

STAT

path for a wheel, compared with a brake equipped with linings made of plastic No. 22. At the same time, to get the calculated brake moment, the first brake requires the lowest pressure.

A chamber brake equipped with linings made of plastic No. 22, when braking under calculated conditions at a sliding speed of the pair of 21.1 m/sec, also gives a longer brake path of the wheel than a chamber brake quipped with linings made of the experimental plastics 6FS, 6FP, and "M". In a chamber brake with linings made of the plastics No. 22, the pressure in the brake required for $M_{T\ max}\ 0.4$ at this speed is no longer lower but higher than in brakes with linings made of the plastics 6FP and 6FS.

At a higher sliding speed of the pair equal to 39.6 m/sec, corresponding to a peripheral speed of v_{okr} = 300 km/hr according to eq. (214), the chamber brake with linings made of the plastic No. 22 gives a shorter brake path length than a brake with linings made of the plastics "M", 6FP, and 6FS. However, the pressure in a chamber brake with facings made of the plastic No. 22 was double at this speed compared to a brake with the plastics 6FP and 6FS. This is explained by changes in the surface of the friction pairs, which take place in the braking process.

Surface Changes of Materials in Braking

Figure 52 gives a photomicrograph of a polished cross-section specimen of a brake shoe friction surface made of the plastic 6FP, while Fig. 53 gives the same for the plastic No. 22.

As can be seen from Fig. 47, the specific feature of the plastic 6FP is a well-defined film on the friction surface of the shoe. This film prevents the metal of the brake jacket from folding over on the shoe.

Figure 54 shows a brake drum and a brake with shoes made of the plastic 6FP. The friction surfaces of the drum and shoes have a smooth polished appearance. Figure 55 shows a brake drum and a brake with shoes made of the plastic No. 22.

STAT

Table 3

Test Data

Lining Material	Speed r_{okr}, km/hr	Speed v_{sk}, m/sec	Pressure p_T, kg/cm²	Pressure p_{ud}, kg/cm²	$M_{T. max}$ 0,4, kg·cm	$M_{T. mean}$, kg·cm	Brake path of wheel L, m	Time of braking until stand stops t_r, sec	Linear wear of lining for one braking Δ, mm	Temperature of brake drum (disk) at end of braking θ, °C	Mean specific friction horsepower $N_{ud} = \frac{A_T}{\Sigma_T^1}$ kgm/cm²·sec.	Relative wear for 1 braking $\Delta_o = \frac{\Delta}{N_{ud}\cdot sp}$
Unidisk Brake												
№ 22	160	17,3	13,5	8,5	12 780	11 240	303	15,2	0,100	358	22,1	0,00452
«М»	160		22	13,9	14 080	12 010	295	14,4	0,06	365	24,2	0,00107
6 FP	163	17,6	16,5	10,4	13 300	12 015	287	14,1	0,0258	347	23,6	0,00109
6 FS	189	20,5	22	13,9	13 385	12 465	273	12,8	0,0248	329	25,4	0,00098
6 FS			22	13,9	18 280	15 410	218	8,5	0,0230	310	38,0	0,0006
Chamber Brake												
№ 22	160	21,1	15,0	12,0	25 830	21 360	396	17,3	0,075	351	25,7	0,00292
	300	39,6	20,0	16,0	26 020	20 680	367	9,1	0,080	329	45,9	0,00174
«М»	160	21,1	14,0	11,2	26 060	21 620	355	15,6	Spreading 0,283	349	28,4	0,00099
	160	21,1	11,5	9,2	26 470	23 370	337	15,4	0,66	324	29,4	0,00224
6 FP	200	39,6	10,0	8,0	24 800	19 480	392	9,2	0,075	339	47,7	0,00157
6 FS	160	21,1	8,0	6,4	26 460	21 595	350	16,5	0,053	324	26,4	0,00200
6 FS	300	39,6	10,0	8,0	27 060	20 740	380	8,9	0,066	336	51,2	0,00129

STAT

The metal of the brake drum, folded over the shoes, formed a hard crust in bands on the friction surfaces of the shoes.

During folding over, the friction surface of a pair is destroyed and its friction qualities deteriorate. When brake shoes are subject to folding over, a part of

Fig. 52 – Friction Surface of a Brake Shoe Made of Plastic 6FP after Operation in a Chamber Brake at $v_{okr} = 300$ km/hr. Cross section of polished specimen, not etched, $\times 140$ (V. M. Gudchenko)

1 – Wood's alloy, 2 – Film on shoe surface; 3 – Plastic; 4 – Brass.

the friction surface of the brake forms a homogenerous pair: cast iron plus cast iron with a friction coefficient considerably lower than that of a pair made of plastic plus cast iron. Folding over disrupts the contact of pair elements; this, in turn,

STAT

decreases the friction force and the uniformity of specific pressure distribution over the contact surface of the shoes and drum. Therefore in the case of folding

Fig. 53 - Friction Surface of Brake Shoe made of Plastic No. 22 after Operation in a Chamber Brake. Cross Section of Polished specimen, not etched, × 200 (V. M. Gudchenko).

1 - Friction surface; 2 - Wood's alloy; 3 - Metal layer, applied to shoe (white layer not etched). 4 - Crumbled layer of burned plastic; 5 - Plastic No. 22 of changed composition

over a higher pressure is required in the brake to reach a calculated brake moment. When folding over takes place, in addition to deterioration of the frictional qualities of the pair, burs appear in the form of deep, ring-like, small grooves

STAT

154
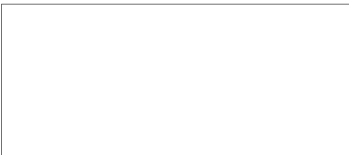
(Fig. 55a). Strips of metal on the surface of a shoe do not remain intact. The metal films, during brakings, is either detached in places from the friction surface of
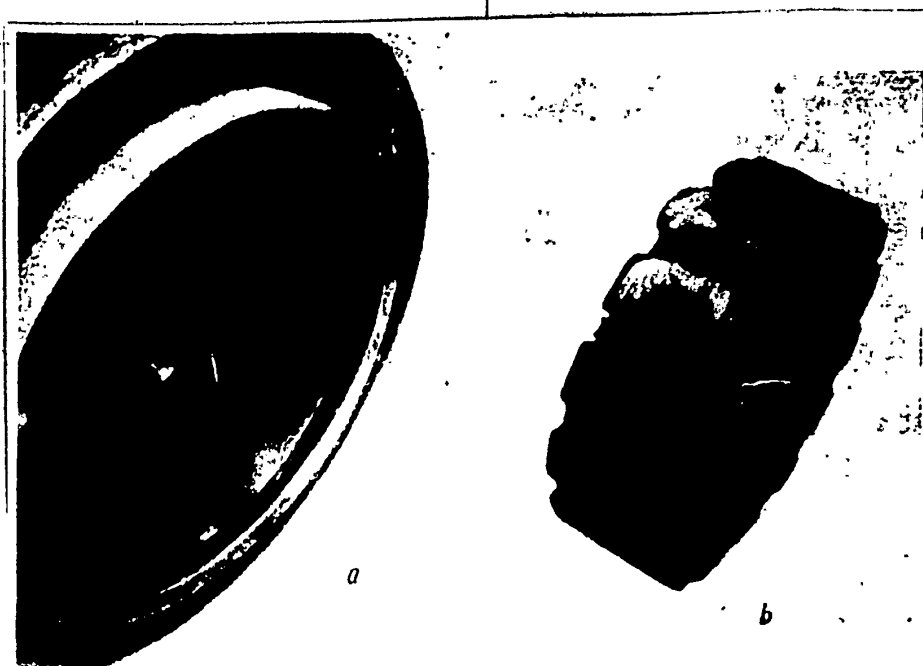
Fig. 54 - Friction Surfaces after Braking.

a - Brake drum (cast iron ChNMKh). b - Shoes (6FP)

the shoes, tearing off pieces of plastic as in the case of linking, or metal appears in another place. This leads not only to considerable destruction of the brake friction surface, but to instability of the brake moment. At the same pressure in the brake, the brake moment changes its value from one braking to another within rather wide limits.

It should be noted that a unidisk brake with shoes of plastic No. 22, during braking under calculated conditions did not show folding over of the disk metal over the friction surface of the linings.

When working under calculated conditions, the unidisk brake with linings made of plastics 6FP and "M" showed no folding over of metal either. At all sliding speeds, the friction surface of the frictional pair in a unidisk brake retained its smooth, clean appearance.

STAT

When working under calculated conditions, the behavior of the plastics 6FP and "M" in a chamber brake changes somewhat. In the chamber brake at v_{sk} = 21.1 m/sec, linings made of plastic "M" showed fold-over of a very thin layer of metal folded over the friction surface in the form of separate ring-like bands. However, even with light folding over the metal, the plastic "M" when tested in a chamber brake

Fig. 55 - Friction Surfaces after Braking

a - Brake Drum (ChNMKh); b - Shoes (plastic No. 22).

showed improved frictional properties: In the chamber brake less pressure was required to produce the calculated moment than in a unidisk brake.

Chamber brake linings made of plastics 6FP and 6Fs showed no fold over on their friction surface. Their friction surfaces were smooth and polished, with traces of surface film in the form of molten, softened brass. The brake drum, coupled with shoes made of plastics 6FP and 6FS, had a perfectly smooth and polished friction surface, just as in braking at an initial speed of v_{okr} = 160 km/hr at a corresponding v_{sk} = 21.1 m/sec, and just as in braking at an initial speed of v_{okr} = 300 km/hr at a corresponding v_{sk} = 39.6 m/sec. On the friction surface of the drum there was

156

STAT

a thin smooth layer of brass transferred from the friction surface of the linings. This folding of brass over the friction surface of the drum did not result in the type of destruction usually caused by folding of cast iron over the friction surface of the lining. On the contrary, this folding over of brass together with other elements of the plastic - barite and brass resins - evidently forms a film which does not destroy the softened friction surface of the cast iron drum and moreover has a lubricating and polishing action. Evidently this is the reason why the plastics 6FP and 6FS increase their friction qualities when operating in a chamber brake. To achieve a calculated brake moment $M_{T\ max}$ the plastic 6FP requires less pressure in a chamber brake than in a unidisk brake, and less than the plastics No. 22 and "M" in a chamber brake. In a chamber brake, the plastic 6FS requires considerably less pressure than No. 22 and "M". In other words, the plastics 6FP, 6FS, and "M" compared to the plastic No. 22, allow the use of a brake with smaller dimensions but of the same force.

Brake Characteristics of a Wheel

Diagrams of brake moments determined in tests on disk and chamber brakes are shown in Fig. 56, 57, and 58. Each diagram is based on data from ten separate brakings.

The completeness of a brake moment diagram characterizes the stability of the friction coefficient of a pair: the more complete the diagram, i.e., the less the value of brake moment is decreased from its maximum in the process of braking, the higher will be the stability of the friction coefficient of a brake pair.

The diagrams of brake moments of a disk brake in braking under calculated conditions at sliding speeds of $v_{sk} = 0.39$ and $v_{okr} = 17.3$ m/sec (Fig. 56) show that the plastic 6FP has the greatest stability of friction coefficient in the process of braking, when combined with cast tiron ChNMKh. The brake moment of a unidisk brake with linings made of the plastic 6FP shows practically no change in value all along

157

STAT

its friction path. The plastics No. 22 and "M" have less stable friction coefficients: The brake moment decreases at the end of the braking (for the plastic No. 22 - 36%).
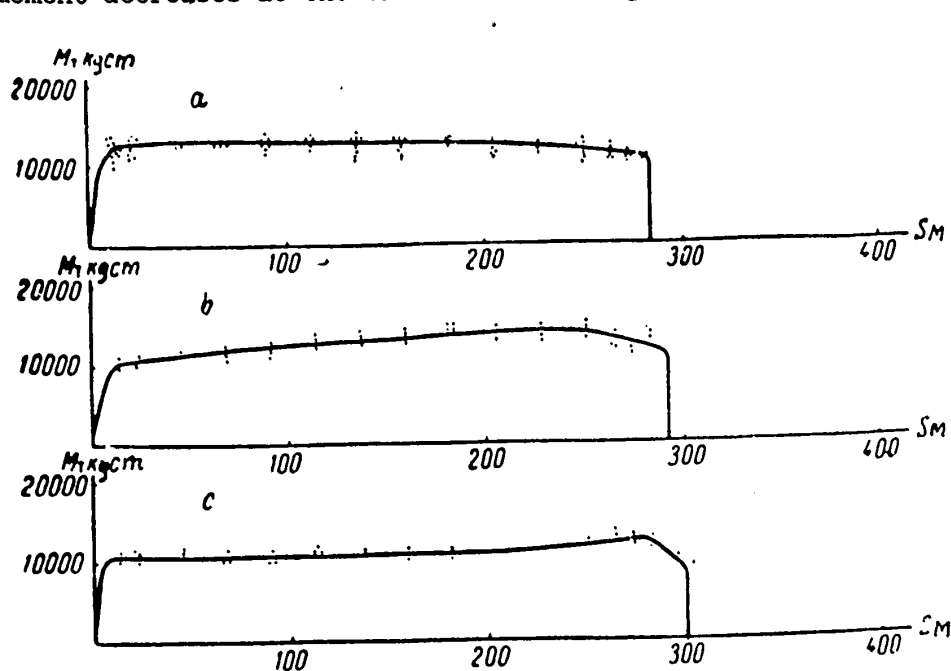
Fig. 56 - Diagram of Brake Moments of a Disk Brake at a Sliding Speed of 17.3 m/sec

a) For the plastic 6FP at p_T = 16.5 kg/cm^2; b) For the Plastic "M" at p_T = 22 kg/cm^2; c) For plastic No. 22 at p_T = 13.5 kg/cm^2.

As a result of the instability of the friction coefficient of a frictional pair, the brake-path length of a wheel equipped with a brake with plastic "M" linings and the brake-path length of a wheel equipped with brakes with plastic No. 22 linings are longer than the brake-path length of a wheel equipped with a brake with plastic 6FP linings.

The diagrams of the brake moment of a chamber brake (Fig. 57), equipped with linings made of the same plastics No. 22, 6FP, "M", plotted in brake tests at a speed of v_{sk} = 21.1 m/sec differ in nature from diagrams of unidisk brake moments.

Each curve presented in Fig. 57 has a saddle-like depression (flexure in the middle).

The nature of the instability of the friction coefficient of the plastics No.22

STAT

and "M" in the case of a chamber brake differs from the nature of the instability in a disk brake. The diagram of the brake moment for a unidisk brake with plastic "M"
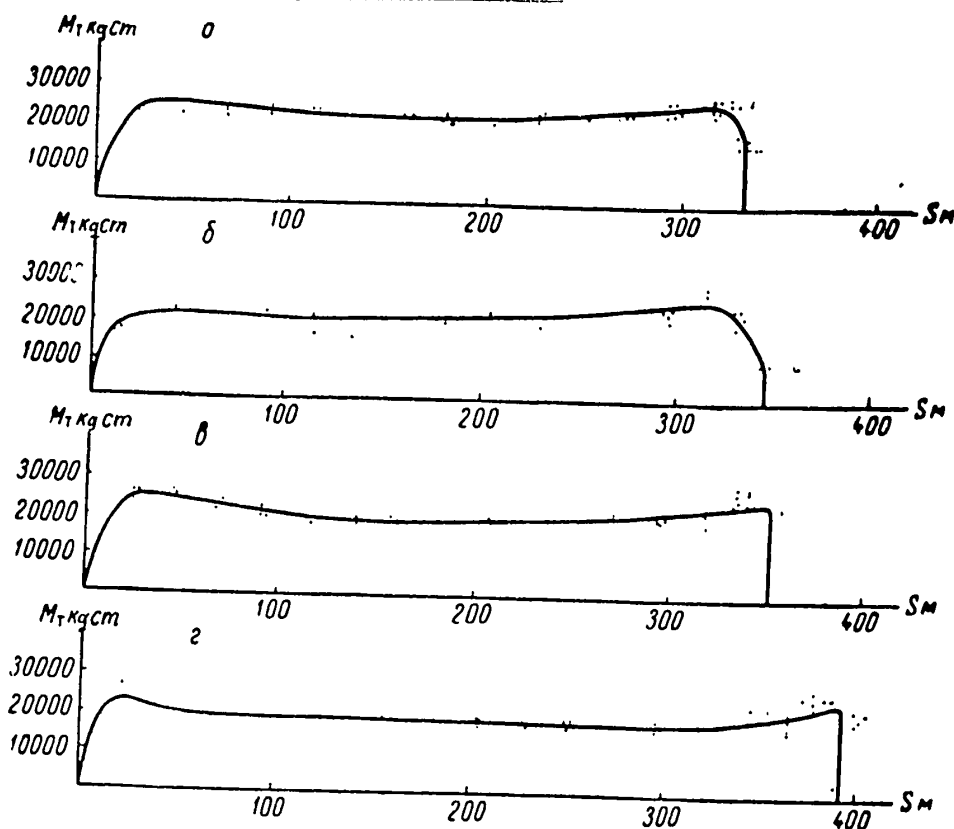
Fig. 57 - Diagrams of Brake Moments of a Chamber Brake at a Sliding Speed of 21.1 m/sec

a) Plastic 6FP at p_T = 11.5 kg/cm^2; b) Plastic 6Fs at p_T = 8 kg/cm^2; c) Plastic "M" at p_T = 14 kg/cm^2; d) Plastic No. 22 at p_T = 15 kg/cm^2.

linings has a hump (rise in the middle) instead of a depression.

The diagrams in Fig. 57 indicate that, for a chamber brake with linings of plastics No. 22, 6FP and "M", there is no decrease in the value of the brake moment at the end of braking under calculated conditions. Only a chamber brake equipped with plastic 6FS (this plastic was not tested on a disk brake) has - besides a depression - a sharp decline of the brake moment at the very end of braking.

STAT

The divergence of the brake-moment value as a result of instability of the friction coefficient of a pair, represented on the diagram by a depression, considerably
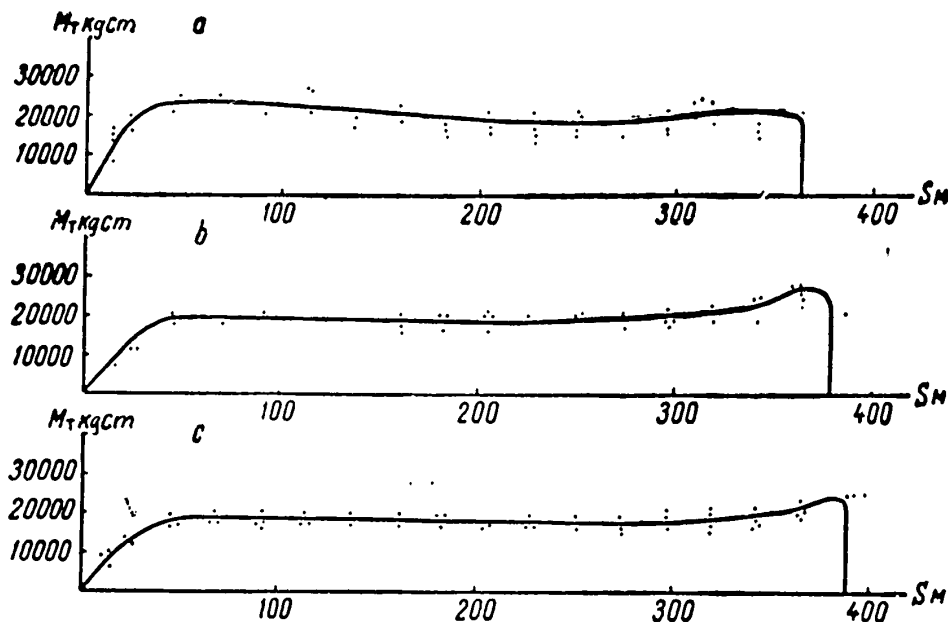
Fig. 58 — Diagrams of Brake Moments of a Chamber Brake at a
Sliding Speed of 39.6 m/sec

a — Plastic No. 22 at p_T = 20 kg/cm^2; b — Plastic 6FS at
p_T = 10 kg/cm^2; c — Plastic 6FP at p_T = 10 kg/cm^2

decreases the braking efficiency: the length of the brake path of a wheel equipped
with a chamber brake made of plastics 6FP, "M", and No. 22 producing a depression in
the moment diagram, is longer than the length of the brake path of a wheel equipped
with a disk brake made of the same plastics but not giving a depression in the dia-
gram.

Figure 58 shows diagrams of the brake moment of a chamber brake with linings
made of plastics 6FP, 6FS, and No. 22. These diagrams were plotted during brake
tests under calculated conditions at considerably higher speeds v_{sk} = 39.6 m/sec,
corresponding to v_{pos} = 300 km/hr).

The diagram shows that an increase in the initial sliding speed of a pair from
21.1 to 39.6 m/sec considerably affects the stability of the friction coefficient of

160

STAT

these plastics when they operate in combination with cast iron ChNMKh. All three

plastics produce a more sharply expressed delay in reaching the calculated brake mo-

ment at the start of braking and produce depressions in the middle of braking. At

the very end of braking, all three plastics produce a sharp rise in the value of the

brake moment; the diagram concludes with a peak at the end of the braking path. The

moment diagram for a brake with linings of plastic No. 22 has the sharpest peak.

The peak-like nature of the growth of the moment at the end of braking is dang-

erous because the nature of such a change in the value of the brake moment shows a

tendency to jamming; besides, the nature of such a change in the brake moment during

the process decreases the braking efficiency most.

The diagrams shown in Fig. 58 indicate that the plastic No. 22 plus the cast

iron ChNMKh react most sharply to an increase of the initial sliding speed, i.e., to

the action of the surface temperature on the friction coefficient of a pair.
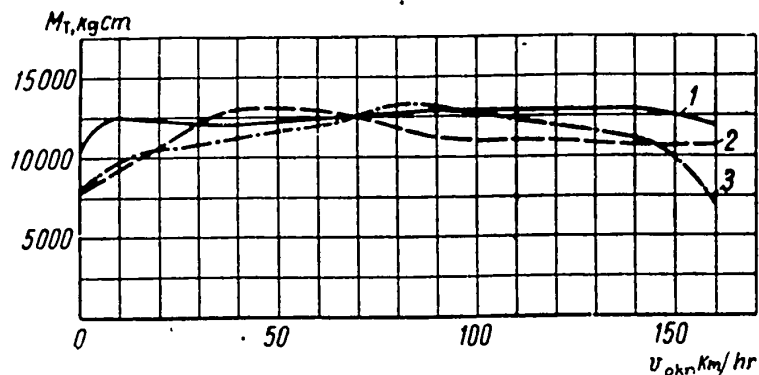
Fig.59 - Dependence of the Brake Moment M_T on the Peripheral Speed v_{okr}

for a Disk Brake of a Wheel 660 × 160 B under Different Pressures, Giving

the Same M_{max} Braking Conditions: A - 125,000 kg-m

1 - Plastic 6FP at P_T = 16.5 kg/cm^2; 2 - Plastic "M" at

p_T = 22 kg/cm^2; 3 - Plastic No.22 at p_T = 13.5 kg/cm^2

A change in the brake moment as a function of the peripheral speed v_{okr} is

shown in Fig.59 for a disk brake and in Fig.60 and 61 for a chamber brake.

The brake moment of a unidisk brake, equipped with linings made of the plastic

6FP changes little with speed. This shows that a friction pair consisting of plastic

161

STAT

6FP and cast iron ChNMKh, under conditions of a disk brake and in the range of sliding speeds from 160 tó 5 km/hr, operates stably and that its friction coefficient depends little on the temperature produced on the friction surface of a pair. Plastics "M" and No. 22, under these conditions, produce a less stable friction coefficient.

At the start of braking, when the sliding speed and consequently the surface temperature have the highest values, the brake moment of a unidisk brake with linings made of the plastic "M" has the lowest value. Then, as the speed decreases, the brake moment gradually increases and reaches a maximum at a speed of 75-80 km/hr. Then, regardless of a decrease in sliding speed, the brake moment decreases. This decrease in the moment apparently is the result of a temperature influence during the second half of the brake path, the temperature in this case being not surface but volume temperature of the brake disk. The plastic No. 22 shows approximately the same change in the frictional properties as a function of the speed.
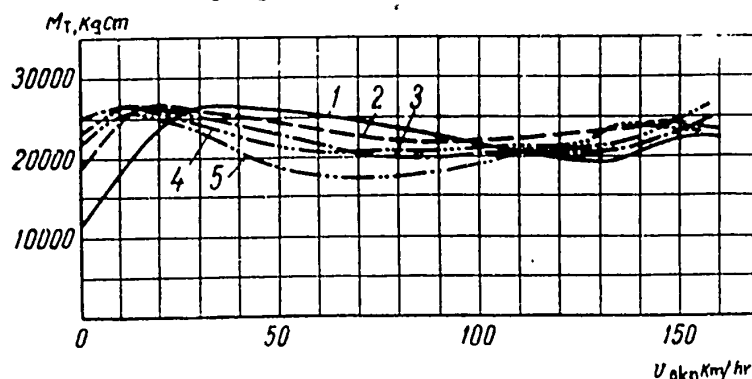
Fig. 60 - Dependence of the Brake Moment M_T on v_{okr} for a Chamber Brake with an Initial Peripheral Speed of 160 km/hr

1 - Plastic 6FS at $p_T = 8$ kg/cm^2; 2 - Plastic 6FP at $p_T = 11.5$ kg/cm^2;

3 - Plastic "M" at $p_T = 14$ kg/cm^2; 4 - Plastic 3FS at $p_T = 8.5$ kg/cm^2;

5 - Plastic No. 22 at $p_T = 15$ kg/cm^2

The plastic 6FP, 6FS, "M", and No. 22 have a somewhat different nature of change in the frictional properties as a function of speed when operating in a chamber brake, combined with cast iron ChNMKh. When braking at a speed of 160 km/hr, the change in the brake moment of a chamber brake equipped with linings of plastics

STAT

6FP, 6FS, "M", and No. 22 differs as follows: At the start of braking, when the speed is near 160 km/hr, the brake moment decreases; then it begins to increase gradually and reaches a maximum at the speed of 40-15 km/hr. Later, at the end of braking, the value of the brake moment decreases again.

The rate at which the greatest decrease in the brake moment during the braking process takes place and at which the curve $M_T = f(v)$ forms a depression is not the same for all tested plastics. Speed has the greatest effect on the value of the brake moment when a brake is equipped with the plastic No. 22. This type of brake, at the start of braking at v_{okr} = 160 km/hr has a brake moment of 27,000 kg/cm; then it decreases and, in the depression of the curve at v_{okr} = 70 km/hr, reaches a value of 17,500 kg/cm. Later at v_{okr} = 15 km/hr the brake moment is restored and again reaches the value of 27,000 kg/cm. At the very end of braking, at a speed approaching zero, the brake moment decreases again from 27,000 kg/cm to 22,500 kg/cm. A chamber brake with the plastic No. 22 shows fluctuations in the value of the brake moment during the process of braking which, in this case, are between the limits of + 3 and - 33%.
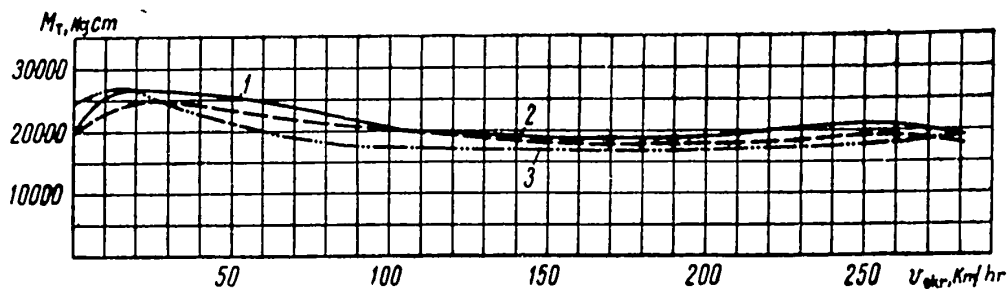
Fig. 61 – Dependence of the Brake Moment M_T on v_{okr} for a Chamber
Brake with an Initial Peripheral Speed of 300 km/hr
1 – Plastic 6FS at p_T = 10 kg/cm^2, 2 – Plastic 6FP at
p_T = 10 kg/cm^2; 3 – Plastic No. 22 at p_T = 20 kg/cm^2

Chamber brakes with the plastics 6FP and "M" have a more stable moment. When braking at a speed of 300 km/hr (Fig. 61), the value of the brake moment of brakes equipped with plastics 6FS, 6FP, and No. 22 is less than the calculated value at the

163

STAT

very start of braking; then it decreases still more and, having reached a minimum at a speed of 150 km/hr, begins to increase slowly again. Only near the end of braking, at a speed of v_{okr} = 15-30 km/hr, does the brake moment reach its calculated value and after that drops sharply.

The phenomenon of sharp decrease in the brake moment at the end of braking, just before the wheel stops, had been noted by us before. It occurs in brakes equipped with all tested plastics. The explanation should be looked for in the prolonged (10-15 sec) action of the volume temperature on a given plastic.

The decrease in the brake moment at high speed (300 - 100 km/hr) apparently can be explained as the action of high temperatures on the friction surface.

Figure 61 shows that a brake equipped with the plastic No. 22, at nearly all speeds, has a brake moment less than the brake moment of brakes equipped with plastics 6FP and 6FS. As mentioned before, this is explained by the fact that a brake with the plastic No. 22, at speeds higher than 200 km/hr, is subject to fold-over which decreases the friction coefficient of a brake pair.

Numerous inertia-stand tests on chamber brakes equipped with shoes made of the plastic No. 22 show: If the specific power absorbed by the brake does not exceed 40 kg/cm^2·sec, then no fold-over occurs; however, as soon as the value of the specific power exceeds 40 kg/cm^2 · sec, then fold-over appears. The more intensive the fold-over, the more specific power is absorbed by the brake. These data refer only to a pair of plastic No. 22 plus cast iron ChNMKh, a chamber brake.

Figure 62 shows the change in the mean and maximum friction coefficients of the plastics No. 22 and 6FS on cast iron ChNMKh, as a function of the sliding speed. These friction coefficients are found by calculation according to the equation

$$f_T = \frac{M_T}{p_y \, S_T r_T} . \qquad\qquad (217)$$

In calculating, the brake moment M_T was taken from the diagram of moments and the specific pressure p_{ud} was found from the equation

164

STAT
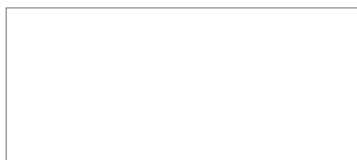
$$p_{ud} = 0,8\, p_{\text{T}}. \qquad\qquad (218)$$

The peripheral speed v_{okr} for a chamber brake with a wheel 660 × 16СВ, is re-
lated to the sliding speed of a pair by the equation (214):

$$v_{\text{SK}} = 0,475\, v_{okr}.$$

When the sliding speed increases, the friction coefficients of the plastics No.
22 and 6FS decrease. The absolute values of the friction coefficient is less for the
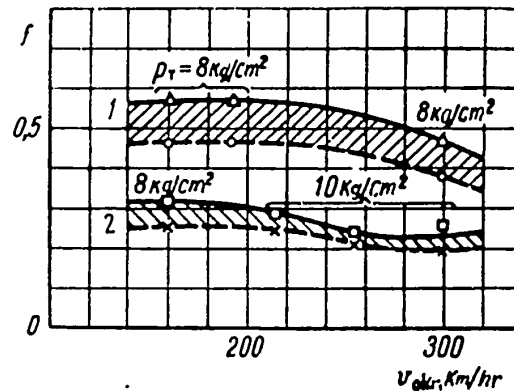
Fig. 62 – Change of Mean (Broken Line) and Maximum (solid line)

      Coefficients of Friction for the Plastics 6FS and No. 22 over

      Cast Iron ChNMKh, as a Function of the Sliding Speed at the

      Specific Pressure p_{ud} = 8 kg/cm^2

      1 – Plastic 6FS; 2 – Plastic No. 22

plastic No. 22 than for the plastic 6FS. The curves of changes, in the friction co-
efficient for the plastic 6FS are steeper than for the plastic No. 22. The differ-
ence in values of maximum and mean friction coefficients for the plastic 6FS over the
entire range of speeds is greater than for the plastic No. 22. This shows that the
stability of the frictional properties of the plastic No. 22 is higher. Comparing
these two plastics, it must be remembered, however, that in starting at a speed of
200 km/hr, the plastic No. 22 folds over, introducing an uncertainty in calculating
the friction coefficient value.

    The data in Fig. 62 were found at a specific pressure on the friction

STAT

surface of the brake shoes of p_{ud} = 8 kg/cm^2. For other values of p_{ud}, the nature of the curves should not change, since the dependence of the friction coefficient on the specific pressure is practically linear. Only the absolute values of the friction coefficient will change. Figure 63 shows curves for changes in the friction coefficients of the plastics 6FP, 6FS and No. 22 over cast iron ChNMKh, as a function of the brake chamber pressure.

These curves are the result of chamber brake tests at an initial peripheral speed of v_{okr} = 300 km/hr.
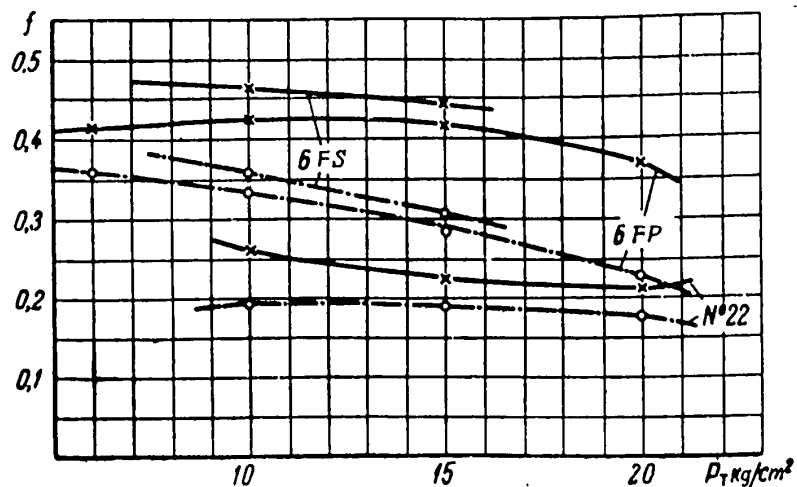
Fig. 63 - Curves for Changes in the Friction Coefficient of the Plastics 6FP, 6FS, and No. 22 over Cast Iron ChNMKh in a Chamber Brake, as a Function of the Pressure at the Initial Speed of Braking v_{okr} = 300 km/hr (Solid Lines f_{max}; Broken Lines f_{mean})

The curves show that, in braking at the speed v_{okr} = 300 km/hr, the plastic No. 22 has the highest stability of friction properties. In the plastic No. 22, the curves of maximum and mean friction coefficients are closest. In this respect, the plastics 6FS and 6FP are lagging behind the plastic No. 22. The curves of change in their friction coefficients are rather far apart and diverge still more as the pressure p_T rises. This means that, under higher pressures, the stability of the fric-

166   STAT

tion coefficient for these plastics will decrease.

Results of tests with the plastics No. 22, 6FP, "M" and 6FS under calculated conditions show that for stability of frictional properties when used in unidisk and chamber brakes, the best are the plastics 6FP and 6FS. The plastic "M" is next in stability.

Table 3 gives data on the wear of the plastics No. 22, 6FP, 6FS, and "M". These data were obtained in actual tests with unidisk and chamber brakes on a stand, under calculated conditions, with brakings at initial speeds of v_{okr} = 160 km/hr and v_{okr} = 300 km/hr.

Absolute values of linear wear of linings for one braking are given in the Table. They are necessary for designers of brakes. Knowing the degree of wear of linings for one braking and the required time of brake service, a designer can find the necessary thickness of the linings in a given brake. Besides the absolute values of linear wear for one braking, the Table gives data for the relative linear wear of linings, i.e., the wear for one braking, as it pertains to the specific power absorbed by the brake at a given braking. Data for the relative wear are necessary for a comparative rating of tested frictional pairs with respect to their wear resistance.

The wear of linings made of the plastic 6FP for one braking is equal to 0.0258 mm when used in a unidisk brake. The wear of linings made of the plastic No. 22 is equal to 0.100 mm. Judging by these data, a unidisk brake, with linings made of the plastic 6FP will be serviceable more than three times longer than a unidisk brake with linings made of the plastic No. 22, under similar conditions.

In testing the plastic 6FP in a chamber brake, the results were worse than in testing it in a unidisk: The wear of chamber brake linings, made of this plastic, for one braking under calculated conditions, is equal to 0.075 mm, i.e., the wear increased nearly three times. The plastic "M", used in a chamber brake, increased insignificantly in wear. The plastic No. 22, when used in a chamber brake even decreased slightly in wear for one braking. The latter is explained by fold-over of

STAT

metal on the brake linings, which results in wear of the metal counterbody of a pair;
i.e., the cast iron ChNMKh.

When evaluating the wear resistance of a given plastic, it is necessary to con-
sider not only its own wear resistance but also the extent of wear of the brake drum
or disk. The plastic No. 22, when operating in a chamber brake, although showing
less wear than in a disk brake, results in a considerable wear of the brake drum.
The plastics 6FP and "M" produce practically no wear of the drum.

To find the effect of the sliding speed on the wear of brake linings, brake
tests were made at a speed of v_{okr} = 300 m/sec with a chamber brake. These tests
showed that at an increase in sliding speed, the wear of the linings increases. How-
ever, despite the fact that the sliding speed was raised rather sharply (from 21.1
to 39.6 m/sec), the wear of the lining increased only slightly.

To obtain a comparative rating of the wear resistance of tested plastics under
calculated conditions, their relative wear should be compared.

Table 3 shows that the plastic 6FP has the lowest relative wear in a unidisk
brake. In a chamber brake, the plastic "M" has the lowest relative wear.

Tests made with the plastics No. 22, 6FP, and 6FS at an increased speed showed
that the plastics 6FP and 6FS have the lowest relative wear at a sliding speed of
v_{sk} = 39.6 m/sec.

The effect of the value of the kinetic energy on the wear of brake linings was
studied in chamber brakes of wheels 1260 × 390B and 660 × 160B. Braking was perform-
ed at a speed of v_{okr} = 160 - 200 km/hr. The pressure in the brake was such that the
calculated brake moment was maintained.

Figure 64 shows curves for the variation in the shoe wear δ for the above-men-
tioned brakes for one braking, as a function of the coefficient C in eq. (2) of the
kinetic energy

$$A_T = C_{saM} P_{sI} v^2_{pos.}$$

168

STAT

The curves show that the wear of the brake lining has a linear dependence on the value of the kinetic energy.

The stability of the friction coefficient and the braking efficiency of the tested plastics 6FP, 6FS, No. 22, and "ПT" as a function of the pressure p_T in the brake
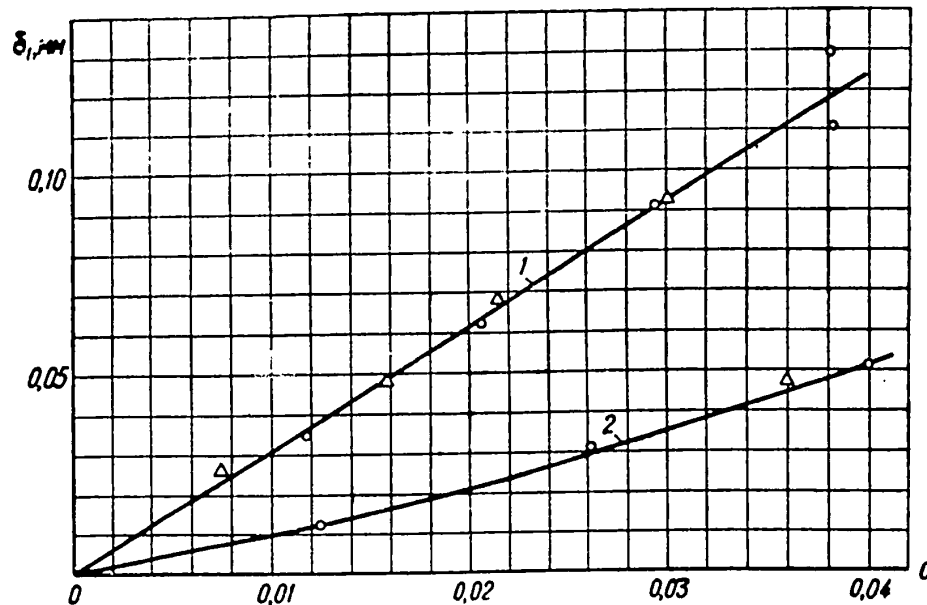
Fig. 64 – Wear of Shoes for one Braking as a Function of the Kinetic Energy (Coefficient C in the Formula $A_{stand} = CP_{st} v^2_{pos}$). The circles denote wear of linings under smooth pressure on the brake from $p_T = 1.5 + 2$ kg/cm^2 at the initial braking to p_T calc at the end of braking; the triangles denote lining wear at sudden application of calculated pressure to the brake and keeping it constant until the end of braking.

1 – Wheel 1260 × 390 B; 2 – Wheel 660 × 160 B

was studied while operating in chamber and unidisk brakes, with brakings at speeds of 160, 214, 254 and 300 km/hr.

When we change the value of the pressure in the brake at a given speed, we vary the power absorbed in the brake. This power, at a given speed and friction radius, is proportional to the specific pressure on the sliding surface and to the

169   STAT

friction coefficient of the frictional pair. The coefficient of friction, in turn, depends (Fig. 63) on the specific pressure.

Consequently, the pressure in a chamber or disk brake, being proportional to the specific pressure on the friction surface of a frictional pair, doubly affects the value of the power absorbed in the brake; on one hand, the pressure in the brake affects the value of the brake power directly, and on the other hand, it affects it indirectly through the friction coefficient of the brake frictional pair.
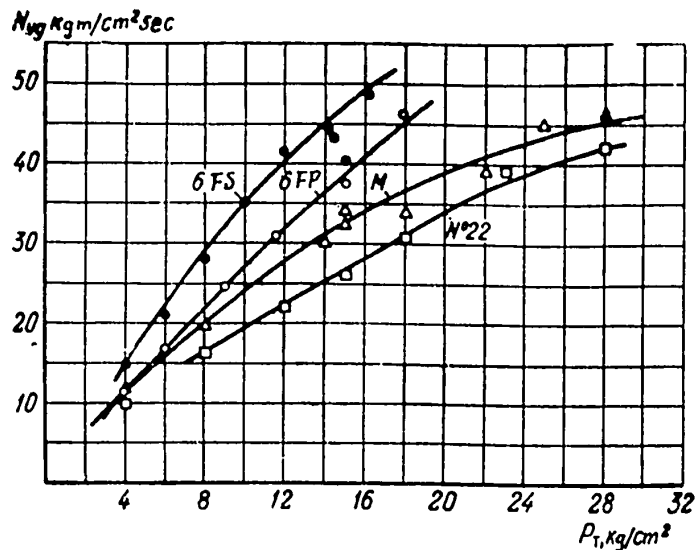
Fig. 65 – Specific Power of the Chamber Brake of a Wheel 660 × 160 B, Equipped with Linings of Different Plastics, as a Function of Pressure in the Brake System. Conditions of braking:

$$A = 0.036 v_{pos}^2 \quad P_{st} = 250,000 \text{ kgm}, \quad v_{okr} = 160 \text{ km/hr}.$$

Figure 65 shows curves for the specific power of friction for the tested plastics combined with cast iron ChNMKh, as a function of the pressure in a chamber brake.

The plastics 6FS and 6FP develop the greatest specific power of friction at a given pressure in a brake. The curves for a change of specific power, as functions of the brake pressure for the plastics 6FS and 6FP are steeper than the curves for the plastics "M" and No. 22. This shows that the frictional efficiency of the plas-

170

STAT

tics 6FS and 6FP must be higher than the efficiency of the plastics "M" and No. 22.

The curves $N_{T\ ud} = f\ (p_T)$ have a practically linear nature.

Rating of the stability of the friction coefficient and of the braking efficiency of a given frictional pair can be done conveniently by means of the stability coefficient

$$\alpha_c = \frac{M_{max}}{M_{T.sp}}, \qquad (219)$$

representing the ratio of the maximum brake moment developed by the brake to the mean brake moment as well as by the efficiency factor

$$\beta_{eff} = \frac{\alpha_{st}}{\varphi_{kol}}, \qquad (220)$$

representing the ratio of the stability coefficient to the brake path of the wheel. Consequently, the most stable coefficient of friction will be obtained by a friction pair whose coefficient α_{st} equals 1, i.e., $M_{T\ max}$ and $M_{T\ sp}$ are equal in magnitude.

The most effective pair is one which has the maximum coefficient B_{eff}, i.e., one whose wheel-brake path, expressed by the total angle ψ_{kol} of wheel revolution during braking, is the smallest.

Data referring to the stability of the friction coefficient and the frictional efficiency of the plastics 6FP, 6FS, "M", and No. 22, obtained in tests of the above plastics in unidisk and chamber brakes under different brake pressures and brakings at different speeds are shown in Table 4.

Figure 66 shows curves for the change of maximum $M_{T\ max}$ and mean $M_{T\ sp}$ brake moments as functions of the pressure p_T in a unidisk brake.

The more closely spaced the curves $M_{T\ max}$ and $M_{T\ sp}$ are, the higher will be the stability of the friction coefficient of a given plastic combined with cast iron ChNMKh in a unidisk brake. When the curve $M_{T\ max}$ coincides with $M_{T\ sp}$, absolute stability is established.

The curves show that, during operation in a unidisk brake, the plastics 6FP,

171

STAT

Table 4

a) P_T, kg/cm^2; b) P_{ud}, kg/cm^2; c) v_{okr}, km/hr; d) v_{sk}, m/sec; e) $M_{T\ max\ sp}$, kg · cm; f) $M_{T\ sp\ sp}$, kg · cm;

g) Length of Brake Path L_{sp} M; h) Braking time t – sec; i) Maximum Friction Coefficient $f_{max} = \dfrac{m_t}{P_{ud}\,S_t\,r_t}$;

j) Mean Horsepower of Friction $N_{ud\ sp} = \dfrac{A_{T\ sp}}{S_T\,t_{sp}}$ kgm/sec^2 · sec; k) Chamber Brake; l) Disk Brake

"M", and No. 22, with an increase in pressure p_T in the brake, i.e., with an increase in specific pressure on the friction surface, cause a decrease in the stability of the friction coefficient; the curves $M_{T\ max}$ and $M_{T\ sp}$ diverge.
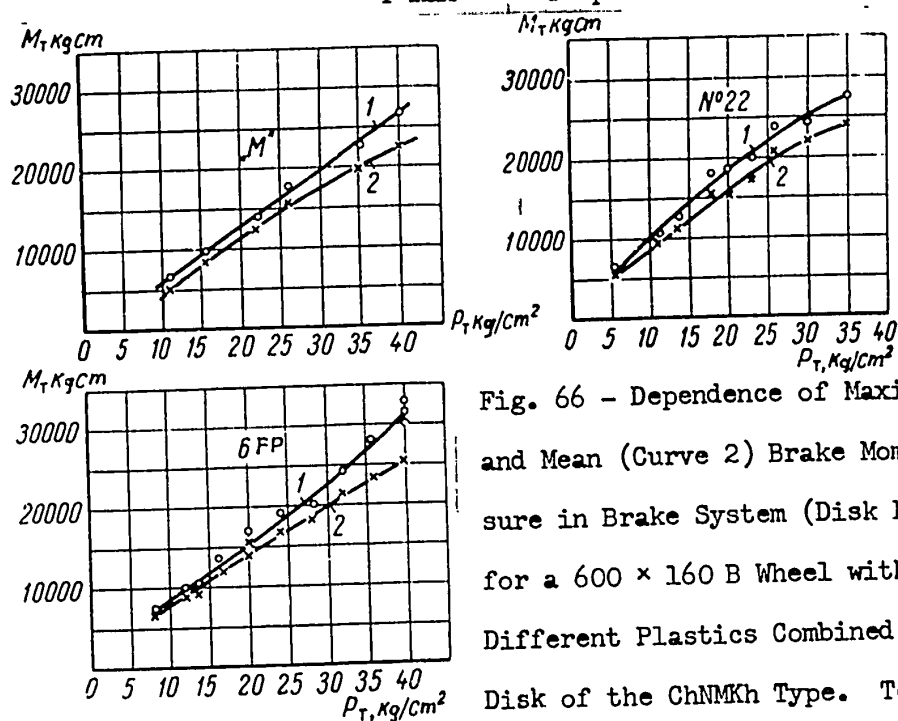

Fig. 66 – Dependence of Maximum (Curve 1) and Mean (Curve 2) Brake Moments on the Pressure in Brake System (Disk Experimental Brake for a 600 × 160 B Wheel with Brake Linings of Different Plastics Combined with a Cast Iron Disk of the ChNMKh Type. Testing Conditions: A = 125,000 kgm, v_{okr} = 160 km/hr

The plastic No. 22 shows the greatest divergence in the curves $M_{T\ max}$ and $M_{T\ sp}$ up to pressures of p_T = 30 kg/cm^2.

The change in the stability of the coefficient α_{st}, as a function of the pressure p_T in a unidisk brake of 6FP, "M", and No. 22 plastics is shown in Fig. 67.

The "M" and 6FP plastics have rather high (0.9) stability of the friction coefficient in a range of pressures p_T from 8 to 32 kg/cm^2. The coefficient of stability in these plastics decreases with higher temperatures. The change in the stability coefficient of the plastic No. 22 takes place differently than in the plastics 6FP and "M"; starting from the smallest pressures and up to pressures of p_T = 20 kg/cm^2, the stability coefficient of the plastic No. 22 decreases and then depending on the extent of the increase in pressure p_T, the coefficient increases reaching a greater

173

STAT

value than the plastic 6FP or "M" at pressures of $p_T > 32$ kg/cm^2.

One can draw the conclusion that, in actual performance, a unidisk brake made of the plastic No. 22 combined with cast iron ChNMKh under specific pressures of $p_{ud} > 20$ kg/cm^2, and with brakings at speeds of $v_{okr} = 160$ km/hr, has an advantage
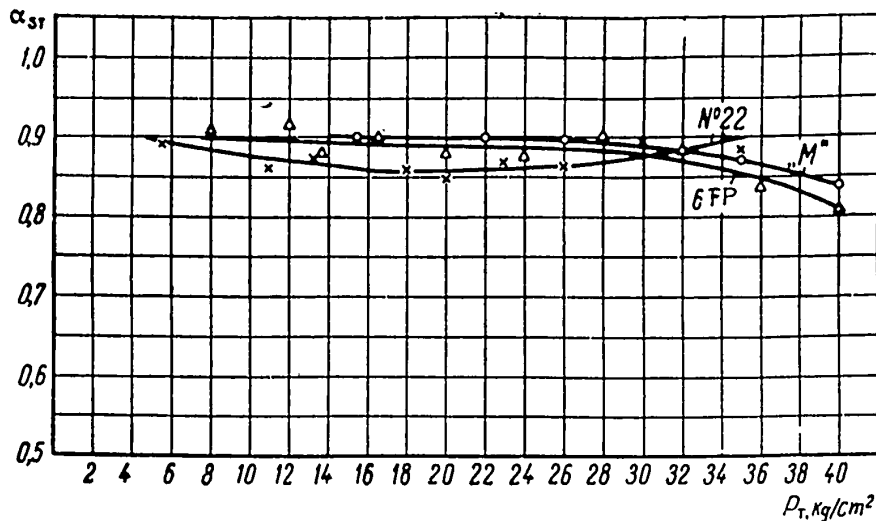

Fig. 67 – Dependence of the Stability Coefficient on Pressure in the
Brake System (Experimental Disk Brake for a 660 × 160 B Wheel with
Brake Linings of Different Plastics Combined with a Cast Iron
Layer of a ChNMKh Disk). Braking conditions: A = 250,00 kgm,
$v_{okr} = 160$ km/hr.

over the 6FP and "M" plastics in its coefficient of stability.

Figure 68 shows the curves for changes in the efficiency factor B_{eff} of 6FP, "M" and No. 22 plastics, depending on p_T when these plastics perform in a unidisk brake.

It is clear from these curves that the functional efficiency of all three plastics grows with an increase in pressure p_T from 6 - 12 to 32 - 40 kg/cm^2. In this range of pressures p_T, the efficiency factor B_{eff} of all three plastics changes practically linearly. The factor B_{eff} reaches its maximum during the pressures of $p_T = 40 - 45$ kg/cm^2, corresponding to the specific pressures $p_{ud} = 25 - 28$ kg/cm^2. In the range of pressures of $p_T = 6 - 40$ kg/cm^2, plastic No. 22 has the highest

174

STAT

coefficient B_{eff}. In a unidisk brake, the plastic No. 22 is superior to the plastics 6FP and "M", not only in stability of the friction coefficient α_{st}, but in its braking efficiency B_{eff}.

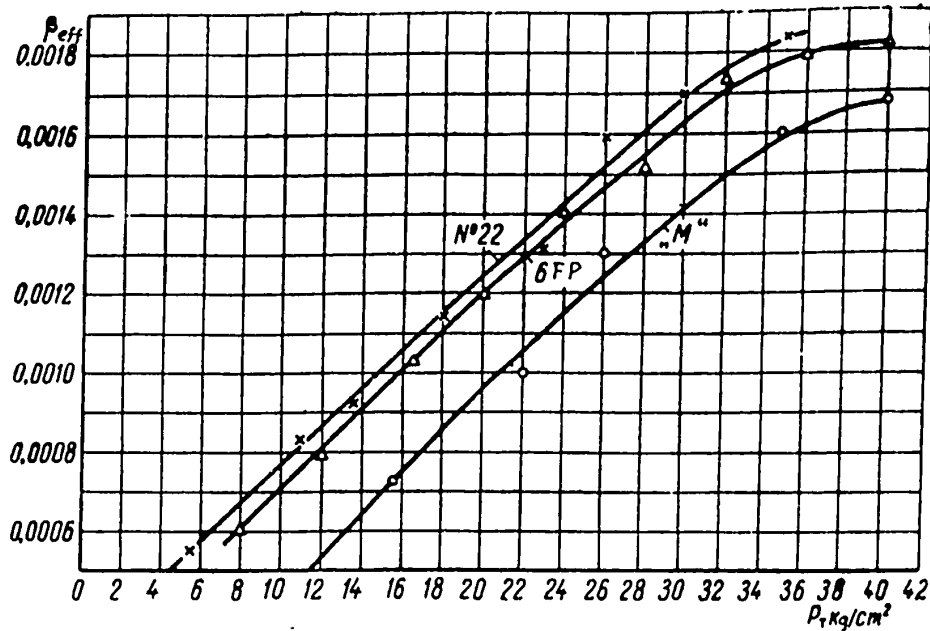The study of the stability in the friction coefficient and of the frictional

Fig. 68 – Dependence of Brake Efficiency B_{eff} on the Pressure in the Brake System. Braking conditions: A = 250,000 kgm, v_{okr} = 160 km/hr

efficiency in 6FP, 6FS, "M", and No. 22 plastics was conducted in a chamber brake at braking speeds of 160, 214, 254, and 300 km/hr. The stability and efficiency characteristics of 6FP, "M", and No. 22 plastics, during performance in a chamber brake, differ greatly from the stability and efficiency characteristics of these plastics when performing in a unidisk brake.

In brakings at speeds of 160 km/hr with 6FP, 6FS, "M", and No. 22 plastics, the brake moment curves $M_{T\ max}$ and $M_{T\ sp}$ (Fig. 69) diverge more sharply depending on increase of pressure in the brake, than the $M_{T\ max}$ and $M_{T\ sp}$ curves of these plastics when performing in a unidisk brake.

STAT

This indicates that, under the conditions of a chamber brake, the stability of the friction coefficient in these plastics deteriorates. Figure 70 shows curves for the change in the stability coefficient α_{st} of the plastics 6FP, 6FS, "M", and No. 22 when performing in a chamber brake.
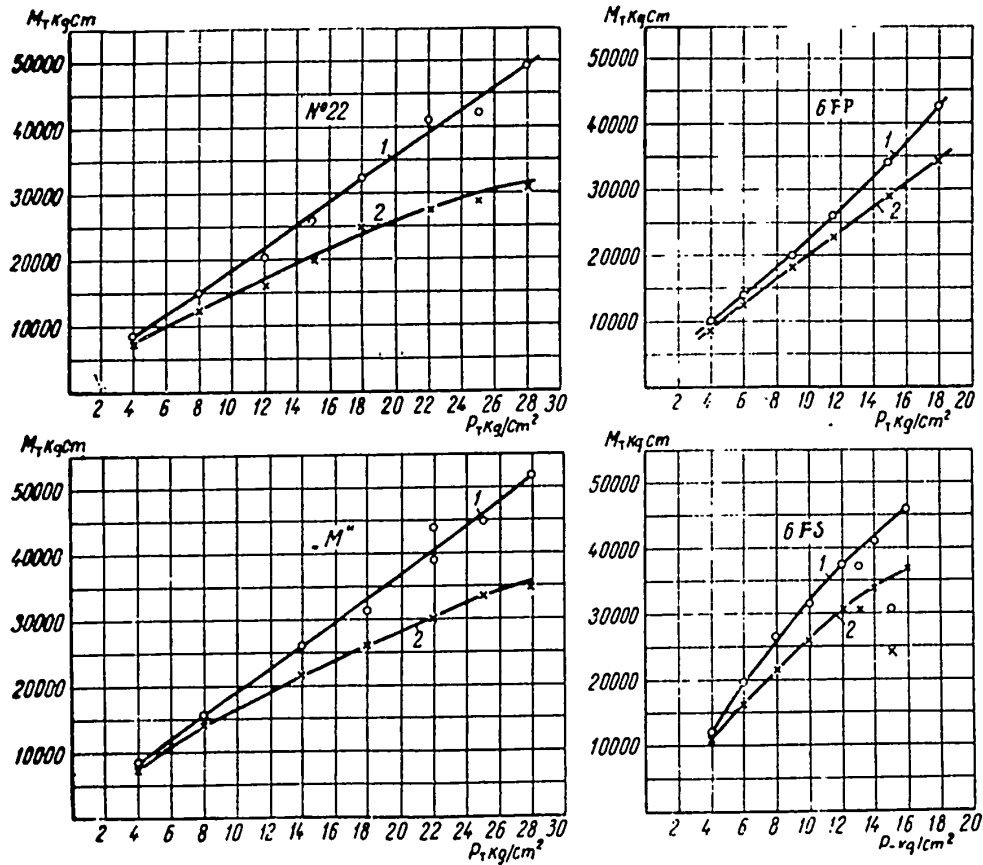
Fig. 69 – Dependence of the Maximum (Curve 1) and Mean (Curve 2) Brake Moments on the Pressure in the Brake System of a T 132 Chamber Brake in a 660 × 160 B Wheel with Brake Linings of Different Plastics. Braking conditions: A = 250,000 kgm, v_{okr} = 160 km/hr

In a unidisk brake, the stability coefficient of the 6FP and "M" plastics in the range of pressures p_T = 6 - 30 kg/cm^2 maintains its value and, starting at pressures of p_T = 30 kg/cm^2, decreases. In a chamber brake, the coefficient of the plastic "M" is stable over the whole range of pressures p_T, while the stability coef-

176   STAT

175

ficient of the plastic 6FP, starting with pressures of $p_T = 9$ kg/cm^2, sharply decreases with an increase of pressure in the brake. Under conditions of a chamber

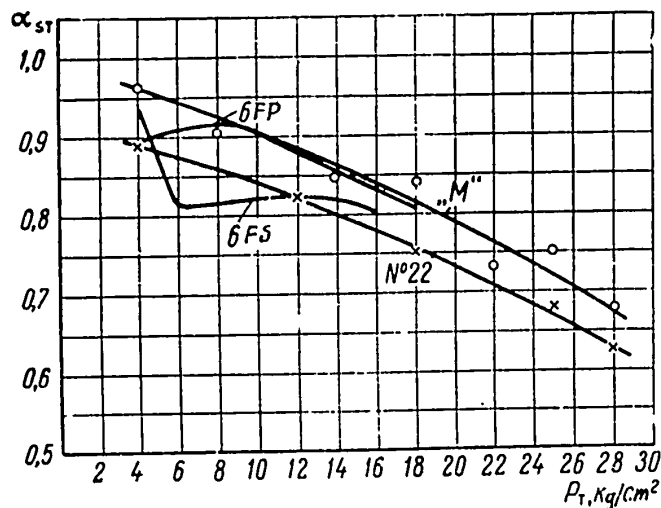Fig. 70 - Dependence of the Stability of the Friction Coefficient in a Pair on the Pressure in the Brake System (in a T 132 Chamber Brake of a 660 × 160 B Wheel with Brake Linings of Different Plastics). Braking conditions: A = 250,000 kgm, v_{okr} = 160 km/hr

brake, the plastic No. 22 also has a stability coefficient which decreases sharply with an increase of pressure in the brake.

Any increase in the initial braking speed in a brake lowers even more the stability of the friction coefficient of all plastics tested, which do not fold over metal on the friction surface of the shoes.

Figure 71 shows curves for the change in the brake moments $M_{T\,max}$ and $M_{T\,sp}$ depending on p_T during brakings in a chamber brake with a speed of ~ 300 km/hr.

It is clear from Fig. 71 that only the curves for the plastic No. 22 $M_{T\,max}$ and $M_{T\,sp}$ diverge somewhat less. However, this decrease in divergence of the moment curves is due to the fold-over of metal on the friction surface of the blocks, and although the decrease makes the friction coefficient more stable up to a pressure of 16 kg/cm^2, it is accompanied by a sharp decrease in the absolute value of the friction coefficient of the pair, reducing the braking efficiency.

177

STAT

When braking in a chamber brake with a speed of $v_{okr} = 300$ km/hr, the coefficient of stability α_{st} in 6FP and 6FS plastics decreases more sharply, depending on p_T (Fig. 72), than in braking with a speed of $v_{okr} = 160$ km/hr.

As for the plastic No. 22, its stability coefficient during brakings in a chamber brake with a speed of $v_{okr} = 300$ km/hr in a range of pressures of $p_T \approx 10 - 15$ kg/cm^2 increases sharply; on further increase in the pressure p_T, the stability coefficient decreases just as sharply.
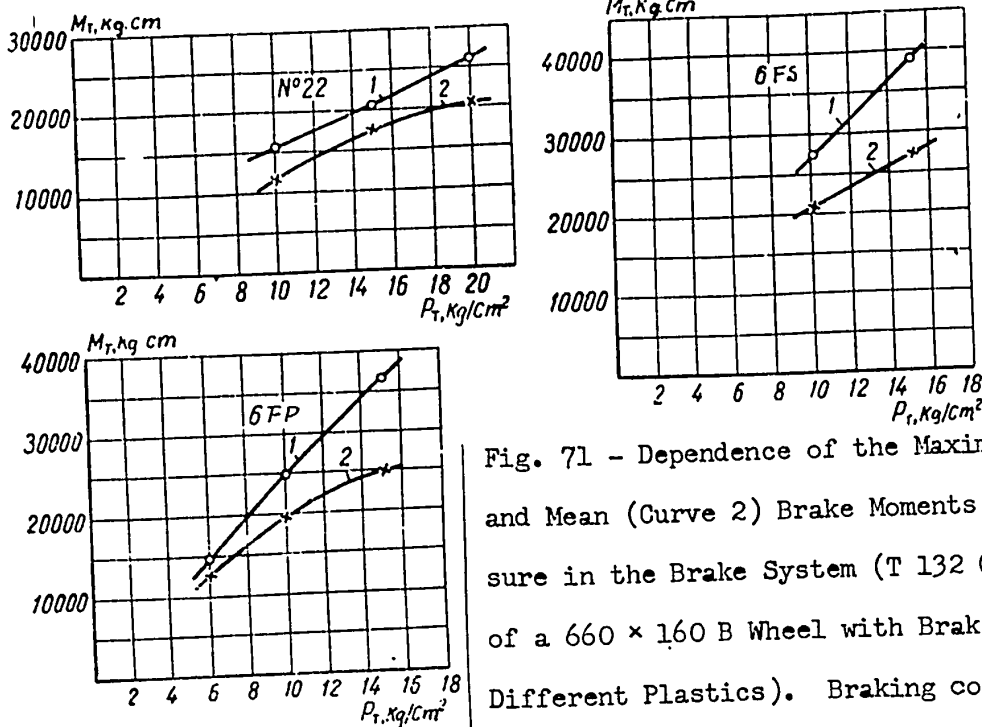

Fig. 71 - Dependence of the Maximum (Curve 1) and Mean (Curve 2) Brake Moments on the Pressure in the Brake System (T 132 Chamber Brake of a 660 × 160 B Wheel with Brake linings of Different Plastics). Braking conditions: $A = 250,000$ kgm, $v_{okr} = 299$ km/hr

The explanation for the nature of such changes in the value of the stability coefficient for the plastic No. 22 lies in the effect of fold-over, which appears in plastics under these braking conditions, on the friction coefficient of the pair.

The magnitude of the braking efficiency B_{eff} changed when working in a chamber brake. The slope of the curves for braking in a chamber brake at a speed of $v_{okr} = 160$ km/hr (Fig. 73), as compared with the slope of these curves when braking at the same speed in a unidisk brake (Fig. 68), showed a decrease. The dependence of the change in the efficiency factor B_{eff} on the pressure p_T in a chamber brake

STAT

produced a clearly expressed nonlinearity. In addition, the plastic No. 22, during operation in a chamber brake, decreased the value of its efficiency coefficient for the whole range of pressures p_T as compared with the values of the efficiency coefficient (Figs. 73 and 68) produced in this plastic during operation in a unidisk brake.
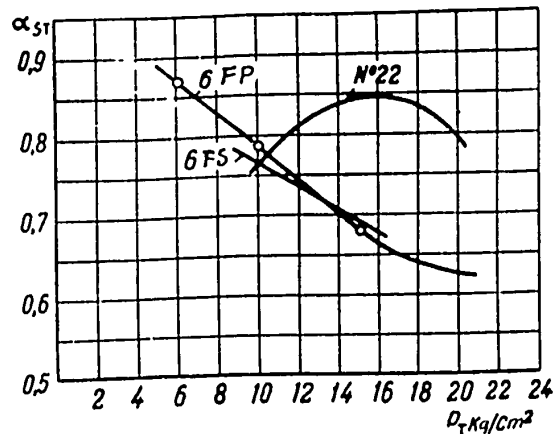

Fig. 72 - Dependence of the Stability Coefficient of the Friction Pair on the Pressure in the Brake System (T 132 Chamber Brake in a 660 × 160 B Wheel with Brake Linings of Different Plastics).

Braking Conditions: A = 25,000 kgm, v_{okr} = 299 km/hr

An increase in the initial braking speed considerably lowered the efficiency of the brake with linings of 6FP and No. 22 plastics. In braking at a speed v_{okr} = 300 km/hr, the efficiency factor of the 6FP and No. 22 plastics grew with an increase in pressure p_T only up to 16–18 kg/cm^2, while it remained unchanged on further increase in pressure (Fig. 74), with B_{eff} = 0.0007.

When braking at a speed of v_{okr} = 160 km/hr and a pressure of p_T = 18 – 20 kg/cm^2, this factor for the plastic 6FP is equal to 0.00115, and for the plastic No. 22 it is equal to 0.00075.

The stability α_{st} and the efficiency B_{eff} factors of the plastics studied, as shown by their tests in a chamber brake, depend on the surface temperature which is higher in a chamber brake since its friction surface is not ventilated and the overlapping coefficient is close to 1 as a result of high sliding speeds. Therefore, in

179

STAT

a chamber brake, the temperature gradients in the elements of the friction pair are not the same as in other brakes. Also, under conditions of a chamber brake, the volume temperature of the frictional pair remains effective for a longer period of time.
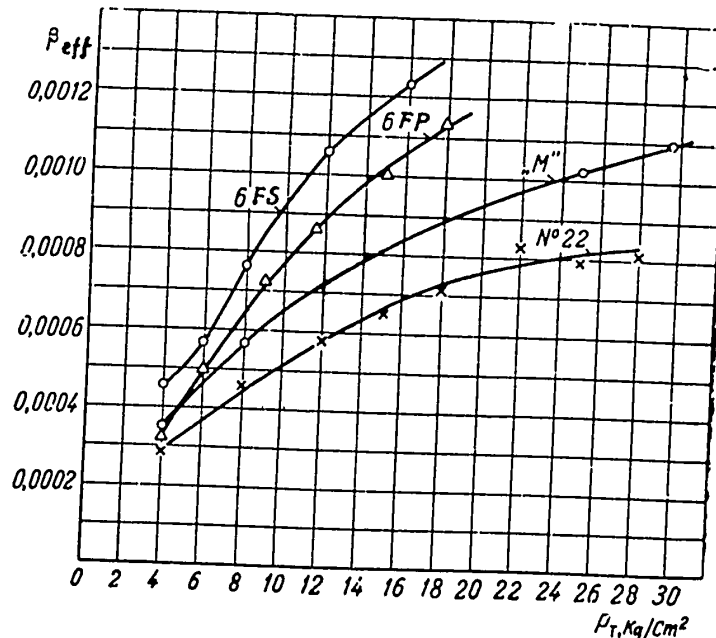

Fig. 73 – Dependence of the Brake Efficiency Factor β_{eff} on the Pressure in the Brake System (T 132 Chamber Brake in a 660 × 160 B Wheel with Brake Linings of Different Plastics). Braking conditions: A = 250,000 kgm, v_{okr} = 160 km/hr

Requirements for Frictional Materials

The basic criterion for rating frictional material of a pair for modern brakes is its heat resistance, i.e., its ability to maintain mechanical strength and value of the friction coefficient when the temperature is raised. Both of these parameters are affected first of all by the temperature in the surface layers of the friction pair. Therefore, to ensure efficiency and a long service life of brake linings, rapid removal of heat from the friction surface which lowers the temperature is just as essential as for brake drum performance.

Practice shows that is is impossible to obtain a complete solution of the prob-

180

lem of steady brake and wheel performance under high temperatures by assuring modu-
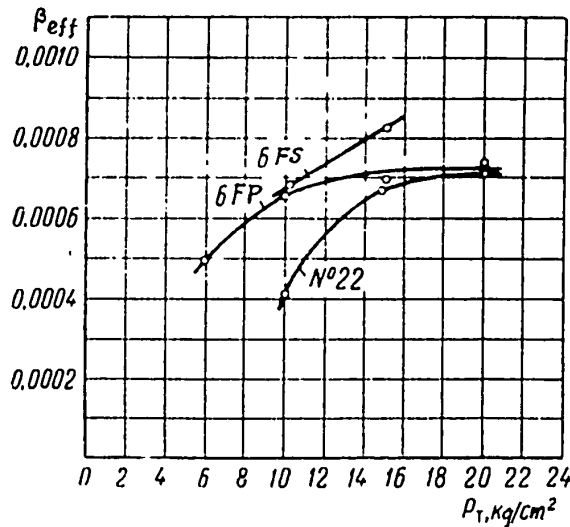lated heat conditions for frictional brake-pair operation. To solve the problem of

Fig. 74 – Dependence of Brake Efficiency Coefficient β_{eff} on the
Pressure in the Brake System (T 132 Brake on a 660 × 160 B
Wheel with Brake Linings of Different Plastics). Braking
Conditions: A = 250,000 kgm, v_{okr} = 299 km/hr

developing a brake design for a modern aircraft wheel for performance under difficult
heat conditions and forced heat and mechanical loads, it is necessary to lower the
heat loads acting on the frictional pair and at the same time to find and use special
heat-resistant materials for the frictional pair.

To achieve this, systematic laboratory and theoretical studies should be con-
ducted to find new materials for wheel brakes and new brake designs which would as-
sure reliable performance of the elements in the wheel brake under forced conditions.

The following general requirements should be met for materials of a frictional
pair in modern aircraft brakes, consisting of a brake drum or a brake disk and brake
linings.

1) Resistance to heat fatigue caused by cyclic heating and cooling;

2) Resistance of the friction surface to wear, erosion, and abrasion

181   STAT

3) Resistance to mechanical destruction.

Requirements of Frictional Materials for Brake Drums and Brake Disks

The material of an ideal brake drum or brake disk should meet the following physical requirements to provide the qualities necessary:

1. High heat conductivity, necessary to prevent reaching the melting point of the material in a thin red-hot layer of the friction surface.

2. Low coefficient of heat expansion, necessary to reduce to a minimum the heat stresses between the inner and outer layers of the brake drum.

3. High specific heat capacity, necessary for the material to accomodate a greater quantity of heat at a minimum increase in temperature.

4. A high melting or softening point, necessary to avoid the possibility of a metal fold-over on the brake linings and jamming of the brakes.

5. A high coefficient of surface heat emission, necessary for a greater quantity of heat to be dissipated by radiation. This property is not so important in the drum during single landings with braking, but when frequent braked landings are made, for example during instruction flights, the radiating capacity of the drum becomes much more important.

6. A high friction coefficient, making it possible to achieve the necessary brake moment at minimum loads, other conditions being equal.

7. A low specific gravity, making it possible to have minimum weight in the design of the brake drum or brake disk.

8. A low ridigity modulus, contributing to a reduction in thermal stresses caused by the temperature gradient.

9. A large volumetric heat capacity, permitting minimum drum (disk) dimensions at a given specific gravity of the material.

During the development of wheel brakes, many materials have been tested for brake drums, but it seems obvious now that high-carbon ferrous alloy meets the re-

182

STAT

quirements better than any of the alloys presently known.

Cast iron with a high carbon content has high heat resistance and excellent compressive strength. It is known that the higher the carbon content in the form of graphite in iron, the higher will be the resistance of the iron to temperature fluctuations. It is possible that a high carbon content in the form of graphite contributes to maintaining a low rigidity modulus which reduces the magnitude of the thermal stress to a minimum.

Even more important is the fact that graphite behaves as a liquid and assures uniform distribution of tensions. This also explains the high compressive strength of cast iron. Cast iron has a compression yield point which, in magnitude, exceeds by three to five times the magnitude of its expansion yield point. The ratio of $\frac{\sigma_{comp}}{\sigma_{exp}}$ is greater in soft cast irons than in hard cast irons. For soft cast irons $\sigma_{comp} = 7000$ kg/cm^2 and $\sigma_{exp} = 1400$ kg/cm^2; therefore $\frac{\sigma_{comp}}{\sigma_{exp}} = 5$.

As a result of the large magnitudes of their compression yield points cast irons with high carbon content have smaller radical shrinkage than steel of average carbon content.

ChNMKh cast iron is used for brake drums in domestic aircraft brakes.

Requirements for Frictional Materials in Brake Shoes and Facings.

The other part of the frictional pair are the plastics of various compositions and the cermet alloys from which the brake shoes and linings are made. Brake linings undergo just as much strain and are as important a part of the friction pair as the drum or disk brake.

For performance under forced braking conditions, characterized by a surface temperature of $\theta_s = 1000\text{--}1200°C$, volume temperature of $\theta_v = 400\text{--}500°C$, a sliding speed of $v_{sk} = 25 - 50$ m/sec, and a specific pressure of $p_{ud} = 15 - 50$ kg/cm^2, the material for the brake linings should meet the following basic requirements:

1) A coefficient of friction which is stable and required by its absolute value.

183

STAT

The value of the friction coefficient should be 0.30 ± 0.03 to 0.40 ± 0.05.

2) Resistance to erosion of the lining should ensure a maximum wear of 0.03 mm for one braking at given θ, v_{sk} and p_{ud}.

3) High mechanical strength.

4) Absence of a tendency to abrade the friction surface of the coupled pair (drum, disk).

5) Smooth performance.

The ideal lining should have a stable friction coefficient not only at positive temperatures but also at negative temperatures of the surrounding medium, and in damp and dry weather as well.

Stability of the friction coefficient is especially important for brakes with servo action.

In certain cases, the brake design may affect the value of the friction coefficient of the pair, as long as it specifies operating heat conditions to a certain extent.

A unidisk brake has a coefficient of overlap that is a ratio of the magnitude of the covered friction surface to the uncovered surface which is equal to 0.25 - 0.5.

This creates favorable conditions for rapid radiation of heat from the friction surface and for ventilating it in the braking process. Usually the chamber brake has a maximum covered friction surface; its coefficient of overlap is close to a unit.

During the braking process in the chamber brake, pratically no heat escapes from the friction surface by radiation; therefore, the temperature of the friction surface in such a brake is higher than in a unidisk brake with a partially uncovered friction surface.

The brake design also affects the general heat conditions of the wheel brake. With all other conditions being equal, the wheel with a unidisk brake has easier heat conditions: The rim of the wheel with a unidisk brake heats up less than a wheel with a chamber brake; the temperature of the friction surface of a frictional pair

STAT

in a disk brake is lower than in a chamber brake.

It is possible to solve satisfactorily the problem of the frictional pair for modern aircraft brakes by using more heat-resistant materials and at the same time using a brake design which would provide the best heat conditions in the pair.

One of the methods of such a solution is the use of a frictional pair made of ChNMKh cast iron and plastic 6FP in a disk brake which has a ventilated friction surface.

The problem of providing modern jet aviation with wheel brakes capable of operating under high rolling speeds requires serious theoretical and experimental studies of the processes taking place in the friction surface of the brake frictional pair during braking.

The laboratory method of studying the performance of a frictional pair in ring models and in actual brakes on an inertia stand makes it possible to determine fully the effect of temperature, speed, sliding, specific pressure, and degree of overlap in the elements of the pair on brake characteristics: stability, friction coefficient, and wear of the frictional pair. Practical experience of laboratory studies shows that the qualitative and quantitative results of tests on models are very close to the results obtained in tests of comparable pairs in actual brakes on an inertia stand.

BIBLIOGRAPHY

1 – RAS, No. 499 (1952)

2 – Product Engineering, November (1946)

3 – SAE Transactions (1953)

4 – SAE Quarterly Transactions, VII, v. 4, No. 3 (1950)

5 – SAE Journal, II (1954)

6 – Aeroplane, No. 1948 (1949)

7 – Flight, No. 2115, 2126 (1949)

STAT

8. - Aeroplane, No.2071 (1951)

9. - SAE Journal, June (1950)

10. Chichinadze,A.V. - Extension Seminar on Problems of Increasing Wear Resistance of Brakes and Friction Units in Machines and Unification of Testing Methods for Brake Materials. Vestnik Mashinostroeniya, No.11 (1952)

11. Kragel'skiy,I.V., Bessonov,L.F., Shvetsova,E.M. - Contacting of Uneven Surfaces. DAN, Vol.93, No.11

12. Kragel'skiy,I.V. - Friction of Rest of Two Uneven Surfaces. Izvestiya AN SSSR, OTN, No.10 (1948)

13. Kaydanovskiy,N.L. and Khaikin,S.E. - Mechanical Relaxation Vibrations. Zh.Tekh. Fiz., Vol.III, No.1 (1933)

14. Kragel'skiy,I.V. - Effect of Fixed Contact on the Magnitude of Friction Power. Zh.Tekh.Fiz., Vol.XIV, No.4 - 5 (1944)

15. Ishlinskiy,L.Iu., Kragel'skiy,I.V. - Interrupted Action During Friction. Collection, Increased Wear Resistance and Service of Machines, Mashgiz (1953)

16. Stoker,D. - Nonlinear Vibrations of Mechanical and Electrical Systems. Publ. Foreign Literature (1953)

17. Shvetsova,Ye.M. and Kragel'skiy,I.V. - Classification of Types of Surface Destruction in Machine Parts under Conditions of Dry and Boundary Friction. Friction and Wear in Machines. Publ.AN SSSR, Collection 8 (1953)

18. Kragel'skiy,I.V. - Geometric Characteristics of Conditions in Surface Friction Interaction. Collection, Increased Wear Resistance and Service of Machines. Mashgiz (1953)

19. Aleksandrov,M.P. - Study of Crane Brakes.

20. Grechin,V.P. - Alloyed Cast Iron Casting. Oborongiz (1952)

21. Yuzefovich,N.A. and Kuvshinskiy,Ye.V. - Study of Mechanical Properties of Polymers in the Field of Softening the Diagram of Stretching in Rubbers and Resins. Zh.Tekh.Fiz., Vol.XXIII, No.8 (1953)

STAT

22. Bowden,F.P. - Friction on Snow and Ice. Proceedings of the Royal Society, Ser. T., No.1131 (1953)

23. Lykov,A.V. - Theory of Heat Conductivity. Gosergoizdat (1949)

24. Bowden,F.P. - Proc.Roy.Soc. A., 154, 640 (1937)

25. Levitskiy,M.P. - Friction Surface Temperatures in Hard Bodies. Zh.Tekh.Fiz., Vol.XIX, No.9 (1949)

26. Block,N. - Second World Petroleum Congress. Paris (1937)

27. Block,N. - General Discussion on Lubrication and Lubricants. Just.Mech.Eng. of London, IV (1937)

28. Iyeger,D.K. - Moving Heat Sources and Friction Temperature. Applied Mechanics and Machine Building. Collection of Translations, Publ. Inostrannoy Literatury, No.6 (1952)

29. Jaeger,J.C. - Philosophical Magazine Journal of Science, No.240 (1944)

30. Khol'm,R. - Temperature in a Heated Contact as Applied to Sliding Friction. Prikladnaya Mekhanika. Collection of Translations, No.4 (1953)

31. Petrusevich,A.I. - Machine Building. Encyclopedic Handbook, Vol.2, Mashgiz (1948)

32. Smirnov,V.I. - Course of Higher Mathematics. Tekhteorizdat (1948)

33. Yanke,Ye, and Emde,F. - Tables of Functions with Formulas and Curves. Nauch-Tekh.Izdat., Kiev (1934)

34. Charron,F. - Heat Transfer between Two Rubbing Bodies. Publications Scientifiques et Techniques du Secretariat d'Etat a l'Aviation, No.182 (1943)

35. Parker,R.C. - The Frictional Behavior of Engineering Materials. Engineering, 4, 11 (March 1949)

36. Kragel'skiy,I.V., Chichinadze,A.V. - Methods of Testing Frictional Materials on the New Friction Setup I-47. Zavodskaya Laboratoriya, No.5 (1954)

37. Chupilko,G.Ye. - Aircraft Brake Devices. Oborongiz (1940)

38. Karslov,Kh.S. - Theory of Heat Conductivity. Gostekhteoretizdat (1947)

STAT